
***Glasnik hemičara i tehnologa
Bosne i Hercegovine***

***Bulletin of the Chemists and Technologists
of Bosnia and Herzegovina***

Print ISSN: 0367-4444
Online ISSN: 2232-7266



Vladimir Prelog
Sarajevo, 23.07.1906. - Zürich, 07.01.1998.

47

December 2016.

***Glasnik hemičara i tehnologa
Bosne i Hercegovine***

***Bulletin of the Chemists and Technologists
of Bosnia and Herzegovina***

Print ISSN: 0367-4444
Online ISSN: 2232-7266

47

December 2016.

**Prirodno-matematički fakultet Sarajevo
Faculty of Science Sarajevo**



Glasnik hemičara i
tehnologa
Bosne i Hercegovine

Print ISSN: 0367-4444
Online ISSN: 2232-7266

Bulletin of the Chemists and Technologists of Bosnia and Herzegovina

Zmaja od Bosne 33-35, BA-Sarajevo
Bosnia and Herzegovina
Phone: +387-33-279-918
Fax: +387-33-649-359
E-mail: glasnik@pmf.unsa.ba
glasnikhtbh@gmail.com

REDAKCIJA / EDITORIAL BOARD

Editor-In-Chief / Glavni i odgovorni urednik Fehim Korać

Faculty of Science Sarajevo
Zmaja od Bosne 33-35, BA-Sarajevo
Bosnia and Herzegovina

E-mail: glasnik@pmf.unsa.ba
glasnikhtbh@gmail.com

Phone: +387-33-279-995 (Administration)
+387-33-279-911 (Executive Editors)
Fax: +387-33-649-359

Editors / Urednici

Milka Maksimović (mmaksimo@pmf.unsa.ba)
Emin Sofić (esofic@pmf.unsa.ba)
Semira Galijašević (semira.galijasevic@gmail.com)
Nurudin Avdić (technoprocur@yahoo.com)

Editorial Board / Članovi redakcijskog odbora

Ivan Gutman (SRB)	Dejan Milošević (B&H)
Željko Jaćimović (MNE)	Ljudmila Benedikt (SLO)
Meliha Zejnilagić-Hajrić (B&H)	Amira Čopra-Janićijević (B&H)
Tidža Muhić-Šarac (B&H)	Sabina Gojak-Salimović (B&H)
Jasna Huremović (B&H)	Emira Kahrović (B&H)
Ismet Tahirović (B&H)	Danijela Vidic (B&H)
Mustafa Memić (B&H)	Andrea Gambaro (ITA)
Dragana Đorđević (SRB)	Aida Šapčanin (B&H)
Jože Kotnik (SLO)	Lucyna Samek (POL)
Angela Maria Stortini (ITA)	Ivan Spanik (SLK)
Mirjana Vojinović Miloradov (SRB)	Heike Bradl (GER)
Lea Kukoč (CRO)	Sanja Čavar-Zeljčković (CZE)

Advisory Editorial Board / Članovi redakcijskog savjeta

Margareta Vrtačnik (SLO)

Alen Hadžović (CAN)

Franci Kovač (SLO)

Franc Požgan (SLO)

Mladen Miloš (CRO)

Mirjana Metikoš (CRO)

Lectors / Lektori

Semira Galijašević (Eng/B/H/S)

Milka Maksimović (Eng/B/H/S)

Administrative Assistants / Sekretari redakcije

Safija Herenda

Alisa Selović

Electronic Edition and Executive Editors / Elektronsko izdanje i izvršni redaktori

Anela Topčagić

Jelena Ostojić

Časopis izlazi polugodišnje, a kompletna tekst verzija objavljenih radova je dostupna na <http://www.pmf.unsa.ba/hemija/glasnik>.

The journal is published semiannual, and full text version of the papers published are available free of cost at <http://www.pmf.unsa.ba/hemija/glasnik>.

Citiran u *Chemical Abstracts Service*.



Cited by *Chemical Abstracts Service*.

Citiran u EBSCO Host.

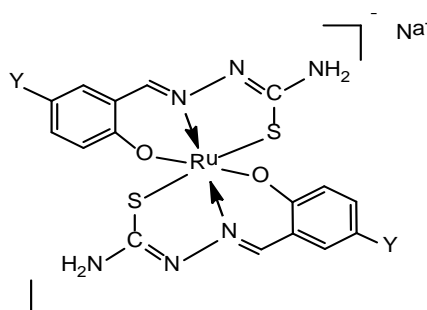


Cited by EBSCO Host.

CONTENT / SADRŽAJ

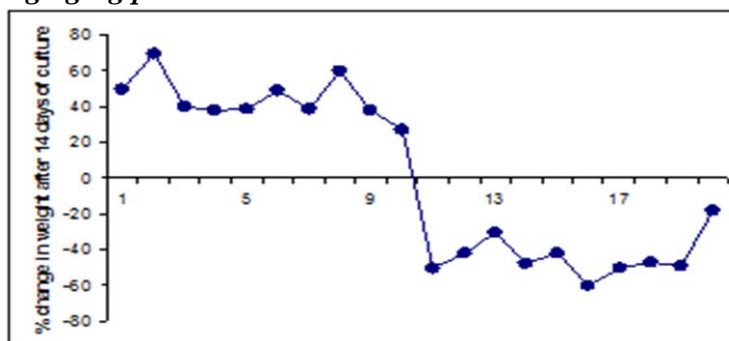
Editorial	I
ORIGINAL SCIENTIFIC ARTICLES	
<i>Synthesis and characterization of Ru(III) complexes with thiosemicarbazide based ligands</i>	1-6

Ljubijankić Nevzeta
Tešević Vele
Grgurić-Šipka Sanja
Jadranin Milka
Begić Sabina
Buljubašić Lejla
Markotić Ena
Ljubijankić Sead



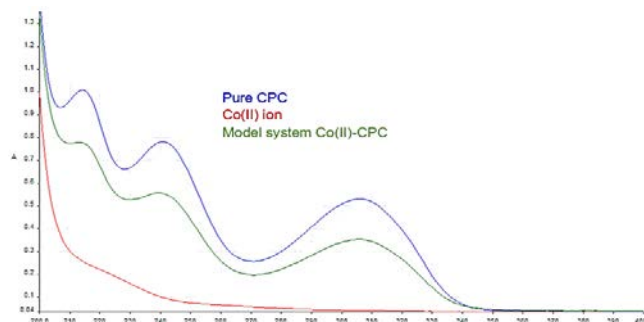
<i>Calcium analysis in bones during aging process</i>	7-10
-------------------------------------------------------	------

Šapčanin Aida
Sofić Emin



<i>Spectroscopic Investigations of Co(II) and Cu(II) Interaction with Imatinib Mesylate and Capecitabine</i>	11-16
--------------------------------------------------------------------------------------------------------------	-------

Cipurković Amira
Horozić Emir
Crnkić Aida
Marić Snježana
Ljubijankić Nevzeta



Antimicrobial effects of garlic (*allium sativum L.*)

17-20

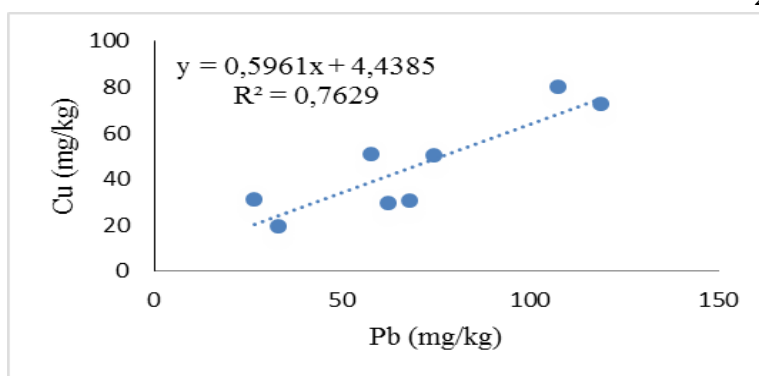
Strika Ilma
Bašić Azra
Halilović Namir



Heavy metals pollution in children playgrounds -an environmental modelling and statistical analysis

21-26

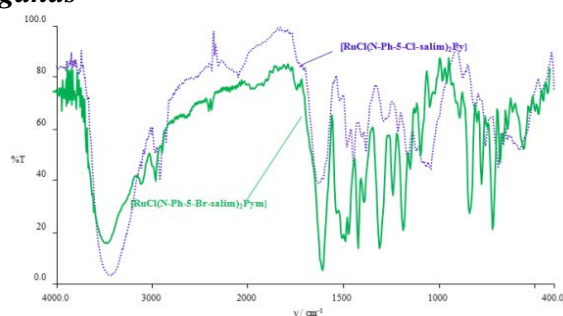
Šapčanin Aida
Čakal Mirsada
Ramić Emina
Smajović Alisa
Pehlić Ekrem



Synthesis and Characterization of Neutral Ru(III) Complexes Containing Schiff Bases and N-donor Heterocyclic Ligands

27-32

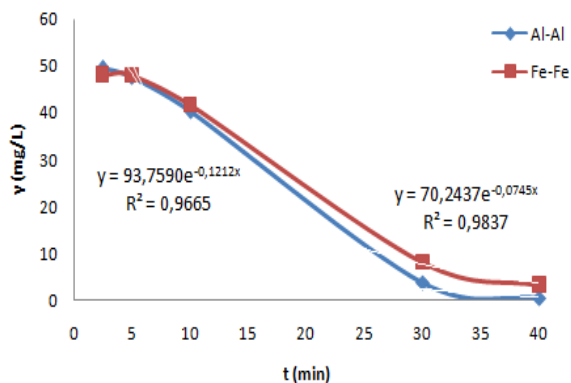
Begić Sabina
Ljubijankić Nevzeta



The phosphate removal efficiency electrocoagulation wastewater using iron and aluminum electrodes

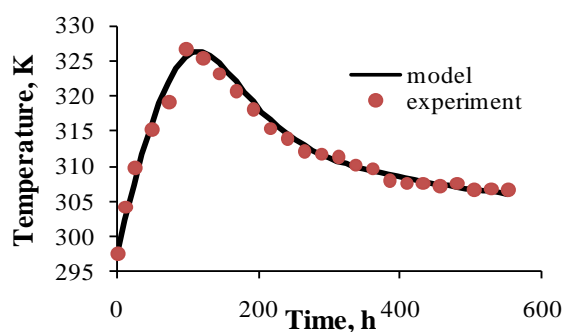
33-38

Đuričić, T.
Malinović, B.N.
Bijelić, D.



Mathematical modeling and simulation of the composting process in a pilot reactor 39-48

Papračanin Edisa
Petric Ivan



Development and validation of the mathematical model for synthesis of maleic anhydride from n-butane in a fixed bed reactor 49-58

Petrić Ivan
Karić Ervin

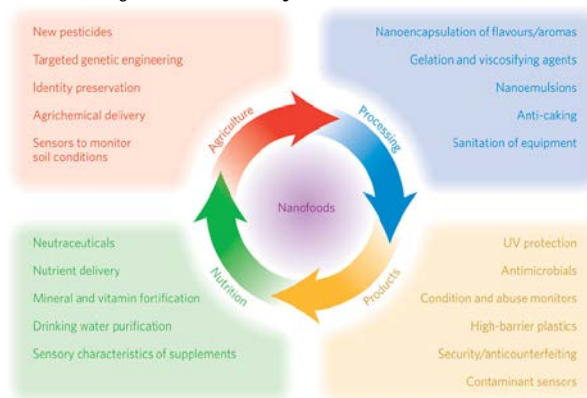


TECHNICAL PAPERS

Nanosensors applications in agriculture and food industry

59-70

Omanović-Miklićanin
Enisa
Maksimović Mirjana



Instructions for authors

71

Sponsors

79

Editorial

The first study, ten years after war activities, to report about the content of heavy metals and metalloides, polycyclic aromatic hydrocarbons (PAHs) and polychlorinated biphenyls (PCBs) found in samples of soils from playgrounds was realized in Sarajevo city. Due to the fact that children, the most vulnerable population, are in direct contact with surface soils, it has been recommended that children's playgrounds should be given special consideration in this respect. The war activities during 1992. to 1995. period caused a variety of damages and contamination of urban land. During the last five years, the background pollution of Sarajevo has been mainly created by atmospheric impurities emitted from different sources. The major polluting source of pollutants such as the heavy metals and metalloides in Sarajevo are vehicles because of high traffic density and also because vehicles (passenger cars and commercial vehicles) below the Euro 3/4 standard are used. Furthermore, heating plants (using crude oil or natural gas) and domestic heating (using wood and coal) are the other sources of inorganic and organic pollutants. Unfortunately, there is still inadequate emission control and soil quality standards in practice.

The goal of this research was to identify and quantify some inorganic and organic pollutants found in the soil of Sarajevo public playgrounds. Some of the consequences, ten years after the war, are evident in the collapse of monitoring programmes, in the severing of links between individuals working at universities and government officials, and in the physical destruction of records, including scientific data that had been painstakingly collected over a long period of time. There is currently little ongoing environmental monitoring at work. It is clear, however, that the consequences of the war for the environment have been different and geografically uneven. Findings of this study suggest that the contaminated playground soils in a war damaged area, as is the Sarajevo area, are still sources of heavy metals and metalloides, PAHs and PCBs contamination. While playgrounds soil characterization would provide an insight into major inorganic and organic pollutants speciation and bioavailability, attempts at environmental remediation of polluted soils would entail knowledge of the source of contamination, basic chemistry, and environmental and other associated children's health risks caused by these pollutants.

Results of this study may contribute to a more accurate health risk assesment of the soils, and may support planning safer and more sustainable urban playground areas; these findings could assist developers in planning projects for a more efficient use of land, or in studies assessing children's health risks, or in studies concerning the soil contamination and related legislation which is not sufficiently regulated in Bosnia and Herzegovina.

Editors



Synthesis and characterization of Ru(III) complexes with thiosemicarbazide-based ligands

Ljubijankić N.¹, Tešević V.², Grgurić-Šipka S.², Jadranin M.³, Begić S.¹, Buljubašić L.¹, Markotić E.¹, Ljubijankić S.⁴

¹Faculty of Science, Department of Chemistry, Zmaja od Bosne 33-35, Sarajevo, Bosnia and Herzegovina

²Faculty of Chemistry, University of Belgrade, Studentski trg 12-16, Belgrade, Serbia

³Center of Chemistry – Institute for Chemistry, Technology and Metallurgy, University of Belgrade, Studentski trg 12-16, Belgrade, Serbia

⁴School of Health Studies, University of Bihać, Žegarska aleja bb, Bihać, Bosnia and Herzegovina

Article info

Received: 15/11/2016

Accepted: 07/12/2016

Keywords:

Thiosemicarbazones

Thiosemicarbazide

Tridentate ligand

ONS donors

Ruthenium

Corresponding author:

Nevzeta Ljubijankić

E-mail: nevezetalj@gmail.com

Phone: 033 279 956

Abstract: Three Ru(III) complexes general formula $\text{Na}[\text{RuL}_2]$ (where L = dibasic tridentate thiosemicarbazone ligands) have been synthesized by reacting RuCl_3 with thiosemicarbazide-based ligands with ONS donors. Ligands of general formula $(\text{X})\text{N-NH-C}(\text{S})\text{-NH}_2$ were prepared through the condensation reaction of salicylaldehyde or its derivatives (X = salicylaldehyde, 5-Cl-salicylaldehyde, 5-Br-salicylaldehyde) with thiosemicarbazide. Complexes have been formulated and characterized by mass spectrometry and infrared spectroscopy. The data showed the formation of a complex with a 1:2 metal:ligand stoichiometries. The ligands coordinated as an ONS tridentate dianion through the oxygen atom of the deprotonated phenolic OH-group, the azomethine nitrogen atom and the sulfur atom after deprotonation of the thiosemicarbazide residue in its thiol form.

INTRODUCTION

Thiosemicarbazones have been the subject of many studies because of their variable bonding modes, promising biological implications and structural diversity (Al-Amiery et al., 2011). Among the most examined compounds of this group is certainly salicylaldehyde thiosemicarbazone (Vojinović-Ješić et al., 2011). The synthesis of the transition metal complexes with thiosemicarbazone ligands has been receiving considerable attention due to the potentially chemotherapeutic properties of both ligands and complexes as antitumor and antibacterial agents (Sampath and Jayabalakrishnan, 2016). It was found that their dibasic tridentate thiosemicarbazones with ONS donors

are of immense importance as they possess a wide spectrum of medicinal properties (El-Bahnasawy et al., 2014). Thiosemicarbazone derivatives are of particular chemical and pharmacological importance for the possession of a number of different biological activities: anticancer, antiviral, antibacterial, antifungal activity, etc. (Kumar et al., 2013). Pharmacological potential of thiosemicarbazone as antitumor agent is one of the most promising areas of its research (Chil J. 2013). Salicylaldehyde thiosemicarbazone and its derivatives are a group of flexible tridentate ONS donors capable of stabilizing the upper and lower oxidation state of transition metal ions (Leovac, et al., 1983). Thiosemicarbazone complexes differs from the free ligand with respect to their biological properties (Chandra et al., 2014). Although the thiosemicarbazone, obtained by

the condensation process with *o*-hydroxyl carbonyl compounds, show antibacterial activity, the metal complexes often manifest effect of a larger order of magnitude compared to the corresponding ligand (Ngan et al., 2011). A particularly important feature is the reduction of the cytotoxic action of thiosemicarbazone, which may be reduced by complexing to the metal cation (Rana et al., 2002). Synthesis of transition metal complexes with thiosemicarbazone ligands attracted considerable attention because of the potentially useful chemotherapeutic properties and ligands and complex in terms of anticancer and antibacterial activity (Al-Amiery et al., 2012). Salicylaldehyde thiosemicarbazone is usually expected to bind to a metal center, *via* dissociation of two acidic protons, as a dianionic tridentate ONS donor forming stable chelate (Datta et al., 2011). Platinum group metal complexes with thiosemicarbazones show a wide range of pharmacological activity (Thangadurai et al., 2001). The aim of this work was to study the syntheses, as well as the spectral and structural characteristics of three Ru(III) complex with salicylaldehyde thiosemicarbazone derived from salicylaldehyde and Cl and Br substituted salicylaldehyde and thiosemicarbazide.

EXPERIMENTAL

Materials and methods

Physical measurements

All chemicals used were commercially available with analytical grade of purity and used without further purification. Infrared spectra were recorded as KBr pellets on a Perkin Elmer spectrum BX FTIR System in region 4000 – 400 cm^{-1} . Agilent 6210 Time-of-Flight LC/MS system (Agilent Technologies, Santa Clara, California, USA) equipped with an ESI interface (ESI-ToF-MS) was used for recording of mass spectra and for the confirmation of molecular formulas of compounds. The ESI was operated in a negative mode and nitrogen was used as the drying gas (12 L/min) and nebulizing gas at 350°C (45 psi). The OCT RF voltage was set to 250 V and the capillary voltage was set to 4.0 kV. The voltages applied to the fragmentor and skimmer were 140 V and 60 V, respectively. Scanning was performed from 100 to 2000 m/z (mass-to-charge ratio). The identification of compound was as follows: compound was dissolved in the acetonitrile (concentration of 1 mg/mL), and a direct injection of 5 μL sample was conducted by 1200 Series HPLC (Agilent Technologies, Waldbronn, Germany) without a separation column. The isocratic mobile phase consisted of 50% acetonitrile and 50% of 0.2% formic acid in water (v/v) at a flow rate of 0.2 mL/min. Using these parameters, the anionic part of the compound was detected as the corresponding $[\text{M}]^-$ ion.

Synthesis of ligands

Thiosemicarbazide (0.01 mol; 0.91 g) was dissolved in ethanol (60 mL) by refluxing at 50°C and ethanolic solution (30 mL) of the salicylaldehyde or 5-Cl-salicylaldehyde or 5-Br-salicylaldehyde (0.01 mol; 0.89 mL, 0.157 g, 0.201 g, respectively) was added. The reaction mixture was refluxed for four hours at 60°C. The

volume of reaction mixture was reduced and then cooled on ice water. The crystals of salicylaldehyde thiosemicarbazone, 5-Cl-salicylaldehyde thiosemicarbazone and 5-Br-salicylaldehyde thiosemicarbazone, hereinafter HL1, HL2 and HL3, respectively, were precipitated out. The crystals were recrystallized in ethanol.

Synthesis of complexes

Ethanolic solution (20 mL) of the thiosemicarbazone ligand HL1 or HL2 or HL3 (1 mmol; 0.195 g or 0.229 g or 0.273 g, respectively) was added to the solution of $\text{RuCl}_3 \cdot 3\text{H}_2\text{O}$ (0.5 mmol; 0.131 g) in ethanol (20 mL) and the reaction mixture was refluxed for 4-5 hours. Volume of the resulting solution was reduced to 10 mL at rotary vacuum evaporator and the solution was left overnight. The precipitation was performed by adding the equimolar amounts of water solution of NaCl. The resulting crystalline compound was filtered under suction, washed with ethanol and ether, and dried in vacuum. Dark green partly crystalline product is air stable, soluble in most common polar organic solvents and insoluble in apolar organic solvents and water. Yield: 63%

RESULTS AND DISCUSSION

Ligands HL1, HL2, HL3, general formula (X)N-NH-C(S)-NH₂ were prepared by mixing equimolar amounts of thiosemicarbazide and salicylaldehyde or its derivatives (X = salicylaldehyde, 5-Cl-salicylaldehyde, 5-Br-salicylaldehyde) in absolute ethanol under reflux for four hours at 60°C (Pahontu et al., 2013) (Figure 1).

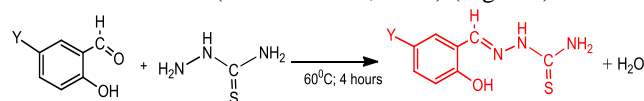


Figure 1. Preparation scheme for ligands L1, L2, L3; Y = H, Cl, Br, respectively

The complexes $\text{Na}[\text{RuL}_2]$ (L = HL1, HL2, HL3) were prepared by the modified synthetic procedure (Kumar et al., 2013) by mixing 1:2 molar ratio of RuCl_3 and the ligands in absolute ethanol (Figure 2).

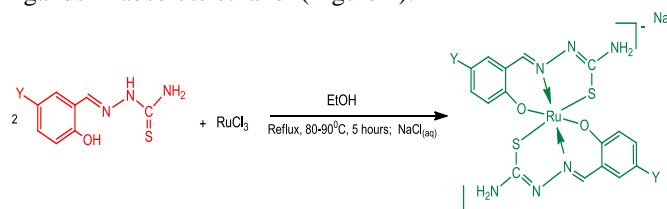


Figure 2. Preparation scheme for complexes $\text{Na}[\text{Ru}(\text{HL}1)_2]$, $\text{Na}[\text{Ru}(\text{HL}2)_2]$, $\text{Na}[\text{Ru}(\text{HL}3)_2]$; Y = H, Cl, Br, respectively

$\text{Na}[\text{Ru}(\text{HL}1)_2]$

ESI-ToF MS m/z : $[\text{C}_{16}\text{H}_{14}\text{N}_6\text{O}_2\text{S}_2\text{Ru}]^-$ 487.96567; FT-IR HL1 (KBr, cm^{-1}): 1616 s $[\nu_s(\text{C}=\text{N})]$, 1269 s $[\nu_s(\text{C}-\text{O}_{\text{phen}})]$; 777 s $[\nu_s(\text{C}=\text{S})]$, FT-IR $\text{Na}[\text{Ru}(\text{HL}1)_2]$ (KBr, cm^{-1}): 1605 s $[\nu_s(\text{C}=\text{N})]$, 1280 s $[\nu_s(\text{C}-\text{O}_{\text{phen}})]$, 723 s $[\nu_s(\text{C}-\text{S})]$, 587 s $[\nu_s(\text{Ru}-\text{N})]$, 509 s $[\nu_s(\text{Ru}-\text{O})]$, 441 s $[\nu_s(\text{Ru}-\text{S})]$

Na[Ru(LH2)₂]

ESI-ToF MS m/z : [C₁₆H₁₂N₆O₂S₂Cl₂Ru]⁻ 555.88615; FT-IR HL2 (KBr, cm⁻¹): 1611 s [ν_s(C=N)], 1280 s [ν_s(C-O_{phen})]; 777 s [ν_s(C=S)], FT-IR Na[Ru(HL2)₂] (KBr, cm⁻¹): 1589 s [ν_s(C=N)], 1266 s [ν_s(C-O_{phen})], 723 s [ν_s(C-S)], 547 s [ν_s(Ru-N), 484 s [ν_s(Ru-O), 438 s [ν_s(Ru-S)]

Na[Ru(LH3)₂]

ESI-ToF MS m/z : [C₁₆H₁₂N₆O₂S₂Br₂Ru]⁻ 643.78526; FT-IR HL3 (KBr, cm⁻¹): 1611 s [ν_s(C=N)], 1261 s [ν_s(C-O_{phen})]; 777 s [ν_s(C=S)], FT-IR Na[Ru(HL3)₂] (KBr, cm⁻¹): 1595 s [ν_s(C=N)], 1278 s [ν_s(C-O_{phen})], 723 s [ν_s(C-S)], 544 s [ν_s(Ru-N), 506 s [ν_s(Ru-O), 438 s [ν_s(Ru-S)]

ESI ToF MS mass spectrometry confirmed existence of [C₁₆H₁₄N₆O₂S₂Ru]⁻, [C₁₆H₁₂N₆O₂S₂Cl₂Ru]⁻ and [C₁₆H₁₂N₆O₂S₂Br₂Ru]⁻ ions with m/z values at 487.96567, 555.88615 and 643.78526, respectively. These ligands are coordinated to ruthenium center as a ONS tridentate dianion through the oxygen atom of the deprotonated phenolic OH-group, the azomethine nitrogen atom and the sulfur atom after deprotonation of the thiosemicarbazide. This was confirmed by IR spectra: shift of azomethine stretching to lower frequencies, shift of C-O(H) vibration to higher frequency and disappearance of the vibration of C=S double bond in the spectra of complexes (El-Bahnasawy et al., 2014).

In order to determine the mode of coordination the most significant infrared spectral frequencies for the metal complexes are compared with the free ligands. A band observed at 1616, 1611 and 1611 cm⁻¹ due to the azomethine C=N stretching frequency of the free ligands

HL1, HL2 and HL3 respectively was shifted to lower frequency in the spectra of the complexes at 1586 – 1605 cm⁻¹ indicating the coordination through N atom. Deprotonated phenolic oxygen – strong absorption band in spectra of ligand positioned at 1261 – 1269 cm⁻¹ after coordination is shifted to 1278 – 1280 cm⁻¹ (Baiu et al., 2009), which corresponds to forming of weaker C-O(Ru) bond comparing to C-O(H) and confirms coordination of ligands to Ru(III) *via* deprotonated phenolic oxygen.

Also, in the IR spectra of ligands, HL1, HL2 and HL3, the characteristic vibration of the (OH) band is observed at 3444, 3410, 3454 cm⁻¹, respectively. The absence of this band in the IR spectra of the complexes indicates the coordination through the phenolic oxygen (Vojinović-Ješić et al., 2011). The ligands showed band at 777 cm⁻¹ for HL1, HL2 and HL2 for the vibration of the C=S double bond (Wiles et al., 1967; Thangadurai et al., 2001). The C=S band was disappeared in the complexes (Al-Amiery et al., 2011) and a new band, C-S appeared at 723–743 cm⁻¹. This confirms that the other coordination site to ruthenium is through thiolate sulphur (Sampath et al., 2016). The appearance of bands in the spectra complexes, Na[Ru(LH1)₂], Na[Ru(LH2)₂] and Na[Ru(LH3)₂] at 1636, 1634, 1629 and 1616, 1588, 1599 cm⁻¹ due to C=N-N=C (Bharti et al., 2013) and new C=N bond, respectively, also indicates that Ru is bonded through thiol sulphur (El Bahnasawy et al., 2014). The medium intensity band in the region 544 – 587 cm⁻¹ is attributed to Ru-N, in the region 484 – 509 cm⁻¹ is attributed to Ru-O, and in the region 438 – 448 cm⁻¹ is attributed to Ru-S bonds (Bahnasawy et al., 2014).

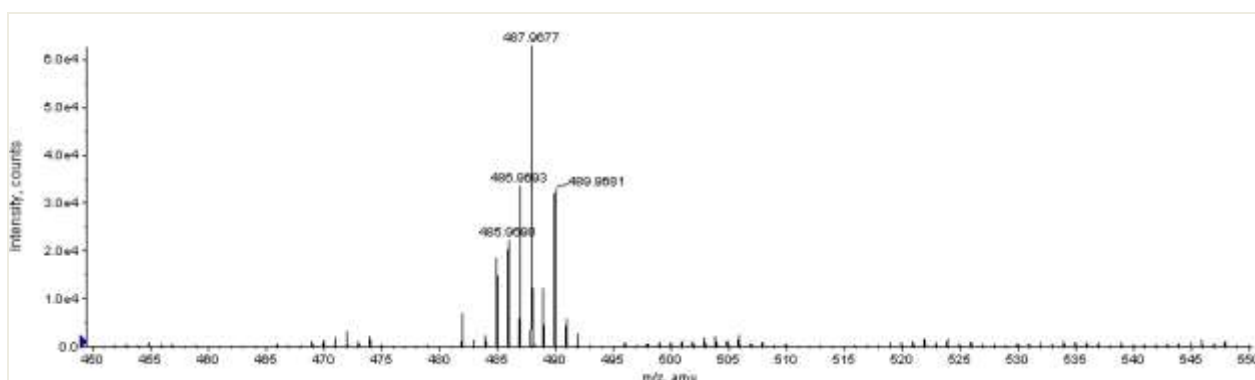
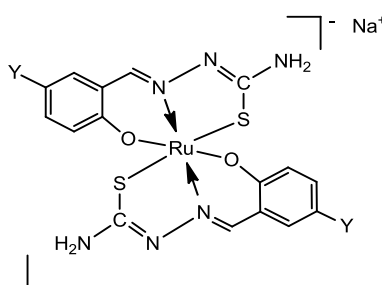
Figure 3. Mass spectrum of Na[Ru(HL1)₂]

Figure 4. Proposed structure for the complexes

Table 1: ESI ToF MS data for molecular ions of compounds

Complex	Molecular ion	Ion Mass	Measured Mass	Error (mDa)	Error (ppm)
Na[Ru(HL1) ₂]	[C ₁₆ H ₁₄ N ₆ O ₂ S ₂ Ru] ⁻	487.96686	487.96770	-1.18976	-2.44
Na[Ru(HL2) ₂]	[C ₁₆ H ₁₂ N ₆ O ₂ S ₂ Cl ₂ Ru] ⁻	555.88892	555.88615	-2.76566	-4.98
Na[Ru(HL3) ₂]	[C ₁₆ H ₁₂ N ₆ O ₂ S ₂ Br ₂ Ru] ⁻	643.78789	643.78526	-2.63104	-4.09

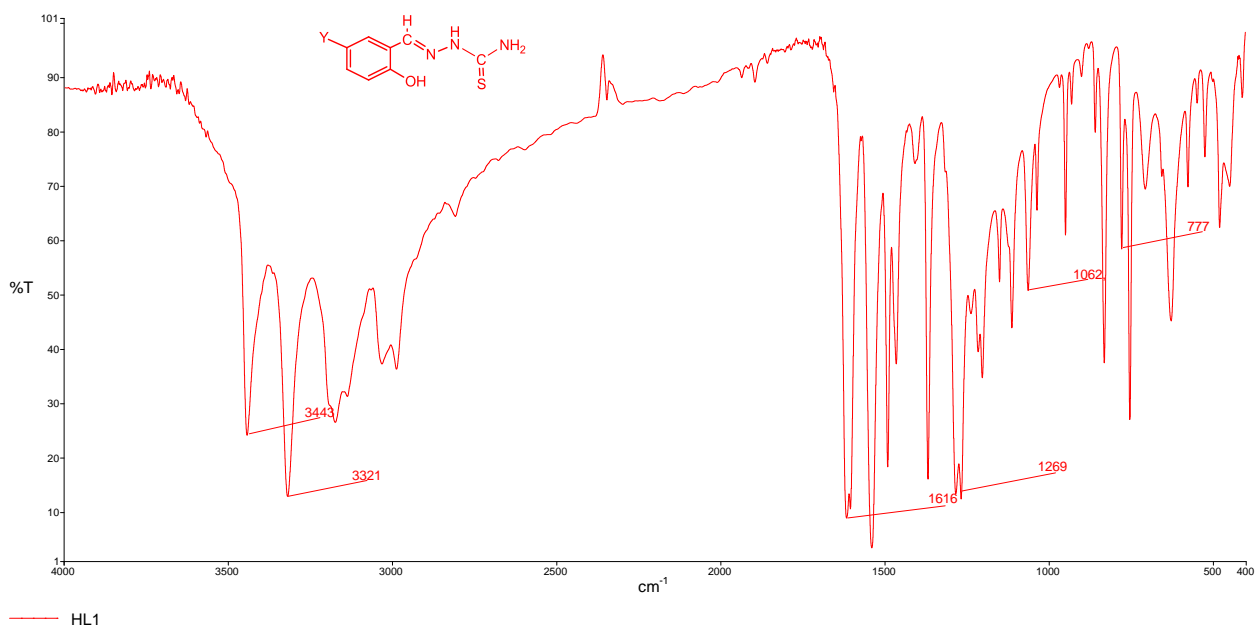


Figure 5. FT IR spectrum of ligand HL1

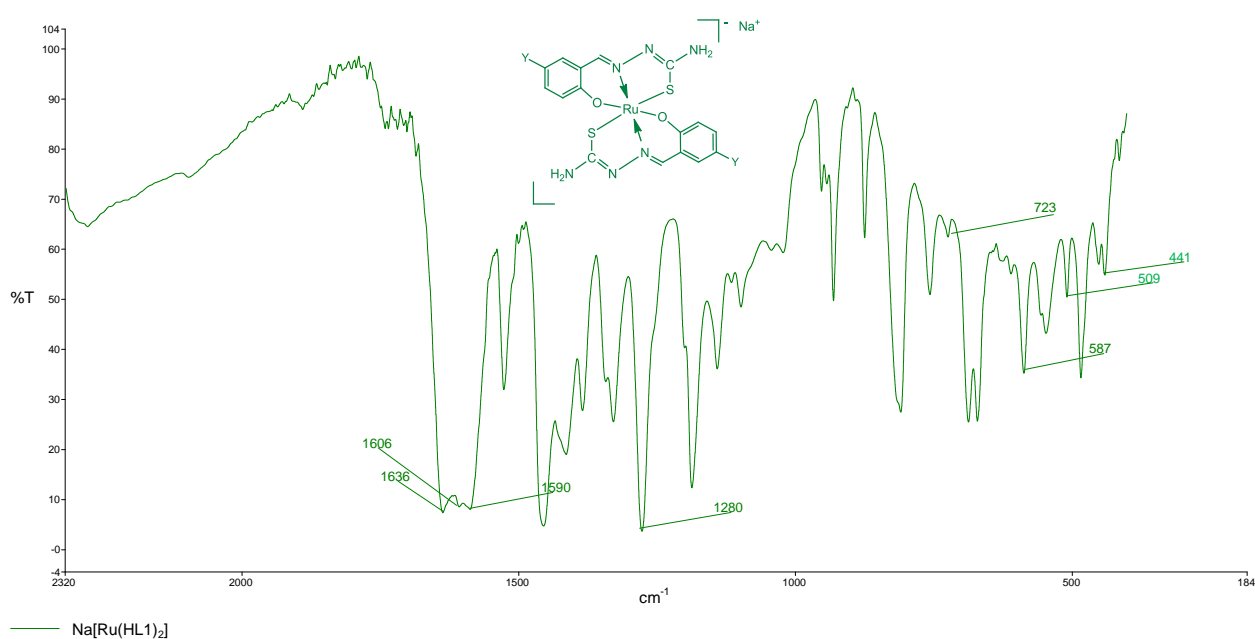
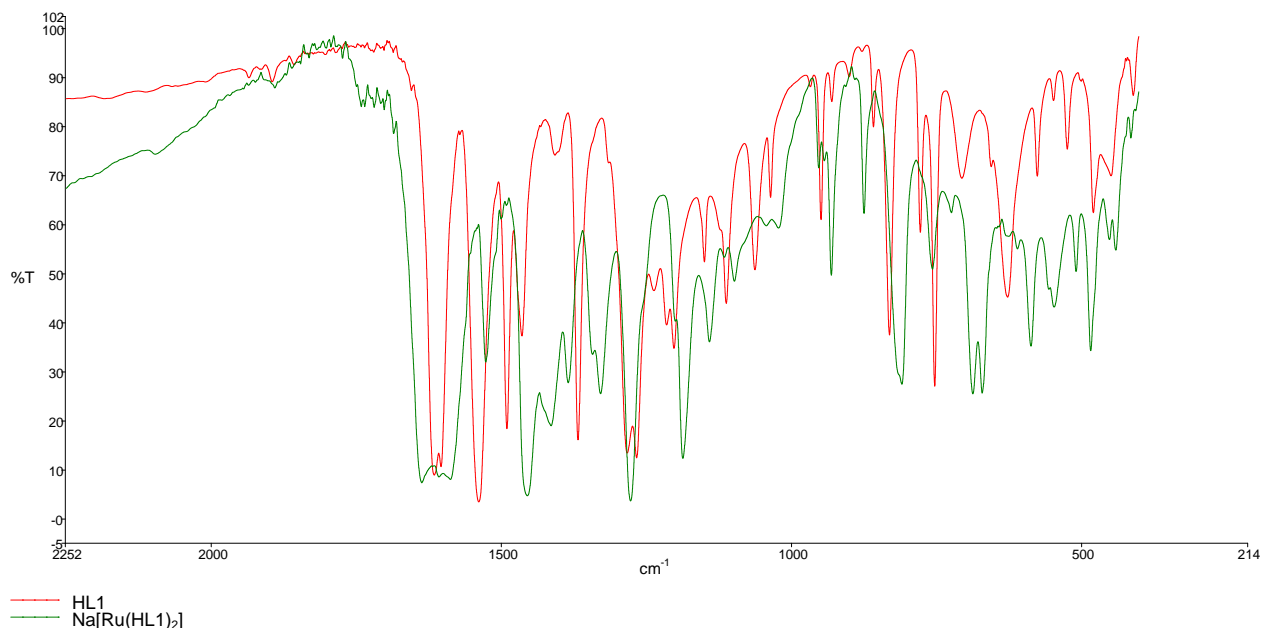
Figure 6. FT IR spectrum of complex Na[Ru(HL1)₂]

Table 2: Characteristic vibrations of ligands and complexes

Ligand/complex	$\nu(\text{C}=\text{N})$, cm^{-1}	$\nu(\text{C}-\text{O})$, cm^{-1}	$\nu(\text{C}=\text{S})$, cm^{-1}	$\nu(\text{C}-\text{S})$, cm^{-1}	$\nu(\text{Ru}-\text{N})$, cm^{-1}	$\nu(\text{Ru}-\text{O})$, cm^{-1}	$\nu(\text{Ru}-\text{S})$, cm^{-1}
HL1	1616	1269	777	-	-	-	-
Na[Ru(HL1) ₂]	1606	1280	-	723	587	509	441
HL2	1611	1266	777	-	-	-	-
Na[Ru(HL2) ₂]	1589	1280	-	723	547	484	438
HL3	1611	1261	777	-	-	-	-
Na[Ru(HL3) ₂]	1595	1278	-	743	544	506	438

Figure 7. Comparative FT IR spectra of ligands HL1 and complex Na[Ru(HL1)₂]

CONCLUSION

Three ruthenium(III) complexes of the type Na[RuL₂] (where L = dibasic tridentate thiosemicarbazone ligand), have been synthesized. Complexes have been synthesized and characterized by mass spectrometry and infrared spectroscopy. The data showed the formation of a complex with a 1:2 metal:ligand stoichiometries. The ligands coordinated as an ONS tridentate dianion through the oxygen atom of the deprotonated phenolic OH-group, the azomethine nitrogen atom and the thiolate sulfur atom after deprotonation of the thiosemicarbazide. ESI ToF mass spectrometry confirmed existence of [C₁₆H₁₄N₆O₂S₂Ru]⁻, [C₁₆H₁₂N₆O₂S₂Cl₂Ru]⁻ and [C₁₆H₁₂N₆O₂S₂Br₂Ru]⁻ ions with *m/z* values at 487.96567, 555.88615 and 643.78526, respectively.

REFERENCES

- Al-Amiery A. A., Al-Majedy Y.K., Abdulreazak H. and Abood H. (2011). Synthesis, Characterization, Theoretical Crystal Structure, and Antibacterial Activities of Some Transition Metal Complexes of the Thiosemicarbazone (Z)-2-(pyrrolidin-2-ylidene)hydrazinecarbothioamide. *Bioinorganic Chemistry and Applications*, 2011: 1-6.
- Al-Amiery A. A., Kadhum A.A.H., Abdulreazak H. and Mohamad A.B. (2012). Antifungal and Antioxidant Activities of Pyrrolidone Thiosemicarbazone Complexes. *Bioinorganic Chemistry and Applications*, 2012: 1-6.
- Bharti J., Meena V. And Suman M. (2013). Synthesis and characterization of Mixed Ligand Complexes of salicylaldehyde Thiosemicarbazone and Pyridine with Iron and Cobalt. *Asian Journal of Biochemical and Pharmaceutical Research*, 4(3), 91-96.
- Baiu S.H., El-Ajaily M.M. and El-Barasi. (2009). Antibacterial Activity of Schiff Base Chelates of Divalent Metal Ions. *Asian Journal of Chemistry*. 21(1), 5-10.
- Chandra S., Raizada S. and Sadwal S. (2014). Synthesis And Characterization Of Cr(III) Complexes With Thiosemicarbazone And Semicarbazone Based Ligands. *International Journal of Advanced Engineering Research and Technology*. ISSN: 2348–8190; 115-118.
- Chil J. (2013). Synthesis, characterization, DNA binding and cleavage activity of ruthenium(II) complexes with heterocyclic substituted thiosemicarbazones. *Journal Chilean Chemical Society*. 58(1):1-11.

- Datta S., Drew M. G. B. and Bhattacharya S. (2011). Synthesis, structure and electrochemical properties of some thiosemicarbazone complexes of ruthenium. *Indian Journal of Chemistry*, 50A, 1403-1409.
- El-Bahnasawy R. M., Sharaf El-Deen L. M., El-Table A. S., Wahba M. A. and El-Monsef. A. (2014). Electrical Conductivity Of Salicylaldehyde Thiosemicarbazone and its Pd(II), Cu(II) and Ru(III) Complexes. *Eur. Chem. Bull*, 3(5), 441-446.
- Kumar S. and Kumar N. (2013). Synthesis, Characterization and Antimicrobial Studies on Some Transition Metal Complexes of Thiosemicarbazone, *International Journal of Research in Pharmaceutical and Biomedical Sciences*, 4(1), 305-311.
- Leovac V. M, Petrović A.F. (1983). Synthesis, structure and spectra of ammonium (2,4-dihydroxybenzaldehyde S-methylthiosemicarbazonato) dioxovanadate (V). *Transition Metal Chemistry*. 8(6), 337-40.
- Ngan N. K, Wong C. S, Mun Lo K.(2011). Synthesis and Crystal Structures of Dioxomolybdenum (VI) Complex with ONS Donor Ligands. *J.Chem Crystalogr.* 41,1700-1706.
- Pahontu E., Fala V., Gulea A., Poirier D., Tapcov V., Rosu T. (2013). Synthesis and characterization of some new Cu (II), Ni (II) and Zn (II) complexes with salicylidene thiosemicarbazones: antibacterial, antifungal and in vitro antileukemia activity. *Molecules*. 18(8), 8812-8836.
- Rana A., Dinda R., Parbati, Parbati S., Ghosh S. and Falvello L. R. (2002). Synthesis, Characterisation and crystal structure of cis-dioxomolybdenum(VI) complexes of some potentially pentadentate but functionally tridentate (ONS) donor ligands. *Polyhedron*. 21 (2002), 1023- 1030.
- Sampath K. and Jayabalakrishnan C. (2016). Ruthenium(III) Thiosemicarbazone Complexes: Synthesis, Characterization, DNA Binding, Antibacterial, In vitro Anticancer and Antioxidant Studies. *DJ Journal of Engineering Chemistry and Fuel*, 1(1), 40-53.
- Thangadurai T.D. and Natarajan K. (2001). Tridentate Schiff base complexes of ruthenium(III) containing ONS/ONO donor atoms and their biocidal activities. *Transition Metal Chemistry*, 26, 717-722
- Vojinović-Ješić LJ. S., Leovac V. M., Lalović M. M., Češljević V.I., Jovanović Lj. S., Rodić M. V. and Divjaković V. (2011). Transition metal complexes with thiosemicarbazide-based ligands. Part 58. Synthesis, spectral and structural characterization of dioxovanadium(V) complexes with salicyl aldehyde thiosemicarbazone, *J. Serb. Chem. Soc.* 76 (6), 865–877.
- Wiles D.M., Gingras BA, Suprunchuk T. (1967). The C=S stretching vibration in the infrared spectra of some thiosemicarbazones. *Canadian Journal of Chemistry*, 45(5), 469-473.

Summary/Sažetak

Sintetizirana su tri Ru(III) kompleksa opšte formule $\text{Na}[\text{RuL}_2]$ (L = dibazni tridentatni tiosemikarbazon ligand), reakcijom RuCl_3 sa ONS donorskim ligandima na bazi tiosemikarbazona. Ligandi opšte formule (X)N-NH-C(S)-NH₂ pripremljeni su reakcijom kondenzacije salicilaldehida i njegovih derivata (X = salicilaldehid, 5-Cl-salicilaldehid, 5-Br-salicilaldehid) sa tiosemikarbazidom. Kompleksi su formulisani i karakterizirani ESI ToF masenom spektrometrijom i infracrvenom spektroskopijom. Podaci pokazuju formiranje kompleksa sa 1:2 metal:ligand stehiometrijom. Ligandi su koordinirani kao ONS tridentatni dianioni preko atoma kisika deprotonizirane OH-grupe, azometinskog atoma azota i atoma sumpora nakon deprotonizacije ostatka tiosemikarbazida u njegovom tiolnom obliku.

Calcium Analysis in Bones During Aging Process

Sapcanin, A.^{a,*}, Sofic, E.^{a,b}

^aFaculty of Pharmacy, University of Sarajevo, Bosnia and Herzegovina

^bFaculty of Science, University of Sarajevo, Bosnia and Herzegovina

Article info

Received: 27/10/2016

Accepted: 06/12/2016

Keywords:

calcium ion-selective electrode
atomic absorption spectrophotometry (AAS)
resorption
aging
bones

*Corresponding author:

E-mail: ida@bih.net.ba

Phone: 00-387-33-586187

Fax: 00-000-00-0000000

Abstract: The resorption process in bone organ culture can be measured and evaluated by only measuring the calcium concentration in the medium with calcium ion-selective electrode. Reliable and consistent calcium resorption from bone using 500 ng/ml prostaglandine E₂ or 250 ng/ml human parathyroid hormone (1-34) have occurred. The results, thus, indicate that calcium can be considered as an independent index of bone resorption. Our preliminary measurements by atomic absorption spectrophotometry (AAS), although statistically unrepresentative the sample – group being 9 babies and 9 adults, point to such conclusion. Bones were taken postmortem or post operationem. Calcium concentration measured by AAS was at range of about 260 mg Ca/ mg ash in the human baby bones (costae) and of about 430 mg Ca/mg ash in the human adults bones (femur). Calcium amount measured also in the calvaria of five-day old mice ICR strain by AAS. Values were at range of about 45 mg Ca/mg ash. AAS is a reference method for calcium determination in human bones, however for simplification it is more appropriate to use calcium ion-selective electrode.

INTRODUCTION

Bone is a specialized connective tissue that together with cartilage makes up the skeletal system. These tissues serve three functions: a) mechanical support and site of muscle attachment for locomotion; b) protective: for vital organs and bone marrow, and c) metabolic: reserve of ions for the entire organism, especially calcium and phosphate. It is also a composite structure, consisting of inorganic mineral crystals an extracellular organic matrix, cells, lipids and waters. The mineral crystals are analogous to the geologic mineral hydroxyapatite (Boskey and Coleman, 2010). The cells which produce, nurture and remodel the mineralized extracellular matrix, also respond to mechanical and other signals, which determine the properties (morphology and function) of the bone (Boskey and Coleman, 2010).

Bone remodelling is a complex process which involves a number of cellular functions directed toward the coordinated resorption and formation of new bone (Ronchetti et al., 1996; Goldhaber, 1997; Jin et al., 2000). Catabolic agents (prostaglandine E₂ (PGE₂) and human parathyroid hormone (h-PTH) fraction 1-34) or anabolic agents (ascorbic acid (AA) and bone morphogenetic protein 4 (BMP4) could stimulate bone resorption or bone

formation directly in a bone organ-culture (Dempster et al., 1993; Goldhaber, 1997; Sampath Kuber, 1999).

The main objective of the current research proposal is to establish calcium as an independent index for observing bone resorption and bone formation processes, which are age dependant.

EXPERIMENTAL

Bone organ-culture system

Calvaria of five-day old mice ICR strain, were dissected aseptically to encompass part of the frontal bone and most of both parietal bones. Dulbecco's Modified Eagle's Medium containing glucose, glutamine, bovine serum albumin, fraction V, penicillin and streptomycin, were added to each bone culture tube. This medium was serum free. Catabolic or anabolic agents were included in the medium. The bone culture tubes were incubated in a roller apparatus for 7 or 14 days at 37⁰ C and oxygenated with 50% O₂, 5% CO₂ and 45% N₂. The media were changed every 2-3 days, and after each change of media the used medium from each bone culture tube was analyzed individually for calcium release from the bone into the medium. Bones were

fixed with formalin and processed for histological examination when the experiment was terminated.

Calcium determination

A Varian spektra AA-10 Atomic Absorption Spectrophotometer for calcium determination in human bones was used. The calcium determination was carried out at the 422 nm line; the light source was a hollow cathode lamp. Weighed bone ash samples were hydrolyzed in 6 M HCl. Used media from the bone organ – cultures were analyzed individually for calcium content using Nova Biomedical Calcium Analyzer, Model 7- Ca^{2+} ion selective electrode (Nova Biochemical, Waltham, MA) according to the instructions of the manufacturer (Yoon *et al.*, 2000). The amount of calcium measured from the bone organ-culture medium after PGE_2 or h-PTH fraction 1-34 was included in the medium.

Analysis of hydroxyproline

Bones without fixing with formalin were hydrolyzed and analyzed for hydroxyproline, using HPLC with fluorescence detection -Pico Tag method -Waters Division of Millipore (Feste, 1992).

Statistical analysis of data

All data were subjected to a one-way analysis of variance (ANOVA) using Fisher's LSD test.

RESULTS AND DISCUSSION

This work is performed to show that calcium analysis is useful for observation and definition of complex biochemical and morphological processes of bone resorption and bone formation. The biological processes of human growth and ageing were reflected in the amounts of calcium in the bones (Boskey and Coleman, 2010)..

Our preliminary measurements by atomic absorption spectrophotometry (AAS), although statistically unrepresentative the sample-group being 9 babies and 9 adults, points to such conclusion. Calcium concentration measured by AAS was in a range of approximately 260 $\mu\text{g Ca} / \text{mg ash}$ in the human baby bones and of approximately 430 $\mu\text{g Ca} / \text{mg ash}$ in the human adults bones. Amounts of calcium were also measured in the calvaria of five-day old mice ICR strain by AAS. The values were in the range of approximately 45 $\mu\text{g Ca} / \text{mg calvaria}$.

Before proceeding with experiments designed to test the agents in our "remodelling system" (Goldhaber, 1997) it was necessary to establish a bone organ culture system that would respond reliably and consistently to bone resorption stimulating agents, such PGE_2 or h-PTH fraction 1-34, so that differences in the amount of resorption could be determined more quantitatively by measuring the amount of calcium released into the medium when the "used" medium was replaced with fresh medium and at the time when the experiment was terminated. Therefore, during the 7-day culture period, therefore, calcium analysis of "used" media was done three times, on day 2 or 3, day 5 and day 7.

From Figure 1. it may be seen that control bones (lacking PGE_2 in the medium) showed little, if any, resorption on gross examination after 7 days in culture. On the other hand, when PGE_2 (500 ng/ml) was added to the culture medium, gross resorption, distortion, and collapse of the

calvaria occurred (Figure 2.). Similar experiments with different concentrations of PTH revealed that 250 ng/ml of h-PTH gave an adequate bone resorption response.



Figure 1. Control group. Picture of calvaria after 7 days of culture. Note intact calvaria



Figure 2. Experimental group. PGE_2 was added as a bone resorption stimulating agent. Note bone resorption

Addition of 500 ng/ml PGE_2 into the medium resulted in increased calcium release and was statistically significant ($P < 0.01$) Figure 3. We observed that calcium release did not occur in the control bones group and group with addition of AA 150 $\mu\text{g/ml}$. Inhibition of increased calcium release occurred when AA was added into the medium with PGE_2 .

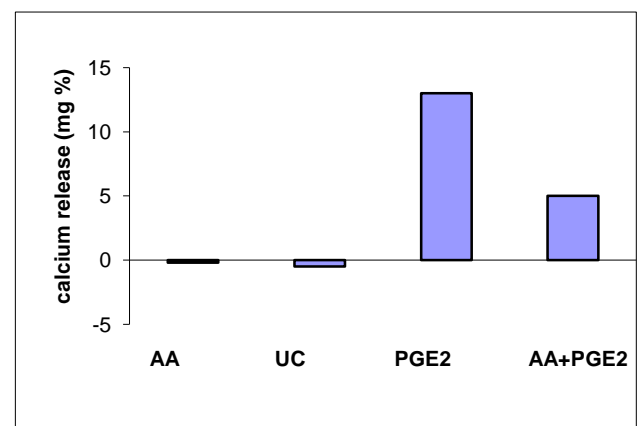


Figure 3. Effect of AA, PGE_2 and combination on calcium release from the bone into the medium, during 7 day culture period. UC -untreated controls; AA -group treated with AA 150 $\mu\text{g/ml}$; PGE_2 -group treated with PGE_2 500 ng/ml; AA + PGE_2 – group treated with combination of AA 150 $\mu\text{g/ml}$ and PGE_2 500 ng/ml; ** $P < 0.01$ (ANOVA)

The addition of AA leads to good new osteoid formation during the culture period.

Biogravimetry of calvaria treated with AA 150µg/ml showed significant increase of calvarial weight (about 50 %) Figure 4.

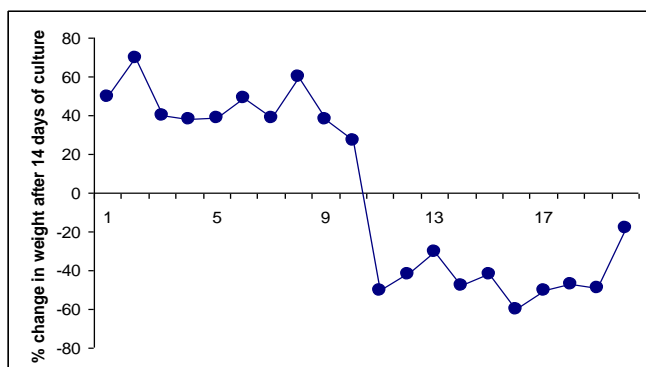


Figure 4. Effect of AA on the weight change of calvaria after 14 day culture period.

150µg/ml AA was added into the medium to stimulate bone formation and biosynthesis of collagen. HPLC analysis of hydroxyproline ("biomarker" for collagen synthesis) approved process of accelerated collagen synthesis and significant increase of hydroxyproline amount compared with untreated control bones (Figure 5.).

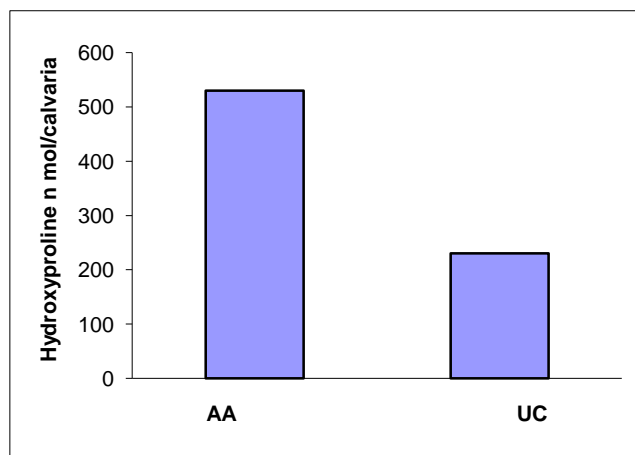


Figure 5. Effect of AA on hydroxyproline amount.
AA – calvaria treated with AA 150µg/ml; UC –untreated controls after 7 day culture period.

The completed experiments confirmed calcium as an independent index of bone resorption and also, as an important parameter in the estimation of bone formation.

CONCLUSION

1. Only with a large number of bone samples would it be possible to draw extrapolation curves reflecting the relationship between the presentation bones calcium amount and human age using AAS.

2. Reliable and consistent calcium resorption from bone using 500 ng /ml PGE₂ or 250 ng /ml h-PTH (1-34) have occurred. The results, thus, indicate that calcium can be considered as an independent index of bone resorption.

3. Reliable and consistent bone formation in bone organ culture using ascorbic acid 150 µg /ml or after addition 50 ng /ml of bone morphogenetic protein 4 have been stimulated. Both substances stimulate osteogenesis. In this case, increased calcium release into medium did not occur.

4. The resorption process in bone organ-culture can be measured and evaluated only by measuring the calcium concentration amount in the medium by calcium ion-selective electrode. Further analysis (for example, histological) is not required.

5. Measuring of calcium release from the bone into the medium using a calcium ion-selective electrode is insufficient for evaluation of bone formation process. Analysis of hydroxyproline by HPLC with fluorescence detection and histological examination of osteoides are necessary.

6. AAS is a reference method for calcium determination in human bones, however for simplification it is more appropriate to use calcium ion-selective electrode.

REFERENCES

- Boskey, A., L., Coleman, R. (2010). Aging and Bone. *J. Dent. Res.*, 89, (12), 1333-1348.
- Dempster, D., W., Cosman, F., Parisien, M., Shen, V., Lindsay, R. (1993). Anabolic actions of parathyroid hormone on bone. *Endocr. Rev.*, 14, (16), 690-709.
- Feste, A., S. (1992). Reversed-phase chromatography of phenylthiocarbonyl amino acids: an evaluation and a comparison with analysis by ion-exchange chromatography. *J. Chromatogr.*, 574,(1), 23-34.
- Goldhaber, P. (1997). Spying on the osteoclast before, during and after bone resorption in tissue culture: In Davidovitch Z, Mah J (ed) *Biological Mechanisms of Tooth Eruption and Replacement by Implants*. Harvard Society for the advancement of Orthodontics, Boston, MA, USA, pp 199-211.
- Jin, L., Briggs, S., Chandrasekhar, S., Chirgadze, N., Clawson, D., Schevitz, R., Smiley, D., Tashjian, A., Zhang, F. (2000). Crystal structure of Human Parathyroid Hormone 1-34 at 0,9-A Resolution. *J. Biol. Chem.*, 275, (35), 27238-27244.
- Ronchetti, I., Quaglino, D., Bergamini, G. (1996). Ascorbic acid and connective tissue. In Robin Haris (ed) *Biochemistry and Biomedical Cell Biology*, vol 25. Subcellular Biochemistry. Plenum press, New York, pp 249-259.
- Sampath, Kuber, T. (1999). Biology of Bone Morphogenetic Proteins - An Overview. *Bone*, 24, (4), 409-431.
- Yoon, H.,J., Shin, J.,H., Lee, S.,D., Nam, H., Cha, G.,S., Strong, T.,D., Brown, R.,B. (2000). Solid-state ion sensors with liquid junction-free polymer membrane-based reference electrode for blood analysis. *Sensors and Actuators.*, B 64, 8-14.

Summary/Sažetak

Resorpcijski proces u organ kulturi kosti može se mjeriti i evaluirati mjerenjem koncentracije kalcija u mediju kalcijevom jon selektivnom elektrodom. Upotreba 500 ng/ml prostaglandina E2 ili 250 ng/ml humanog paratiroidnog hormona (1-34) ostvaruje pouzdan i konzistentan resorpcijski proces. Stoga rezultati indiciraju da kalcij služi kao neovisni indikator koštane resorpcije. Naša preliminarna mjerenja atomskom apsorpcionom spektrofotometrijom (AAS), statistički nereprezentativnih uzoraka od 9 beba i 9 odraslih poentiraju takav zaključak. Kosti su uzete postmortem ili post operationem. Koncentracija kalcija mjerena AAS kretala se od 260 mg Ca/ mg pepela u humanim bebi kostima (costae) do 430 mg Ca/mg pepela u humanim kostima odraslih (femur). Količina kalcija mjerena je AAS takođe i u kalvariji 5 dana starog miša ICR vrste. Vrijednosti su se kretale oko 45 mg Ca/mg pepela. AAS je referentna metoda za mjerenje koncentracije kalcija u humanim kostima, iako je radi pojednostavljenja prikladnija upotreba kalcijeve jon selektivne elektrode.

Spectroscopic Investigations of Co(II) and Cu(II) Interaction with Imatinib Mesylate and Capecitabine

Cipurković A.^a, Horozić E.^a, Crnkić A.^a, Marić S.^a, Ljubijankić N.^b

^aDepartment of Chemistry, Faculty of Science, University of Tuzla, Univerzitetska 4, 75 000 Tuzla, B&H

^bDepartment of Chemistry, Faculty of Science, University of Sarajevo, Zmaja od Bosne 33-35, 71000 Sarajevo, B&H

Article info

Received: 15/11/2016
Accepted: 18/12/2016

Keywords:

Copper,
Cobalt,
FTIR,
UV spectroscopy,
Microscopic analysis

*Corresponding author:

Amira Cipurković
E-mail: amira.cipurkovic@untz.ba
Phone: + 387 35 320 753

Abstract: Cobalt and copper are present as trace elements in biological systems and they are very important for the activity of many enzymes with different functions in the body. Their biological functions derive from the possibility of potential interaction of their M(II) ions with O, N and S donor atoms of various ligands and biomolecules in the living organism. Capecitabine and imatinib mesylate (ImM) are synthetic organic compounds which are used in a treatment of some oncological diseases thus disturbing homeostasis of biological system. In this study, UV and FTIR spectroscopic methods are used to investigate metalligand interactions and products of their interaction at physiological conditions using model test systems. FTIR spectrum of Co(II)-capecitabine model systems show lack of absorption bands characteristic for -OH (at 3230 cm⁻¹) and C=O groups positioned at pyrimidine cycle (at 1718 cm⁻¹) for pure capecitabine. It indicates interaction of Co(II) ion with capecitabine via O-donor atoms. FTIR spectrum of pure ImM deviates from spectrum of Co(II)-ImM system at 1250-1050 cm⁻¹ wavelength region. This region corresponds to peaks characteristic for mesylate ions (O₃S-CH₃), which indicates on interaction between Co(II) and donor atoms containing molecule ligands (O and/or S). UV results for model systems of M(II) with capecitabine and ImM show similar absorption bands as those of pure ligand, while absorbances are different (except for Cu(II)-ImM). Since these investigations are done at approximately at physiological conditions, it is expected that, after application of these ligands as pharmacological agents, the same interactions are happening in the human body.

INTRODUCTION

Cobalt and copper are present as trace elements in biological systems and are very important for the activity of many enzymes with different functions in human body. Biological functions of these metal ions derive from possible interaction of Co(II) and Cu(II) ions with O, N and S donor atoms of various ligands and biomolecules in human organism. (Krstić et al., 2015). Capecitabine (CPC) is an orally-administered chemotherapeutic agent used in the treatment of metastatic breast, stomach, pancreas and colorectal cancers (Kathiravan and Pandey, 2014). CPC (5-deoxy-5-fluoro-N-[(pentylloxy)carbonyl]-

cytidine), is fluoropyrimidine carbamate pro-drug of 5-fluorouracil (5-FU) and its absorption is higher than 5-FU (Kandimalla and Nagavalli, 2012; Sunkara et al., 2013). Structure of CPC is presented at Figure 1.

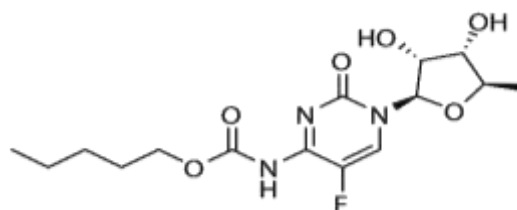


Figure 1. Structure of Capecitabine

Imatinib mesylate (ImM) is a tyrosine kinase inhibitor, that was found to be one of the most recent drugs used for the treatment of chronic myeloid leukemia and gastrointestinal stromal tumor (Zaharieva *et al.*, 2013). Structure of ImM is presented at Figure 2.

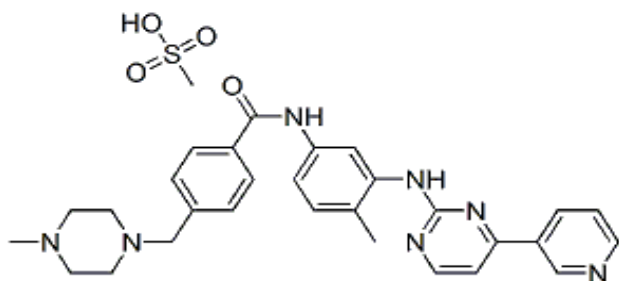


Figure 2. Structure of Imatinib Mesylate

Complexes of Cu(II) and Co(II) with these reagents were synthesized and characterized.

EXPERIMENTAL

Materials and methods

Modeling System for UV spectroscopy: In the case of testing interactions of M(II) ions with natural and synthetic ligands, distilled water and ethanol-water solutions were used as solvents in ratios between 50/50 and 80/20 (v/v.) Concentrations of metal and ligand solutions were in order of 10^{-6} molL⁻¹. After stirring samples in 1: 1 volume ratio, the same have being left to stand for about one hour. After that, absorption spectra of prepared solutions were recorded on Perkin Elmer λ 25 UV/Vis spectrophotometer, in the wavelength region of 200-400 nm at room temperature ($T = 25^\circ\text{C}$) in the quartz cuvette, the optical path length $l = 1.0$ cm, with deuterium lamp as a source of light. Measurements were performed in the laboratory of Department of Physical Chemistry and Electrochemistry at Faculty of Technology, University of Tuzla.

Modeling System for FTIR spectroscopy: Metal and ligand were mixed in 1: 2 (n/n) molar ratio. Solution of dissolved metal (15 mL) and solution of ligand (15 mL) were mixed in a beaker and stirred with a magnetic stirrer without heating, with the appropriate adjustments of pH values in solutions. pH-values were measured on Mettler Toledo MP 220 pH-meter. In order to extract solid products of M-L interactions, stock solutions were prepared by adjusting pH values after stirring for 30 minutes and then left in a dark area for three days at room temperature. After that, if precipitation occurred*, solid phases were separated from solutions by filtration on filter paper (blue ribbon) and thereafter dried in an oven at temperatures between 40-50 °C. Isolated solid products of M-L interactions were prepared as KBr pellet to record FTIR spectra on FTIR Spectrum BX, Perkin Elmer, in wavelength region 450-4000 cm⁻¹, resolution of 2 cm⁻¹ at room temperature (in Laboratory of Faculty of Pharmacy, University of Tuzla).

* Because of the extremely small quantities of separated precipitates in the case of model systems Cu(II)-CPC and Cu(II)-ImM, the same could not be subjected to FTIR analysis.

RESULTS AND DISCUSSION

UV spectroscopic characterization

UV spectra of pure CPC and Co(II)-CPC model system are showed at Figure 3. UV spectrum of CPC shows several absorption maxima at 214, ~ 240 and 305 nm, which completely corresponds to literature data (Piórkowska, 2014). The binary system of Co(II)-CPC shows maximum peak at low absorbance values. There is hypo-chromic shift in comparison to the spectrum of pure CPC, in which the last peak (with the highest λ_{max}) is not clearly defined as in the case of pure CPC. It can be concluded that the Co(II) ions interacted with the CPC. Calculated value of energy splitting for Co(II)-CPC system is 559 kJmol⁻¹.

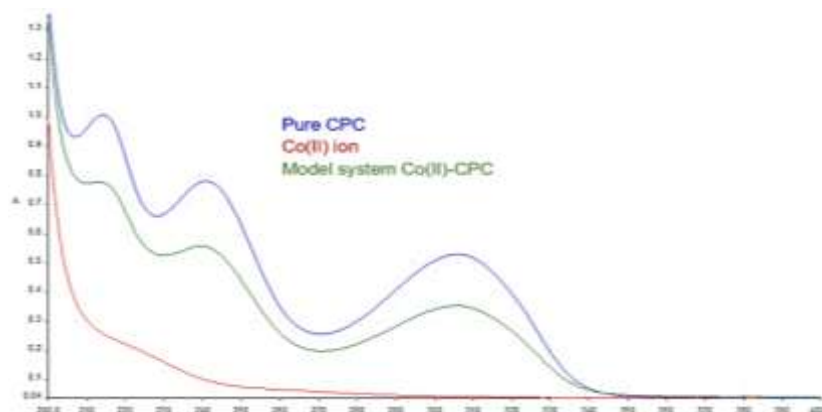


Figure 3. UV spectra of CPC and model system Co(II)-CPC

UV spectra of pure ImM and Co(II)-ImM model system are showed at Figure 4. ImM spectrum shows an absorption maximum at about 255 nm which corresponds to the literature data (Kumar Raja, 2010). The product of

interaction Co(II)-ImM gives new hypo-chromic shifted spectrum with absorption maximum slightly dislocated toward longer wavelengths at ~ 258 nm. Calculated value of energy splitting for Co(II)-ImM system is 464 kJmol^{-1} .

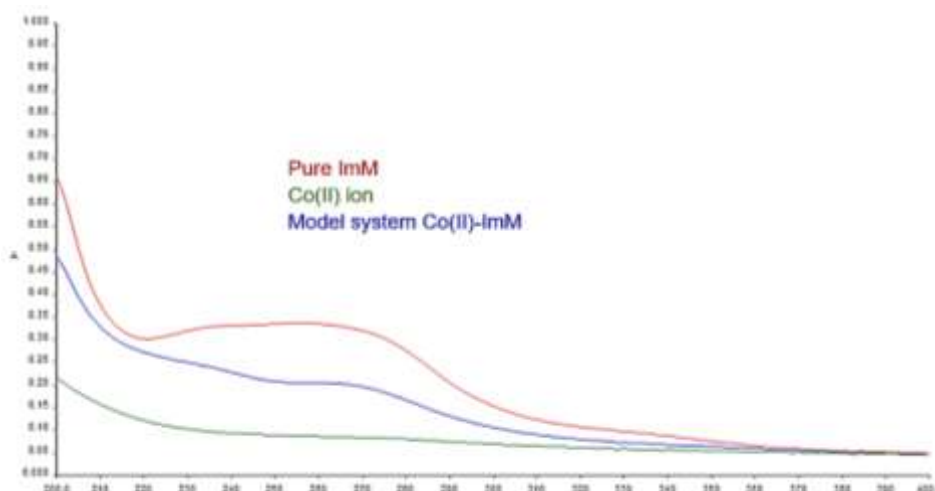


Figure 4. UV spectra of ImM and model system Co(II)-ImM

UV spectra of pure CPC and Cu(II)-CPC model system are showed at Figure 5. Spectrum of CPC and spectrum of Cu(II)-CPC binary system have very similar profiles of absorption bands, but different in the absorbance intensity. Significant absorption values for model system

Cu(II)-CPC are less comparable to that of pure CPC. Spectra of Cu(II) and Cu(II)-CPC are almost identical, but with a very small deviations of the absorbance values. The value of energy d-splitting is also 559 kJmol^{-1} .

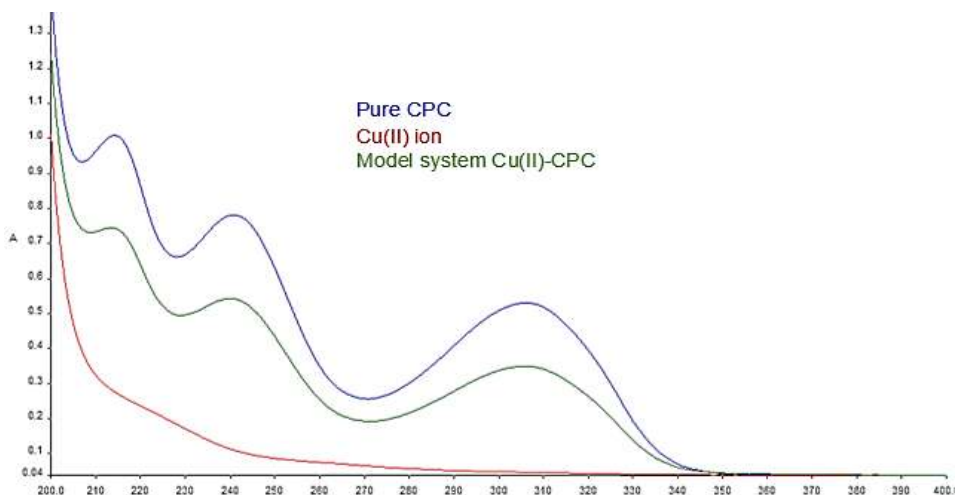


Figure 5. UV spectrum of CPC and model system Cu(II)-CPC

UV spectra of pure ImM and Cu(II)-ImM model system are showed at Figure 6. Spectrum of pure ImM and spectrum of binary system Cu(II)-ImM shows significantly different absorption bands with a positive difference from 200 to 255 nm and a negative difference from 255 to ~ 286 nm, and again positive difference to 400 nm.

Absorption band of model system shows hyper-chromic shift, with absorption maximum shifted towards smaller wavelengths. Based on the absorption maximum at about 216 nm, calculated energy splitting value is 554 kJmol^{-1}

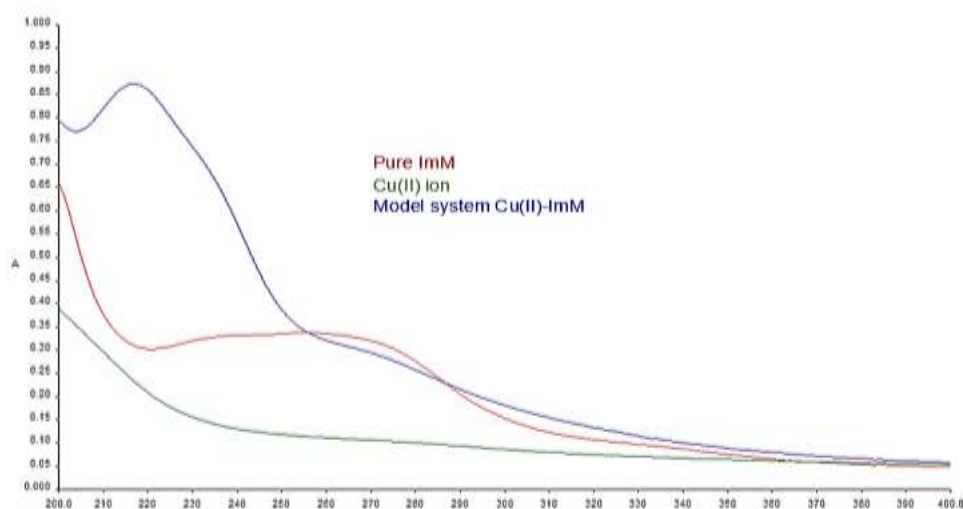


Figure 6. UV spectrum of ImM and model system Cu(II)-ImM

The spectrum of pure ImM and the spectrum of binary system Cu(II)-ImM shows significantly different absorption bands with a positive difference at 200 - 255 nm and negative difference at 255 to ~ 286 nm, and after that positive difference to 400 nm. Absorption band of the model system shows hyper-chromic shift, with the absorption maximum shifted towards smaller wavelengths. Based on the absorption maximum at about 216 nm, calculated energy splitting value is 554 kJmol^{-1} .

FTIR spectroscopic characterization

FTIR spectra of pure CPC and Co(II)-CPC model system are showed at Figure 7. Comparison of these FTIR

spectra clearly shows a number of differences which indicates on the interaction of Co(II) ion with CPC. Wide, medium sharp peak at 3230 cm^{-1} in CPC, characteristic for free -OH group is not visible at FTIR spectrum of Co(II)-CPC model system indicating on a link between oxygen atom as electron-donor and Co(II) ion. Very intense peak at 1718 cm^{-1} visible at CPC spectrum corresponds to the carbonyl group positioned on pyrimidine ring. This peak is not visible for Co(II)-CPC model system which points on the interaction between metal ion and oxygen atom, which could cause delocalization of electron pair of double bond to oxygen.

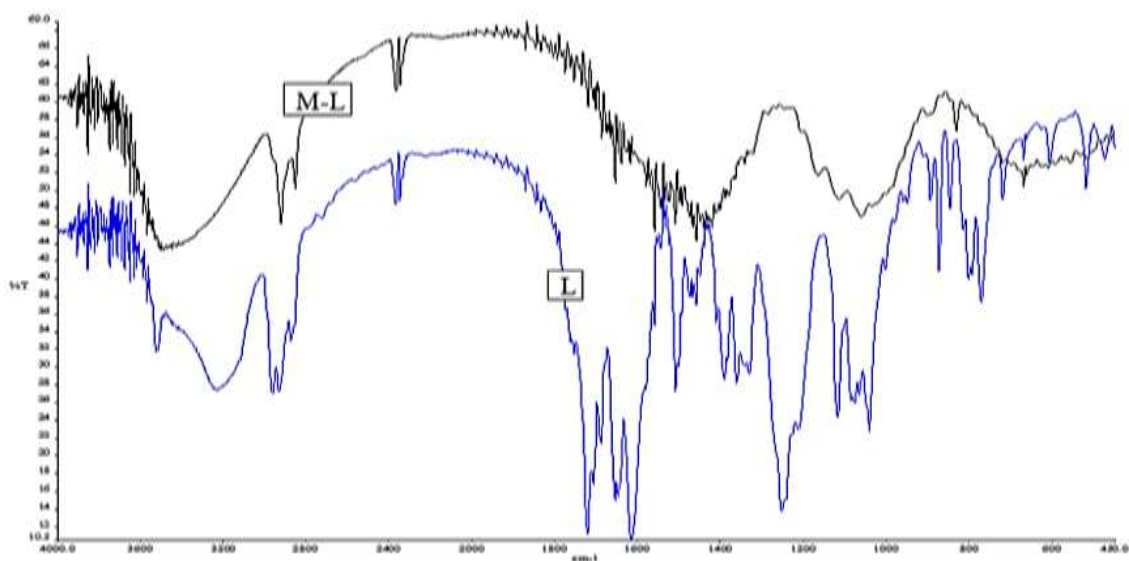


Figure 7. FTIR spectrum of pure CPC and model system Co(II)-CPC

Peaks visible at CPC spectrum at the $1000\text{-}1600 \text{ cm}^{-1}$ wavelengths range obviously change because of the interaction of Co(II) ion and ligand so the most of peaks

are lost or changed intensity (peaks of high intensity become less pronounced and stretched).

Very intensive peak at 1647 cm^{-1} which corresponds to the $\text{C}=\text{N}$ group of CPC (Sunkara, 2013) is also not visible in Co(II)-CPC system suggesting on some changes in the structure of pyrimidine ring after chemical reaction.

FTIR spectra of pure ImM and Co(II)-ImM model system are showed at Figure 8.

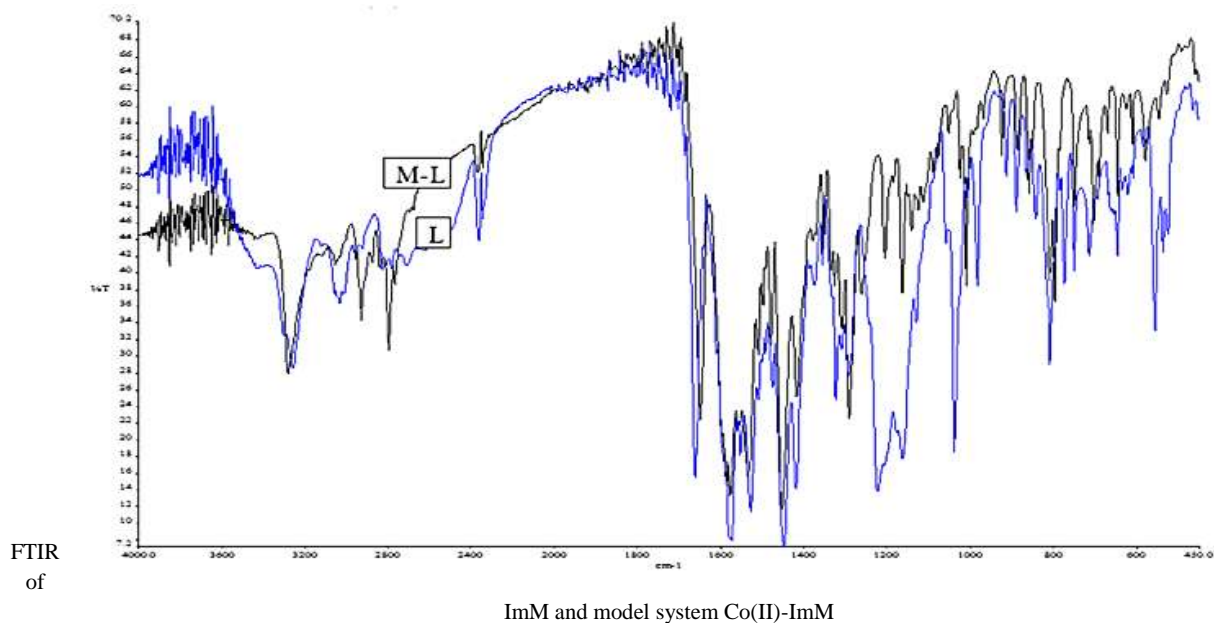


Figure 8.
spectrum pure

FTIR spectrum of pure ImM is very complicated. There is an intensive series of bands, especially at wavenumbers $<1700\text{ cm}^{-1}$. On the other hand, FTIR spectrum of model system Co(II) - ImM differs from the spectrum of pure ImM, indicating the interaction of ions with this ligand. The greatest changes in these spectra are observed in the areas of $3200\text{-}2800\text{ cm}^{-1}$ and $1300\text{-}1000\text{ cm}^{-1}$. The spectrum of pure ImM and Co(II)-ImM system at 3258 cm^{-1} is characterized by a medium intense peak of secondary amino-group. Very intense peak in the spectrum of ImM visible at about 1660 cm^{-1} which corresponds to a $\text{C}=\text{O}$ stretching vibration of amide group, is shifted toward lower values in the spectrum of complex. Several more intense peaks of pure ImM in the area of $1450\text{-}1200\text{ cm}^{-1}$ are characteristic of SO_2 groups of mesylate ion. These peaks are not clearly visible at the spectrum of model system Co(II)-ImM , which shows possible interactions of Co(II) ions with O- or S- donor atoms of mesylate ion. Aromatic amine moiety of ImM molecule shows $\text{C}-\text{N}$ vibration stretching in the area of $1342\text{-}1266\text{ cm}^{-1}$ which is caused by the increase of the force in $\text{C}-\text{N}$ connections due to the resonance in the ring.

Microscopic characterization of solid products of M-L interaction

Microscope images of pure ligands and their solid products with Co(II) -ions are showed at Figure 9.

Comparing microscopic images of ImM and the product of its interaction with Co(II) ions, it can be observed that there are differences in sizes and colors of their crystals.

Crystals of pure ImM are not clearly visible, while the product of Co(II)-ImM interaction is characterized by clearly defined crystals, predominantly pink color, which indicates the presence of Co(II) ions. Ligand CPC and Co(II)-CPC interaction product are of fine-grounded crystal structure, with visible differences between crystals (crystals of product are clearly visible).

CONCLUSION

The results obtained by UV and FTIR spectroscopy clearly indicated on chemical interactions between metal ions, Co(II) and Cu(II) , and investigated ligands, capecitabine and imatinib mesylate. These interactions were probably achieved via O-donor atoms of both ligands. Microscopic images confirmed the results obtained with spectroscopic methods. There are noticeable differences in sizes and colors of crystals. Biological activities and cytotoxicity of these compounds have not been thoroughly investigated yet.

REFERENCES

- Kandimalla R. and Nagavally D. (2012). Validated estimation of Capecitabine by UV-spectroscopic, RP-HPLC and HPTLC method. *International Research Journal of Pharmacy*, 3 (11), 163-166.
- Kathiravan P. and Pandey V. P. (2014). Selection of excipients for polymer coated capsule of Capecitabine through drug-excipient compatibility testing. *International Journal of PharmTech Research*, 6 (5), 1633-1639.

- Krstić N., Nikolić R., Stanković M., Nikolić N. and Đorđević D. (2015). Coordination Compounds of M(II) Biometal Ions with Acid-Type Anti-inflammatory Drugs as Ligands – A Review. *Tropical Journal of Pharmaceutical Research* February, 14 (2), 337-349.
- Kumar Raja J., Sundar V. D., Magesh A. R., Nandha Kumar S., Dhanaraju M. D. (2010). Validated spectrophotometric estimation of imatinib mesylate in pure and tablet dosage form. *International Journal of Pharmacy & Technology*, 2 (3), 490-495.
- Piórkowska E., Kaza M., Fitatiuk J., Szlaska I., Pawinski T., Rudzki P. J. (2014). Rapid and simplified HPLC-UV method with on-line wavelengths switching for determination of capecitabine in human plasma. *Pharmazie* 69, 500–505.
- Sunkara S., Sravanthi D., Maheswari K. M., Salma S. and Nalluri B.N. (2013). Development of modified release tablet dosage forms of capecitabine for better therapeutic efficacy. *Journal of Chemical and Pharmaceutical Research*, 5 (1), 320-328.
- Zaharieva M. M., Amudov G., Konstantinov S. M., Guenova M. L. (2013). Leukemia (book), Chapter 7 - *Modern Therapy of Chronic Myeloid Leukemia*. (p.p. 228-244). INTECH.

Summary/Sažetak

Kobalt i bakar su kao elementi u tragu prisutni u biološkim sistemima i veoma su značajni za aktivnost mnogih enzima sa različitim funkcijama u tijelu. Njihova biološka funkcija proističe iz potencijalne interakcije njihovih dvovalentnih iona sa O, N i S donorskim atomima različitih liganda i biomolekula u organizmu. Kapecitabin i imatinib mesilat su sintetski organski spojevi koji se koriste u tretmanu nekih onkoloških bolesti i pri tome narušavaju homeostazu biološkog sistema. U ovom radu korištene su UV i FTIR spektroskopske metode za ispitivanje metal-ligand interakcija i produkata njihove interakcije pri fiziološkim uslovima, korištenjem modelnih test sistema. FTIR spektar model sistema Co(II)-kapecitabin pokazuje izostanak apsorpcionih traka karakterističnih za -OH (na 3230 cm⁻¹) i C=O (na 1718 cm⁻¹) grupe smještene na pirimidinskom prstenu čistog kapecitabina. To ukazuje na interakciju Co(II) iona sa kapecitabinom preko O-donorskih atoma. FTIR spektar čistog ImM razlikuje se od spektra model sistema Co(II)-ImM u oblasti talasnih dužina od 1250 do 1050 cm⁻¹. Ovo područje odgovara pikovima karakterističnim za mesilatne ione (O3S-CH3), što ukazuje na interakciju između Co(II) i atoma donora koje sadrže molekule liganda (O i/ili S). UV rezultati za model sisteme M(II) sa CPC i ImM pokazuju slične apsorpcione trake kao i čisti ligandi, dok su apsorbanice različite (osim za Cu(II)-ImM). S obzirom da su ova istraživanja izvedena pri približno fiziološkim uslovima, može se očekivati da će se nakon primjene ovih liganada kao farmakoloških reagenasa iste interakcije odvijati u ljudskom tijelu.



Antimicrobial effects of garlic (*Allium sativum* L.)

Strika, I.^a, Bašić, A.^b, Halilović, N.^b

^aUniversity of Sarajevo, Faculty of Science, Department of Biology, Zmaja od Bosne 33-35, 71000 Sarajevo, Bosnia and Herzegovina

^aUniversity of Sarajevo, Faculty of Science, Department of Chemistry, Zmaja od Bosne 33-35, 71000 Sarajevo, Bosnia and Herzegovina

Article info

Received: 16/10/2016

Accepted: 12/12/2016

Keywords:

Allium sativum
antimicrobial activity
fresh local garlic

*Corresponding author:

E-mail: ilma.strika2512@gmail.com

Phone: 00-387-62-182670

Abstract: Garlic has been used as a source of food and medicine for thousands of years. Given that the garlic contains different biologically active materials and acts as an antibiotic and a fungicide, the purpose of this research was to estimate the degree of sensitivity of three different Gram-positive bacteria: *Staphylococcus aureus*, methicillin-resistant *Staphylococcus aureus* (MRSA) and *Bacillus subtilis*; two types of Gram-negative bacteria: *Escherichia coli* and *Salmonella enteritidis*; as well as the fungus *Candida albicans*. The degree of sensitivity of tested microbes with regards to the agency of fresh and thermally processed local and imported garlic was determined using the disc-diffusion method. Examined antimicrobial-test substances exhibited antibacterial effect on all tested gram-positive bacteria and gram-negative bacteria, as well as the fungistatic agency upon fungus *C. albicans*. The strongest antimicrobial effect on all tested species was exhibited by fresh local garlic. Preparates based on *A. sativum* could be introduced in clinical practice for the treatment of infections caused by *C. albicans*.

INTRODUCTION

Garlic (*Allium sativum* L.) is a plant from the family of arcs (Aliaceae). It is a herbaceous plant with height of 20-40 cm, a bulb of strong odour and pungent taste. Sulphur compounds in garlic are responsible both for its strong smell, and for its medicinal properties. The undamaged plant contains alliin (S-allyl-L-cysteine sulfoxide). Alliin is a soluble, crystal, odourless compound. It is a cysteine derivative and has antimicrobial properties. Standardized garlic powder contains 1.3% of alliin. Slight damage causes changes in alliin, which is broken down under the influence of enzymes allinase into lactic acid and 2-propenyl-sulfonic acid. This acid instantly dimerizes and builds allicin - diallyl sulfate or diallyl disulfide. Allicin was first isolated in 1940 and has been shown to have antimicrobial activity against many viruses, bacteria, fungi and parasites. Allicin produces diallyl sulfide, the most important volatile compound of garlic and gives it its characteristic smell. Garlic acts as an antibiotic, antiseptic, antitoxic, antiviral, bactericide, carminative, hipoholesterolemik, depurative, diuretic, expectorant, fungicide, hypoglycemic, hipotensiv, and stomachic. It is

used in the food and pharmaceutical industries (Agarwall, 1996). Given that garlic contains a variety of biologically active substances and at the same time acts as an antibiotic and fungicide, objectives of this study were to examine the *in vitro* antimicrobial activity of both fresh and thermally processed domestic and imported garlic onto selected representatives of Gram-positive and Gram-negative bacteria and fungus *Candida albicans*, compare the antimicrobial effectiveness of heat treated and fresh domestic and imported garlic and assess the degree of sensitivity of selected microorganisms to the effect of garlic.

MATERIALS AND METHODS

This study examined the antimicrobial activity of both fresh, and heat treated *Allium sativum* as well as the garlic of domestic origin (Kakanj) and the imported (China) garlic. The study used three Gram-positive bacteria: *Staphylococcus aureus*, methicillin-resistant *Staphylococcus aureus* (MRSA), and *Bacillus subtilis*, two Gram-negative bacteria: *Escherichia coli*, *Salmonella*

enteritidis and the fungus *Candida albicans*. The practical part of this work performed in the microbiology laboratory of Faculty of Sciences in Sarajevo. The aseptic technique applied during the research.

All experiments performed using sterile dishes and utensils. Culture medium Mueller-Hinton agar prepared for the growth of bacterial cultures used in the study, (Mueller & Hinton, 1941). For the cultivation of *Candida albicans* Sabouraud Dextrose agar was used (Sabouraud, 1892). The juice of fresh domestic and imported garlic prepared by crushing small pieces of garlic in a mortar until a thick mass. The content sieved through sterile gauze in order to obtain the juice. Juice of the heat treated domestic and imported garlic was obtained by a number of cleaned pieces of garlic placed in separate beakers and cooked at 100 °C for 5 minutes. Once the cooking was completed, such garlic was shredded in a mortar and sieved through sterile gauze. The study used method seeding on the agar plate. The degree of sensitivity of the tested bacteria and fungi *Candida albicans* activity of the garlic was determined by the disk diffusion method (Bauer et al., 1966). The sterile filter paper discs of 8 mm in diameter used and soaked in prepared juices.

After completing the procedure, the dishes carefully closed with the parafilm and left in the incubator (manufacturer Sutjeska) for 24 hours at 37 °C, after which the results recorded. After the incubation period, the zones of inhibition measured in all of the Petri dishes by using graph paper.

RESULTS AND DISCUSSION

In this research based on the measured zones of inhibition, it determined that the fresh homemade garlic manifests the best antimicrobial effect. It had the highest level of inhibition on the fungus *Candida albicans* (62 mm), while the lowest level of antimicrobial activity recorded in *Bacillus subtilis* (13mm) (Table 1). Heat-treated domestic garlic demonstrated the weakest inhibitory effect in MRSA and the fungus *Candida albicans*, wherein the zone of inhibition was 0 mm, while the other type of bacteria, both Gram-positive and Gram-negative show slightly better anti-microbial activity (Table 1.). The highest inhibitory effect recorded for *Salmonella enteritidis* (11mm).

Table 1. Results of the study on the antimicrobial effects of fresh and thermally processed domestic and imported garlic

SPECIES	Zone of inhibition (mm)			
	Fresh domestic garlic	Heat treated domestic garlic	Fresh imported garlic	Heat treated imported garlic
<i>Staphylococcus aureus</i>	31	9	9	9
MRSA	29	0	27	0
<i>Bacillus subtilis</i>	13	8	12	9
<i>Escherichia coli</i>	19	8	13	8
<i>Salmonella enteritidis</i>	15	11	11	9
<i>Candida albicans</i>	62	0	54	0

The largest zone of inhibition of 54 mm measured for *Candida albicans*, while the least antimicrobial activity demonstrated by the imported fresh garlic against the *Staphylococcus aureus* where the zone of inhibition was 9 mm (Table 1). Heat-treated imported garlic shows little or no antimicrobial effects. On MRSA and *Candida albicans*, heat-treated imported garlic showed no antimicrobial effect while the effects on the other type of bacteria, indicate a very weak activity (Table 1). In addition to the bactericidal and fungicidal activity on selected types of microbes, fresh local and imported *A. sativum* showed bacteriostatic activity, or affect their reproduction that it ends their metabolic activity. Bacteriostatic effect observed for MRSA with the best performance shown by the fresh homegrown *A. sativum*. Zones of inhibition measured, and the results presented in Table 2.

Table 2. Bacteriostatic agency of *A. sativum* on MRSA

Type of Garlic Juice	Zone of inhibition (mm)
Fresh Domestic	5
Boiled Domestic	0
Fresh Chinese	4
Boiled Chinese	0

Comparative analysis showed better effects of fresh garlic in relation to heat treatment. In comparing the zones of inhibition of fresh domestic and imported fresh, it is important to emphasize that the strongest antimicrobial effects showed fresh garlic of domestic origin. The biggest difference in the measured zones of inhibition that emerged because of the activity of domestic and imported *Allium sativum* L., was observed on the tested bacteria *Staphylococcus aureus*, where the difference between fresh local garlic, which showed the strongest antimicrobial effects, and imported fresh garlic, which showed weak antimicrobial effect on the bacteria was even 22 mm (Table 1). From the research conducted that the domestic fresh garlic had the best effects to the type of fungus *Candida albicans*.

Numerous research has demonstrated that allicin, one of the active ingredients of fresh crushed garlic exhibits different antimicrobial activity (Ankri & Mirelman, 1999; Goncagul, 2010; Ross et al., 2001).

Allicin has been shown that in pure form it displays: antibacterial activity against a broad spectrum of Gram-positive and Gram-negative bacteria, particularly anti-fungal activity against *Candida albicans*, anti-parasitic activity and antiviral activity (Ankri & Mirelman, 1999). Allicin and its derivatives inhibit the cysteine protease, thereby acting antiparasitic on the human and animal pathogenic protozoa (Waag et al., 2010).

From the research conducted that the domestic fresh garlic had the best effects to the type of fungus *Candida albicans*.

Studies have shown that scanning electron microscope and the failure of cells that were treated with garlic, affects the structure and integrity of the outer surface of fungi cells (Ghannoum, 1988).

Since the cells of Gram-negative bacteria have beside a peptidoglycan layer also an outer lipid membrane, for a substance to exhibit any antibacterial activity on these bacteria, the lipid membrane must at least be partially

dissolved or pores created in it to act on the permeability of the membrane, leading to molecules and ions from bacterial cells leaking, and at the end, cracking the bacteria (Zaika, 1988).

Results of this research correlated with the reference literature (Gongacul, 2010; Ghannoum, 1988; Lemar, 2002; Shuford, et al., 2005; Zaika, 1988) where in both domestic and imported *Allium sativum* L. showed weaker antimicrobial activity against Gram-negative bacteria *Escherichia coli* and *Salmonella enteritidis* than the tested Gram - positive bacteria (*Staphylococcus aureus*, MRSA and *Bacillus subtilis*).

CONCLUSIONS

Tested domestic and imported garlic showed antimicrobial effect against all tested of the Gram-positive (*Staphylococcus aureus*, MRSA and *Bacillus subtilis*) and Gram-negative bacteria (*Escherichia coli* and *Salmonella enteritidis*), and the fungus *Candida albicans*. The investigated fresh domestic and imported garlic showed bacteriostatic activity against the methicillin-resistant *Staphylococcus aureus* (MRSA). Fresh domestic and imported garlic showed better antimicrobial effect compared to heat treated domestic and imported garlic. The strongest antimicrobial activity against all species tested was found in fresh homemade garlic. Fresh domestic and imported garlic showed the strongest antimicrobial activity against *Candida albicans*. Following these findings, particularly the intense antimicrobial effect of *Allium sativum* L. against *Candida albicans*, we believe that the preparations based on *A. sativum* L. could be introduced into clinical practice in the treatment of infections caused by *C. albicans*.

REFERENCES

- Agarwal, K. C. (1996). Therapeutic actions of garlic constituents. *Med. Res. Rev.*, 16, 111-124.
- Ankri, S. & Mirelman D. (1999). Antimicrobial properties of allicin from garlic. *Microbes and Infection*. 1, 125-129.
- Bauer, A. W, Kirby, W. M., Sherris, J. C., Turck, M. (1966). Antibiotic susceptibility testing by a standardized single disk method. *Am J Clin*. 45, 493-496.
- Ghannoum, M. A. (1988). Studies on the anticandidal mode of action of *Allium sativum* (garlic). *J. Gen. Microbiol.*, 134, 2917-2924.
- Gongacul, G. (2010). Antimicrobial effect of garlic (*Allium sativum*). *Recent Pat Antiinfect Drug Discov.*, 5 (1), 91-3.
- Lemar, K. M., Turner, M. P. & Lloyd, D. (2002). Garlic (*Allium sativum*) as an anti-*Candida* agent: a comparison of the efficacy of fresh garlic and freeze-dried extracts. *J. Appl. Microbiol.* 93, 398-405.
- Mueller, J. H. & Hinton, J. (1941). A protein-free medium for primary isolation of gonococcus and meningococcus. *Proc. Soc. Exp. Biol. Med.* 48, 3330-333.
- Ross, Z. M., O'Gara, E. A., Hill, D. J., Sleightholme, H. V. & Maslin, D. J. (2001). Antimicrobial Properties of Garlic Oil against Human Enteric Bacteria: Evaluation of Methodologies and Comparisons with Garlic Oil Sulfides and Garlic Powder. *Appl Environ Microbiol.*, 67 (1), 475-480.
- Sabouraud, R. (1892). *Ann. Dermatol. Syphilol.* 3, 1061.
- Shuford, J. A., Steckelberg, J. M. & Patel, R. 2005. Effects of Fresh Garlic Extract on *Candida albicans* Biofilms. *Antimicrob. Agents Chemother.*, 1, 473.
- Waag, T., Gelhaus, C., Rath, J., Stich, A., Leippe, M., Schirmeister, T. (2010). Allicin and derivaates are cysteine protease inhibitors with antiparasitic activity. *Bioorg Med Chem Lett.*, 20, 5541-5543.
- Zaika, L. L. (1988). Spices and herbs: their antibacterial activity and its determination. *J Food Saf.* 23, 97-118.

Summary/Sažetak

Bijeli luk već hiljadama godina se koristi kao hrana i lijek. Budući da bijeli luk sadrži različite biološki aktivne materije i pri tome djeluje kao antibiotik i fungicid, svrha ovog istraživanja je ispitati osjetljivost tri vrste Gram-pozitivnih bakterija: *Staphylococcus aureus*, meticilin-rezistentni *Staphylococcus aureus* (MRSA) i *Bacillus subtilis*; dvije vrste Gram-negativnih bakterija: *Escherichia coli* i *Salmonella enteritidis*, te gljivicu *Candida albicans*. Step en osjetljivosti ispitivanih mikroorganizama na djelovanje svježeg i termički obrađenog domaćeg i uvoznog bijelog luka određivan je disk difuzionom metodom. Testirana antimikrobna-test supstanca pokazala je antimikrobni efekat na sve ispitivane vrste Gram-pozitivnih i Gram-negativnih bakterija kao i fungicidno djelovanje na gljivicu *Candida albicans*. Najjače antimikrobno djelovanje na sve testirane vrste pokazao je svježi domaći bijeli luk. Preparati na bazi *A. sativum* mogli bi se uvesti u kliničku praksu kod liječenja infekcija uzrokovanih *C. albicans*.



Heavy metals pollution in children playgrounds -an environmental modelling and statistical analysis

Šapčanin A^{1,2,*}, Čakal M², Ramić E¹, Smajović A¹, Pehlić E³

¹Faculty of Pharmacy, University of Sarajevo, Zmaja od Bosne 8, 71 000 Sarajevo, Bosnia and Herzegovina

²Faculty of Mechanical Engineering, University of Sarajevo, Vilsonovo šetalište 8, 71 000 Sarajevo, B&H

³Faculty of Biotechnical Sciences, University of Bihać, Luke Marjanovića bb, 77 000 Bihać, Bosnia and Herzegovina

Article info

Received: 05/11/2016
Accepted: 10/12/2016

Keywords:

Soil Pollution
Children Playgrounds
Heavy Metals
Modelling
Correlation Coefficient.

*Corresponding author:

E-mail: aidasapcanin@bih.net.ba
Phone: 00-387-33-586187

Abstract: Models could be used to simulate target variable responses to changes in very complex systems such as soils polluted by heavy metals. Chemical properties of soil such as pH in H₂O, pH in 1 mol/L KCl, humus and CaCO₃ could influence metal mobility and can be used to assess impact of various antropogenic activities. The soil samples were collected from playgrounds located in different areas of Sarajevo. Heavy metals: Cd, Pb, Cu and Zn and basic chemical properties of soil were determined. Statistical analysis was conducted to obtain the correlation coefficient of two selected variables in a data sample, as a normalized measurement of how the two are linearly related. Determined content (mg/kg) for Cd, Pb, Cu and Zn in the spring season were in the ranges of: 0.91-2.15; 26.69-118.97; 19.14-80.21; 75.85-161.45 and in the autumn season were in the ranges of: 0.80-2.14; 41.07-152.71; 29.46-140.74; 71.77-199.04, respectively. The results showed that the highest correlation coefficient was 0.91, for the total content of Cu in the soils in regard to the content of Pb in the autumn season and this indicates a strong and positive correlation. Generally, our results could be used for prediction of heavy metal distribution in playground soil.

INTRODUCTION

Mathematical and computer modelling help us with understanding processes occurring in soils. A number of models are being developed now which can quantitatively predict movements and sorption of heavy metals in soil with good accuracy (Dube et al., 2001). In recent years, researchers have focused on modelling of multicomponent reactive transport and have developed models to study the mobility of potentially toxic heavy metals in the surface soils. The heavy metals are reactive and undergo various chemical transformations in the contaminated soil. Numerous studies have shown that the major sources of heavy metal pollution in urban soils include emissions from traffic (exhaust, tire wear debris particles, particles formed by weathering street), industrial wastes (from power plants, coal combustion, metallurgical industry, automobile repair plants, chemical plants), household garbage, building and weathered particles of sidewalk and precipitation in the atmosphere, etc (Hu et al., 2013; Su et al., 2014). The content of heavy metals in soils can vary widely, even in uncontaminated soils (Qayyum et al., 2015). All inorganic pollutants are considered to be the most common and potentially harmful substances in urban soil in areas affected by anthropogenic pollution (EC, 2013). Due to the fact that children, the most vulnerable population, are in direct

contact with surface soils, it has become clear that soils from children playgrounds should be examined with special care and attention. Polluted soils can directly affect children's health as pollutants and particles from playgrounds can enter their bodies through oral ingestion, inhalation, or in a dermal contact. That is why soil samples, and the soils generally, affect human health, have become a very good diagnostic tool for an assessment of the environmental status of the city (Šapčanin et al., 2016). In urban environments such as children playgrounds, polluted soils can have a direct influence on infants and children's health, because of heavy metals inherent toxicity.

Heavy metals once introduced to the environment by one particular method may spread to various environmental components, which may be caused by the nature of interactions occurring in this natural system. Heavy metals may chemically or physically interact with the natural compounds, which changes their forms of existence in the environment. In general, they may react with particular species, change oxidation states and precipitate (Dube et al., 2001.) Heavy metals are ecologically very important, they are not biodegradable and they move through the ecosystem.

Models could be used to simulate target variable responses to changes in very complex systems such as

soils polluted by heavy metals. Determination of chemical properties of soil such as pH in H₂O, pH in 1M KCl, humus and CaCO₃ could influence metal mobility and can be used to assess impact of various antropogenic activities in soils of interest and to give the environmental buffering capacity and to model pathways in the polluted soils leading to the human health risk of exposure (Kabata-Pendis and Mukherjee, 2007). Every model is created by using the data received as an experimental result from natural or simplified (pseudo-natural) system, which must be accurately defined and in controlled conditions. Obtained results are transformed into a general formula. On the basis of this formula, the scientist chooses a suitable model (Altman, 1991; Armitage and Berry, 1994). The last step is checking the model in different physiochemical conditions to define where and when this model can be applied. There are two types of approach to modelling the system, the predictive and the descriptive ones. In the predictive modelling, the primary objective is to obtain the best possible fit to the available data, since in that way there will be the maximum possible confidence in the predictions made by the model in regions where there are no experimental data with which to compare it. In the descriptive modelling, on the other hand, the goal is to use the model to gain more information about the way in which the real system functions. Furthermore, the primary intent is not to obtain the best possible fit to experimental data, but rather to increase knowledge of the binding process. In any case, one of the first stages in the modelling process is the correlational and regression analysis. By using the regression and correlation, the correlation between two or more variables is analyzed. The correlation implies the analysis of the strength and direction of the correlation, while the regression implies the analysis of the shape and direction of the correlation, and the analysis in terms of independent/dependent (predictor/outcome) variables, with the intent of making prediction. (Altman, 1991; Armitage and Berry, 1994; Bland, 2005). In the regression model, knowledge of values of independent variables enables predicting values of the dependent variables.

Whenever there is a significant correlation between the two variables, the value of one variable can be used for predicting the value of the other variable. (Nedunuri *et al.*, 1995).

MATERIAL AND METHODS

For the purpose of this study, the soil samples were collected from selected public children playgrounds located in eight different urban areas of Sarajevo according to ISO 11047 protocol, in the spring and autumn seasons.

Ten sub-samples were collected from the top 10 cm layer of the soil and mixed to obtain a bulk composite sample. Samples were collected with a stainless trowel and transferred to the laboratory in plastic bags. Stones and foreign objects were hand-removed, and the samples were air-dried for seven days.

Furthermore, the samples were then ground in order to obtain a fine homogenous powder. Basic properties (pH in H₂O, pH in 1M KCl, humus and CaCO₃) of the examined soil samples were determined by standard methods of soil analysis (Sapčanin *et al.*, 2016).

Samples for the determination of heavy metals Cd, Pb, Cu, and Zn were prepared by microwave – assisted acid digestion and determined by using an atomic absorption spectrophotometer, Shimadzu AA 6800, according to Environmental Protection Agency (EPA) protocols.

Mathematical-statistical analysis

Statistical analysis was conducted to obtain the correlation coefficient of two selected variables in a data sample, as a normalized measurement of how the two are linearly related. Estimation of dependence of the selected variables has been carried out according to the following criteria:

if the value of the correlation coefficient is ≥ 0.70 , then correlation is strong;

if the value of the correlation coefficient between 0.30 – 0.69, then correlation is medium;

if the value of the correlation coefficient is < 0.30 , then correlation is weak,

And if the value of the correlation coefficient is 0.0, then there is no linear correlation (which does not exclude the possibility of having a non-linear form of correlation).

RESULTS AND DISCUSSION

The results of the determination of some basic properties of the examined samples from the public park and playground soils in the spring and autumn seasons are presented in Table 1.

Results of the pH values for the active acidity in the soil in the selected public children playground soils range from: 7.94 to 8.29, so that the examined soils are classified as alkaline ones. Results of the pH values for the substituted acidity in the soil on the selected public children playground soils range from: 7.26 to 7.68, so that the examined soils are classified as alkaline ones – in alkaline soils sorption of metals is lower, however, metals remain for longer periods in the soils. The content of humus in the soil in the selected public children playground soils ranges from: 2.94-11.75, and based on the humus content, the examined soils are classified as soils with weak or strong presence of humus.

Table 1. Basic chemical properties (pH in H₂O, pH in 1 mol dm⁻³ KCl, humus, and CaCO₃) of the soil samples from selected playgrounds in the spring and autumn seasons.

Playground	pH in H ₂ O		pH in 1M KCl-u		Humus (%)		CaCO ₃ (%)	
	Spring	Autumn	Spring	Autumn	Spring	Autumn	Spring	Autumn
1	8.17	8.16	7.59	7.30	5.83	5.63	14.26	18.28
2	8.26	8.17	7.73	7.58	3.38	5.54	15.88	17.95
3	8.34	8.14	7.74	7.68	2.94	4.14	17.63	20.73
4	8.14	7.97	7.57	7.54	4.48	4.66	25.20	27.23
5	8.20	8.22	7.63	7.63	11.75	6.48	17.88	36.31
6	8.12	8.04	7.63	7.51	5.16	5.16	5.90	17.15
7	8.29	8.06	7.26	7.61	6.02	6.23	19.73	1.49
8	8.13	7.94	7.41	7.46	2.97	3.85	5.49	4.57

The content of CaCO₃ in the soil in the selected public children playground soils ranges from: 1.49-36.31, and based on the content of CaCO₃ in the soil, the examined soils are classified as soils with weak or strong carbon content.

Table 2 shows basic statistical parameters: mean value, standard deviation, median, variance, minimum and maximum value and the range of the content (mg/kg) of metals/metalloids, in the soil collected from the old children playground in the spring season in Sarajevo.

Table 2. Basic statistical parameters calculated for the content of metal (mg/kg) in public children playground areas in Sarajevo in the spring season

Heavy metal	Mean (mg/kg)	SD	Median	Variance	Min	Max	Range
Cd	1.42	0.56	1.49	0.32	0.48	2.1596	1.68
Pb	68.65	32.15	65.21	1033.71	26.7	118.9793	92.28
Cu	45.36	21.94	40.5	481.46	19.14	80.2156	61.07
Zn	129.94	35.99	137.66	1295.24	75.85	173.44	97.58

Results show that maximum values for the content of metals Cd, Pb, Cu i Zn are higher from the target value according to the Dutch legislation. Obtained maximum values have not exceeded the values which may require intervention in form of remediation, nevertheless, the obtained values do not exclude risks which may be posed to the ecosystem.

According to the results obtained for maximum values of the content of metals/metalloids, the order is as follows: Zn > Pb > Cu > Cd.

Table 3 shows basic statistical parameters: mean value, standard deviation, median, variance, minimum and maximum value and the range of the content (mg/kg) of metals/metalloids, in the soil collected from the old children playground in the autumn season in Sarajevo.

Table 3. Basic statistical parameters calculated for the content of metal (mg/kg) in public children playground areas in Sarajevo in the autumn season

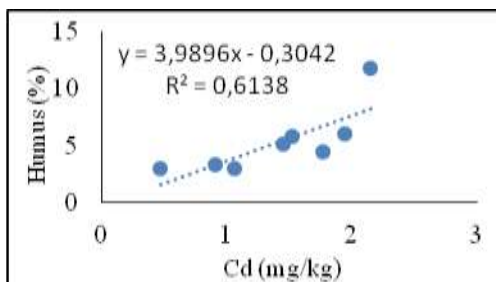
Heavy metal	Mean (mg/kg)	SD	Median	Variance	Min	Max	Range
Cd	1.56	0.47	1.64	0.23	0.81	2.14	1.34
Pb	79.13	46.30	55.33	2144.12	41.07	152.72	111.65
Cu	54.54	39.72	40.73	1577.69	18.92	140.74	121.81
Zn	125.94	40.95	123.75	1677.18	71.76	199.04	127.27

Determined content (mg/kg) for Cd, Pb, Cu and Zn in the spring season were in the ranges of: 0.91-2.15; 26.69-118.97; 19.14-80.21; 75.85-161.45 and in the autumn season were in the ranges of: 0.80 - 2.14; 41.07-152.71; 29.46-140.74; 71.77-199.04, respectively. The results showed that the soils of public parks and playgrounds could be marked as slightly to medium contaminated by determined heavy metals.

Results show that maximum values for the content of metals Cd, Pb, Cu i Zn are higher from the target value according to the Dutch legislation (VROM, 2000). Obtained maximum values have not exceeded the values which may require intervention in form of remediation, nevertheless, the obtained values do not exclude risks which may be posed to the ecosystem.

According to the results obtained for maximum values of the content of metals/metalloids, seasonal variations have been noticed, ie. maximum values of the content of Pb and Cr were higher in autumn in respect to spring, while maximum values of the content of Ni, Cu, Zn, and Se, were higher in spring in respect to autumn. Based on the results obtained for maximum values of the content of metals/metalloids, the order is as follows: Zn > Pb > Cu > Cd.

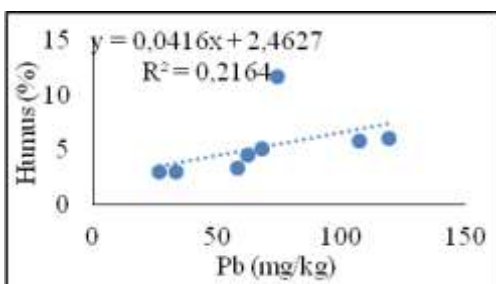
Results of the correlation of the total content of Cd in relation to the content of humus in the spring season are shown in Graph 1.



Graph 1. The total content of Cd in the soil in relation to the content of humus in the spring season

The results show that the highest correlation coefficient for the total content of Cd in the soils in relation to the content of humus in the spring season was 0.78, which indicates to a strong and positive correlation. That means that the increase of the content of humus affects the increase of the total content of Cd.

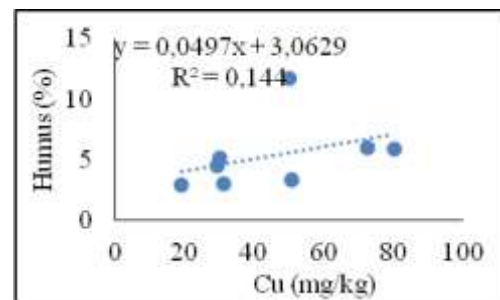
Results of the correlation of the total content of Pb in relation to the content of humus in the spring season are shown in Graph 2.



Graph 2. The total content of Pb in the soil in relation to the content of humus in the spring season

The results show that there is a correlation between the total content of Pb in the soil and the content of humus as the value of the correlation coefficient is 0,47, which indicates to a medium and positive correlation.

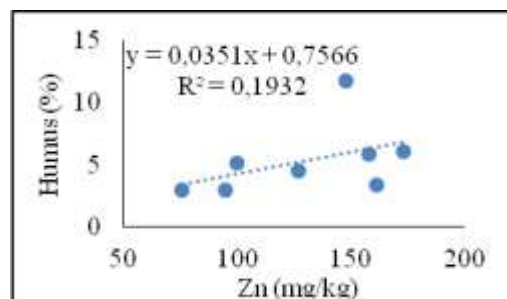
Results of the correlation of the total content of Cu in relation to the content of humus in the spring season are shown in Graph 3.



Graph 3. The total content of Cu in the soil in relation to the content of humus in the spring season

The results show that the correlation coefficient for the total content of Cu in relation to the content of humus is 0,38, which indicates to a medium and positive correlation of these two parameters.

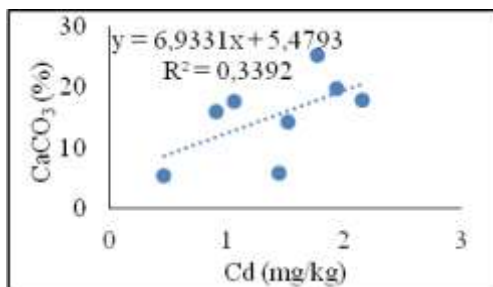
Results of the correlation of the total content of Zn in relation to the content of humus in the spring season are shown in Graph 4.



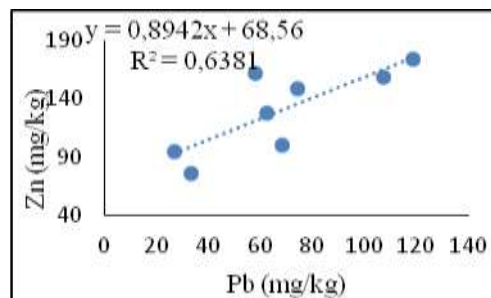
Graph 4. The total content of Zn in the soil in relation to the content of humus in the spring season

The results show that the correlation coefficient for the total content of Zn in relation to the content of humus is 0,44, which indicates to a medium and positive correlation of these two parameters.

Results of the correlation of the total content of Cd in relation to the content of CaCO₃ in the spring season are shown in Graph 5.



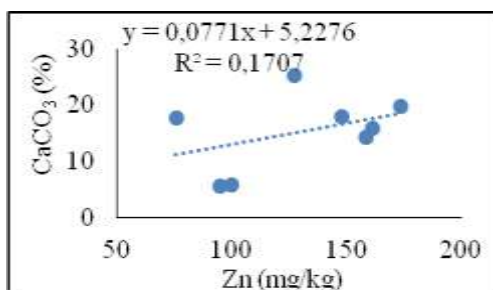
Graph 5. The total content of Cd in the soil in relation to the content of CaCO₃ in the spring season



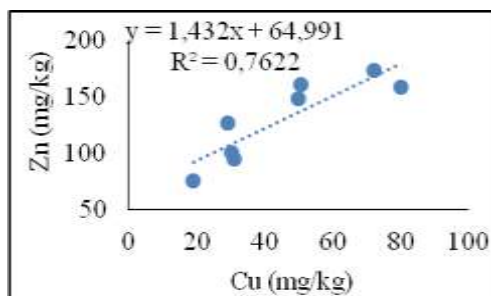
Graph 8. The total content of Pb in the soil in relation to the content of Zn in the spring season

The results show that the correlation coefficient for the total content of Cd in relation to the content of CaCO₃ is 0,58, which indicates to a medium and positive correlation of these two parameters.

Results of the correlation of the total content of Zn in relation to the content of CaCO₃ in the spring season are shown in Graph 6.

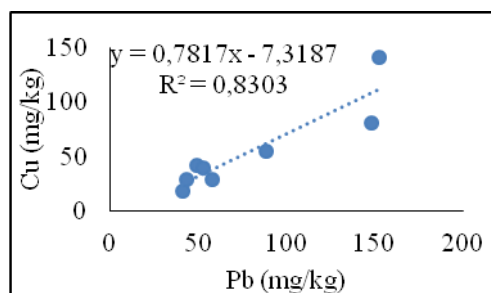


Graph 6. The total content of Zn in the soil in relation to the content of CaCO₃ in the spring season



Graph 9. The total content of Cu in the soil in relation to content of Zn in the spring season

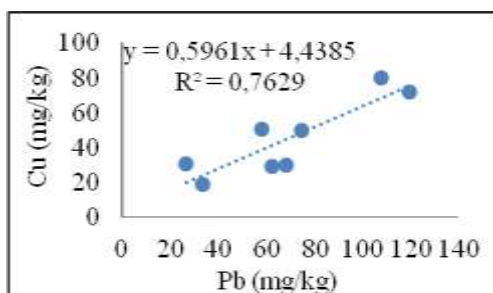
The results show that the correlation coefficient for the total content of Zn in relation to the content of CaCO₃ is 0,41, which indicates to a medium and positive correlation of these two parameters.



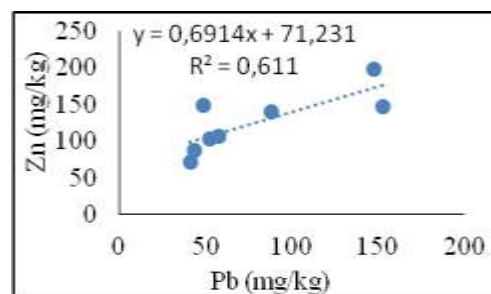
Graph 10. The total content of Pb in the soil in relation to the content of Cu in the autumn season

Basic chemical properties of soil such as pH in H₂O, pH in 1 mol dm⁻³ KCl, humus, and CaCO₃ could influence metal mobility and the determined values could be used to model pathways in the polluted soils.

The correlations between the heavy metals studied are shown in the Graphs 7 to 11, as follows:



Graph 7. The total content of Pb in the soil in relation to the content of Cu in the spring season



Graph 11. The total content of Pb in the soil in relation to the content of Zn in the autumn season

Results of the correlation between the heavy metals studied offer remarkable information on the sources and pathways of the heavy metals. Pb was strongly correlated with Cu ($r=0,87$) and Zn ($r=0,8$) in the spring season. Cu was strongly correlated with Zn ($r=0,87$) in the spring season. Pb was strongly correlated with Cu ($r=0,91$) and Zn ($r=0,78$) in the autumn season.

The highly significant positive correlation between the heavy metals investigated indicates that their compounds occurred from various anthropogenic activities in the children playgrounds environment.

CONCLUSIONS

The presence of heavy metals in soils represents a significant environmental hazard, and one of the most difficult contamination problems to solve. There are two main reasons: firstly, due to the chemical character of heavy metals - they are not subjected to biodegradation processes, and they accumulate in the environment; and secondly, due to the complexity of the soil matrix. The inhomogeneity of soils is so high, that we cannot provide all the features of soil samples without employment of some approximations. Simplification of this matrix increases chances of recognition of basic soil processes. Another option which could enable us to understand better processes occurring in the soils is to employ a computer simulation. However, it seems most effective to apply computer methods with the simulation of natural physicochemical processes in a simplified soil matrix. It can be concluded that, generally speaking, the results obtained from this research can be used for predicting the distribution of content of heavy metals in the soil in the children playground areas.

REFERENCES

- Altman, D.G. (1991). *Practical Statistics for Medical Research*. London. Chapman & Hall.
- Armitage, P., Berr, P. (1994). *Statistical Methods in Medical Research*. Oxford, Blackwell Science Ltd.
- Bland, M. (2005). *An Introduction to Medical Statistics* (3rd Ed). Oxford, Oxford University Press.
- Dube, A., Zbytniewski, R., Kowalkowski, T., Cukrowska, E., Buszewski, B., (2001). Adsorption and Migration of Heavy Metals in Soil. *Polish Journal of Environmental Studies*, 10(1), 1-10.
- Hu, Y., Liu, X., Bai, J., Shih, K., Zeng, E.Y., Cheng, H. (2013). Assessing heavy metal pollution in the surface soils of a region that had undergone three decades of intense industrialization and urbanization. *Environ Sci Pollut Res*, 20, 6150–6159.
- Kabata-Pendis, A., Mukherjee, A.B. (2007). *Trace Elements from Soil to Human*. Berlin, Springer Verlag, p.p. 9-38.
- Rogozan, G.C., Micle, V., Coste (Bina), A. (2013). *Mathematical Models of Heavy Metals Mobility in Soils*. *ProEnvironment*, 6, 450 – 458.
- Qayyum, S., Khan, I., Meng, K., Zhao, Y., Peng, C. (2015). Remediation technologies for heavy metals contaminated soil. *Journal of international academic research for multidisciplinary*, 3(11), 96-105.
- Schnoor, L.J., (1996). Modeling trace metals. In: Schnoor L.J. Ed. *Environmental modeling, Fate and transport of pollutants in water, air and soils*. United States of America, John Wiley & Sons, Inc. p.p. 381.
- EC (2013). *Science for Environment Policy In-depth Report: Soil Contamination: Impacts on Human Health*. Report produced for the European Commission DG Environment, September 2013. Science Communication Unit, University of the West of England, Bristol .Available at: <http://ec.europa.eu/science-environment-policy>
- Nedunuri, K.V., Govindaraju, R.S., Erickson, L.E., Schwab, A.P. (1995). Modeling of heavy metal movement in vegetated, unsaturated soils with emphasis on geochemistry. In the *Proceedings of the 10th Annual Conference on Hazardous Waste Research*, p.p. 57-66.
- Sapčanin, A., Cakal, M., Jacimovic, Z., Pehlic, E., Jancan, G. (2016). Soil Pollution fingerprints of children playgrounds in Sarajevo city, Bosnia and Herzegovina. *Environmental Science and Pollution Research*, doi:10.1007/s11356-016-6301-5
- Su, C., Jiang, L., Zhang, W. (2014). A review on heavy metal contamination in the soil worldwide: situation, impact and remediation techniques. *Environmental Skeptics and Critics*, 3(2), 24–38.
- VROM (2000) Circular on target values and intervention values for soil remediation. Ministry of Housing, Spatial Planning and Environment, VROM, <http://www.minvrom.nl/minvrom/docs/bodem/S&I2000.pdf>

Summary/Sažetak

Modeli se mogu koristiti za simulaciju odgovora ciljnih varijabli na promjene u veoma kompleksnim sistemima kao što su zemljišta kontaminirana teškim metalima. Karakteristike zemljišta kao što su pH u void, pH u KCl-u, humus i CaCO₃ mogle bi utjecati na mobilnost metala i mogu biti upotrebljena za procjenu djelovanja raznolikih antropogenih aktivnosti. Uzorci tla prikupljeni su sa igrališta lociranih u različitim dijelovima Sarajeva. Teški metali: Cd, Pb, Cu i Zn kao i osnovne hemijske karakteristike tla su određeni. Statistička analiza je izvedena da se dobiju podaci o korelacijskim koeficijentima za dvije odabrane varijable u uzorku podataka kao normaliziranog mjerenja da li su varijable linearno povezane. Izmjereni sadržaj (mg/kg) za Cd, Pb, Cu i Zn u proljetnoj sezoni kretali su se u rasponu od: 0.91-2.15; 26.69-118.97; 19.14-80.21; 75.85-161.45 i u jesenjoj sezoni kretali su se u rasponu od: 0.80-2.14; 41.07-152.71; 29.46-140.74; 71.77-199.04, respektivno. Rezultati pokazuju da je najveća vrijednost korelacijskog koeficijenta iznosila 0.91, za ukupni sadržaj Cu u

tlu, u odnosu na sadržaj Pb u jesenjoj sezoni i to indicira jaku i pozitivnu korelaciju. Generalno bi se naši rezultati mogli upotrijebiti za predviđanje raspodjele teških metala u tlu igrališta.

Synthesis and Characterization of Neutral Ru(III) Complexes Containing Schiff Bases and *N*-donor Heterocyclic Ligands

Begić S. *, Ljubijankić N.

Department of Chemistry, Faculty of Science, University of Sarajevo, Sarajevo 71 000, Bosnia and Herzegovina

Article info

Received: 04/12/2016

Accepted: 22/12/2016

Keywords:

Ru(III)
neutral complex
Schiff base
pyridine
pyrimidine

*Corresponding author:

E-mail: sabinab@pmf.unsa.ba

Phone: 00-387-33-279950

Fax: 00-387-33-649359

Abstract: Two new neutral complex compounds of Ru(III) with Schiff bases and *N*-donor heterocyclic ligands have been synthesized. Based on MALDI TOF/TOF mass spectra, CHN elemental analysis, infrared and electronic spectra the synthesized compounds were formulated as $[\text{RuCl}(\text{N-Ph-5-X-salim})_2\text{B}]$, where X = Cl for B = Py and X = Br for B = Pym. In the octahedral environment of Ru(III), bidentate Schiff bases acts as anionic ligand where coordination occurs *via* deprotonated phenolic oxygen and azomethine nitrogen atom. Coordination of monodentate *N*-donor heterocyclic ligands occurs through free electronic pair on the nitrogen atom.

INTRODUCTION

The interest in the synthesis and characterization of Ru(III) complexes containing a Schiff base is due to their many significant biological activities, especially anticancer (Ejidike *et al.*, 2016) or antibacterial (Kahrovic, Bektas, *et al.*, 2014; Priya *et al.*, 2009) activities. Schiff bases derived from the condensation of 5-*X*-salicylaldehyde (where X = Cl or Br) and aniline represent an important class of chelating ligands. There are relatively small number of complexes containing these Schiff bases whose structures are stored in Cambridge Structural Database (Blagus *et al.*, 2010). Ruthenium(III) complexes with Schiff bases derived from 5-substituted-salicylaldehyde are described as DNA intercalators (Ljubijankić *et al.*, 2013; Kahrovic *et al.*, 2014; Begić-Hairlahovic *et al.*, 2014) and electrochemical mediators (Turkusic and Kahrovic, 2012, Kahrovic *et al.*, 2012, Kahrovic and Turkusic, 2012). Pyridine, pyrimidine and their derivatives have been widely used in medicinal applications (Akalın and Akyuz, 2008; Quin and Tyrell, 2010). The pyridine and pyrimidine ring

systems provides a potential binding site for metals. Complex compounds containing pyridine or pyrimidine ring systems possesses a broad range of biological activities and can be used as potentially active therapeutic compounds (Colluccia, Natile, 2007; Kostova, 2006).

In this study, we report the synthesis and spectral characterization of Ru(III) neutral complex compounds with *N*-phenyl-5-*X*-salicylideneimine (where X = Cl or Br) and *N*-donor heterocyclic ligands, pyridine (py) or pyrimidine (pym). The present work is a continuation of our previously reported study on the synthesis, characterization and interaction with CT DNA of Ru(III) complexes with indazole and Schiff base derived from 5-Chlorosalicylaldehyde (Begić-Hairlahovic *et al.*, 2014). The Schiff base and *N*-donor heterocyclic ligands used in this study are shown in (Fig. 1).

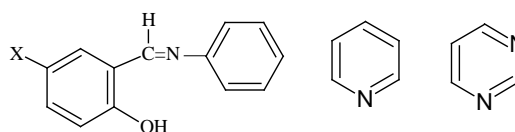


Figure 1: Structure of the Schiff bases (where X = Cl or Br), pyridine and pyrimidine.

EXPERIMENTAL

Materials

All chemicals were of analytical grade and were used as received without any purification with exception of aniline which is purified by distillation.

Starting materials

Schiff bases, *N*-phenyl-5-*X*-salicylideneimine (where *X* = Cl or Br) were synthesized according to the literature procedures (Dholakiya and Patel, 2002) and freshly prepared solutions were used for the synthesis of starting materials.

Sodium dichloro-bis-*[N*-phenyl-5-*X*-salicylideneiminato-*N,O*]ruthenate(III), hereinafter Na[RuCl₂(*N*-Ph-5-*X*-salim)₂] where *X* = Cl or Br were prepared using the reported procedures (Ljubijankic *et al.*, 2013) and were used without any purification as starting Ru(III) compounds in the synthesis of new neutral complexes. The purity of starting Ru(III) compounds were checked by infrared spectroscopy.

Synthesis of Complex 1

The preparation of Chloro(pyridine)bis[*N*-phenyl-5-chlorosalicylideneiminato-*O,N*]ruthenium(III), [RuCl(*N*-Ph-5-Cl-salim)₂py], hereinafter **Complex 1** was carried out by refluxing an ethanolic solutions of Na[RuCl₂(*N*-Ph-5-Cl-salim)₂] and an excess of pyridine. Absolute ethanol was added to 60 ml of ethanolic solution of Na[RuCl₂(*N*-Ph-5-Cl-salim)₂] (41.04 mg; 0.062 mmol) and pyridine (10 μL; 0.124 mmol). The mixture was refluxed for 10.5 hours at temperature 75 °C whereby the solution changed color from dark green to violet blue. The resulting solution was filtered off and kept in an ice-salt bath for seven days. The dark blue product was washed with water and diethyl ether to remove sodium chloride and excess of pyridine. The synthesized complex was dried under vacuum in a desiccator.

Yield: 68 %.

Complex 1: Anal. calcd for C₃₁H₂₃Cl₃N₃O₂Ru: C 55.00, H 3.42, N 6.21. Found: C 53.68, H 3.79, N 6.37. MALDI TOF/TOF MS (*m/z*) calcd for [C₃₁H₂₃Cl₃N₃O₂Ru], 676.9883; found, 676.9889; IR (KBr, cm⁻¹) 1589 s [v(ring mode)], 1004 m [(ring breathing mode)], 669 vw [v(Ru–N)], 438 wv [v(Ru–O)]; UV-Vis (CH₂Cl₂, λ/nm) 245, 260, 350, 607.

Synthesis of Complex 2

The compound, Chloro(pyrimidine)bis[*N*-phenyl-5-bromosalicylideneiminato-*O,N*]ruthenium(III), [RuCl(*N*-Ph-5-Br-salim)₂Pym], hereinafter **Complex 2** was prepared by stirring an ethanolic solutions of Na[RuCl₂(*N*-Ph-5-Br-salim)₂] and an excess of pyrimidine. The solution of pyrimidine (5 μL; 0.06 mmol) in 2 mL absolute ethanol was added to the solution of Na[RuCl₂(*N*-Ph-5-Br-salim)₂] (25.1 mg; 0.034 mmol) in absolute ethanol (40 mL). The mixture was stirred at room temperature for 29 hours until a light green solution

was obtained. The resulting solution was evaporated to dryness and residue washed several times with diethylether and water to remove excess of pyrimidine and sodium chloride. The green product was dried in a vacuum desiccator.

Yield: 50 %.

Complex 2: Anal. calcd for C₃₀H₂₂Br₂ClN₄O₂Ru: C 46.99, H 2.89, N 7.31. Found: C 45.04, H 2.94, N 7.02. MALDI TOF/TOF MS (*m/z*) calcd for C₃₀H₂₂Br₂ClN₄O₂Ru, 766.8823; found, 766.8804. IR (KBr, cm⁻¹) 1589 s [v(ring mode)], 1002 m [(ring breathing mode)], 663 wv [v(Ru–N)], 434wv [v(Ru–O)]. UV-Vis (CH₂Cl₂, λ/nm) 245, 260, 350, 607.

Instrumentation – Physical measurements

Synthesized compounds were characterized by MALDI TOF/TOF mass spectrometry, CHN analysis, cyclic voltammetry, IR and UV/Vis spectrometry.

The mass spectra were recorded on a MALDI TOF/TOF (matrix-assisted laser desorption / ionization-time-of-flight) Analyzer model 4800 Plus (Applied Biosystems Inc., Foster City, CA, USA). Small amount of sample was mixed with 10 μL of MALDI matrix (DHAP (2,6-dihydroxyacetophenone); 5 mg/mL) and 1 μL was spotted on MALDI plate. The mass spectra were acquired in *m/z* range from 10 to 1000 Da (focus mass 500 Da, delay time 300 ns). Thiamine mononitrate, azithromycin and angiotensin were used as internal standards to calibrate the instrument.

The analysis of carbon, hydrogen and nitrogen was carried out by a Perkin Elmer 2400 Series CHNS/O Analyzer.

Infrared spectra (4000 – 400 cm⁻¹) were collected on a BX FTIR Perkin Elmer Spectrum System with samples prepared as KBr pellets.

The electronic spectra were obtained on a Perkin Elmer UV/Vis spectrometer model Lambda 35.

The characterization of Ru(III) complexes by cyclic voltammetry (CV) was investigated using a potentiostat/galvanostat Autolab PGSTAT 12 Analyzer equipped with glassy carbon (GC), Ag/AgCl and Pt wire as working, reference and auxiliary electrode, respectively. The cyclic voltammograms of the complexes were recorded in acetonitrile (MeCN) at scan rate 0.2 V s⁻¹ where tetraethylammonium bromide (Et₄NBr) was used as supporting electrolyte.

RESULTS AND DISCUSSION

The starting Ru(III) compounds, Na[RuCl₂(*N*-Ph-5-*X*-salim)₂] (where *X* = Cl or Br) were synthesized by reacting RuCl₃ with freshly prepared Schiff bases, 5-*X*-salicylideneimine (Dholakiya and Patel, 2002) in 1 : 2 molar ratio in absolute ethanol. The freshly prepared Na[RuCl₂(*N*-Ph-5-*X*-salim)₂] compounds were used for the synthesis of new complex compounds.

Neutral ruthenium(III) complex compounds of general formula [RuCl(*N*-Ph-5-*X*-salim)₂B] (where *X* = Cl for B = py or *X* = Br for B = pym) were prepared by reacting Na[RuCl₂(*N*-Ph-5-*X*-salim)₂] with an excess of py or pym in absolute ethanol as shown in (Fig. 2). The synthesis of

the complexes was carried out in relative mild conditions by replacement of easily outgoing chloride ion in $\text{Na}[\text{RuCl}_2(\text{N-Ph-5-X-salim})_2]$ with py or pym. The products are stable in air, insoluble in water, soluble in dimethyl sulfoxide (DMSO), dichloromethane, acetonitrile (MeCN), dimethylformamide (DMF),

tetrahydrofuran (THF).

Based on mass spectra, CHN elemental analysis, infrared and electronic spectra the synthesized compounds were formulated as $[\text{RuCl}(\text{N-Ph-5-X-salim})_2\text{B}]$, where X = Cl for B = py and X = Br for B = pym.

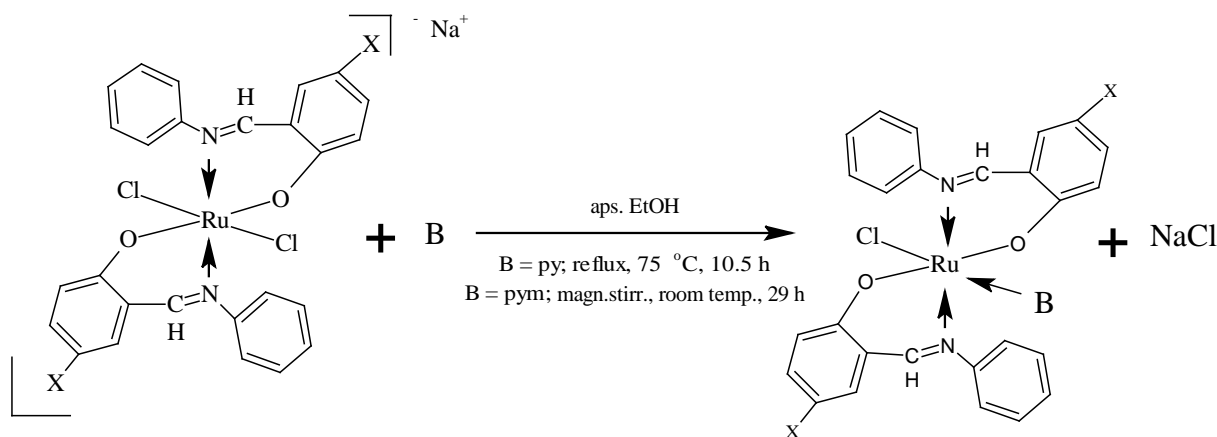


Figure 2: Formation of new Ru(III) complexes. (Where X = Cl for B = py and X = Br for B = pym).

MALDI-TOF/TOF mass spectrometry results confirmed existence of neutral molecules with general formula $[\text{RuCl}(\text{N-Ph-5-X-salim})_2\text{B}]$ (Table 1).

Table 1: MALDI TOF/TOF results of synthesized compounds

Compound	Empirical formula	Calc. mass m/z (100 %)	Measured mass m/z (100 %)	Mass error / ppm
Complex 1	$\text{C}_{31}\text{H}_{23}\text{Cl}_3\text{N}_3\text{O}_2\text{Ru}$	676.9883	676.9889	0.88
Complex 2	$\text{C}_{30}\text{H}_{22}\text{Br}_2\text{ClN}_4\text{O}_2\text{Ru}$	766.8823	766.8804	2.48

The compounds were characterized by IR spectroscopy in the solid state (KBr pellets). The main characteristic vibrations are given in Table 2. In studying coordination effects of metal complexes with pyridine or pyrimidine, ring breathing mode can be used as a guide which shifts to higher wavenumbers upon coordination (Bayari *et al*, 2003). Also when pyridine or pyrimidine ring nitrogen is involved in complex formation certain vibrational modes increase in value due to both coupling with M-N (pyridine or pyrimidine) vibration and alterations of the force field (Akalin, Akyuz, 2008; Bayari *et al*, 2003). The strong bands at 992 and 991 cm^{-1} could be attributed to the ring breathing mode of free pyridine or pyrimidine molecule, respectively. After coordination this bands were shifted for 12 or 11 cm^{-1} to higher wavenumbers.

Coordination of pyridine or pyrimidine to Ru(III) *via* electronic pair on the atom nitrogen affects ring stretching vibrations. This frequencies were shifted towards higher wavenumber, which is indicative of coordination of pyridine or pyrimidine through nitrogen atom to the Ru(III). The new weak bands in Complex 1 at 669 and 438 cm^{-1} could be assigned to Ru-N and Ru-O, respectively. This bands in Complex 2 appears at 663 and 434 cm^{-1} . Characteristic IR vibrations of starting Ru(III) compounds are azomethine C=N, C-O phenolic, Ru-N and Ru-O. After coordination of *N*-heterocyclic donor ligands this bands are not affected. Infrared spectra of synthesized complexes demonstrate that Schiff bases acts as anionic bidentate ligands while *N*-heterocycle as monodentate ligand.

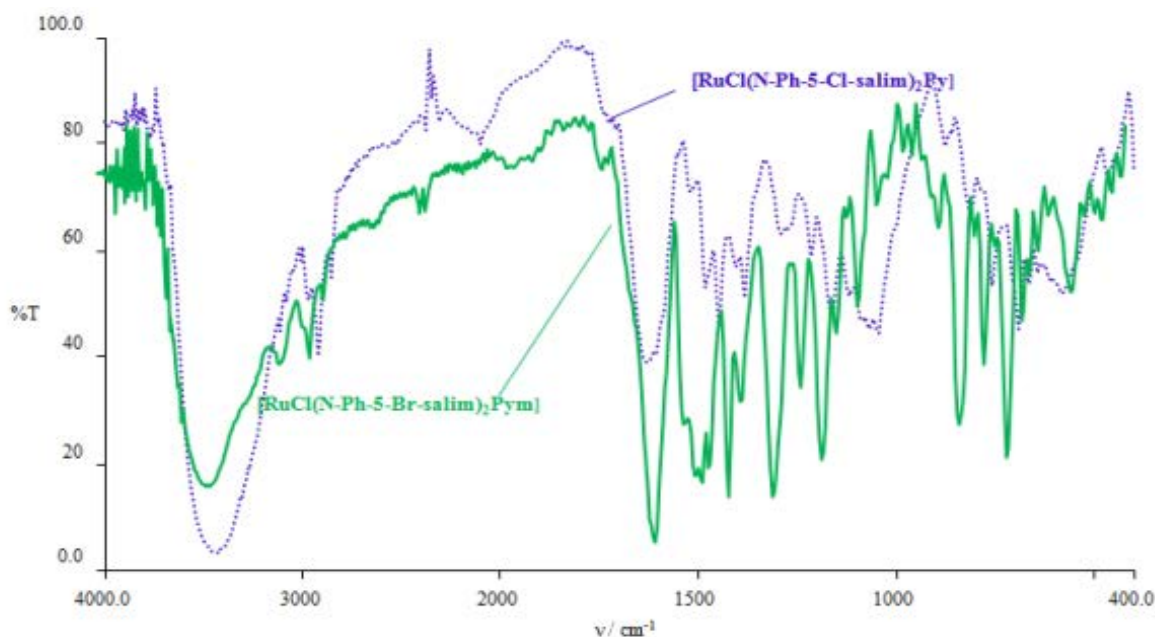


Figure 3: FT- IR spectra of Complex 1 and Complex 2

Table 2: Characteristic vibrations (cm^{-1}) in FT-IR spectra of starting Ru(III) compounds, neutral complexes, free pyridine and pyrimidine

	Complex 1	Complex 2	Py	Pym
$\nu(\text{ring})_{\text{py, pym}}$	1589	1589	1580	1570
ring breathing py, pym	1004	1002	992	991
$\nu(\text{C}=\text{N})_{\text{SB}}$	1603 (1602)	1600 (1601)	-	-
$\nu(\text{C}=\text{O}_{\text{Ph}})_{\text{SB}}$	1295 (1295)	1291 (1289)	-	-
$\nu(\text{Ru}-\text{N})$	669 (668)	663 (663)	-	-
$\nu(\text{Ru}-\text{O})$	438 (436)	434 (433)	-	-

SB – assigned vibrations in Schiff base; Py, Pym – assigned vibrations in pyridine or pyrimidine; values in parentheses refer to starting Ru(III) compound

UV/Vis spectra of starting Ru(III) compounds, synthesized compounds and *N*-donor ligands were recorded in dichloromethane. Electronic spectra exhibit a few characteristic absorptions which are presented in Table 3. UV/Vis spectra of pyridine has one absorption band which could be attributed to $\pi \rightarrow \pi^*$ transition, while pyrimidine showed two bands attributed to $\pi \rightarrow \pi^*$ and $n \rightarrow \pi^*$ transitions. In the electronic spectra of starting Ru(III) compounds weak broad absorptions bands centered at 609 nm for X = Cl or 625 nm for X = Br can be attributed to ${}^2T_{2g} \rightarrow {}^2A_{2g}$. In the spectra of neutral complexes this transitions moves towards lower value of wavelength (565 nm for B = py and 609 nm for B = pym). *N*-donor ligands in the synthesized complexes splits stronger crystal field than chloride ion in the starting material results in higher separation energies of

d-atomic orbitals and moves *d-d* transitions to higher energies.

Since the synthesized complexes are insoluble in water, cyclic voltammograms were recorded in non-aqueous solvent. The complete scan in the range -1.0 – 0.0 V of Complex 1 and Complex 2 in MeCN/ Et_4NBr system showed one cathodic wave (-0.981 V and -0.931 V, respectively) and one anodic wave (-0.740 V and -0.738 V, respectively) (Fig. 4). This quasi-reversible waves can be assigned to the couple Ru(III)/Ru(II).

Table 3: Characteristic absorptions in electronic spectra of $\text{Na}[\text{RuCl}_2(\text{N-Ph-5-X-salim})_2]$, Complex 1, Complex 2 and nitrogenous bases in dichloromethane

Compound	$\pi \rightarrow \pi^*$	$n \rightarrow \pi^*$	IL (SB)	d-d
$\text{Na}[\text{RuCl}_2(\text{N-Ph-5-Cl-salim})_2]$	244	sh	348	613
Py	253	-	-	-
Complex 1	244	sh	348	565
$\text{Na}[\text{RuCl}_2(\text{N-Ph-5-Br-salim})_2]$	244	sh	351	625
Complex 2	244	sh	350	611
Pym	243	287	-	-

$\pi \rightarrow \pi^*$ - electronic transition of delocalized electrons of the aromatic system; $n \rightarrow \pi^*$ - electronic transitions of the atoms of azomethine group or free electron pair on the N atom of pyridine or pyrimidine with aromatic π electrons; IL (SB) – intraligand transition of whole molecule of Schiff base; d-d – transition of low spin complex; sh-shoulder.

In Table 4 are given characteristic half-wave potentials and peak-to-peak separation values of Complex 1 and Complex 2.

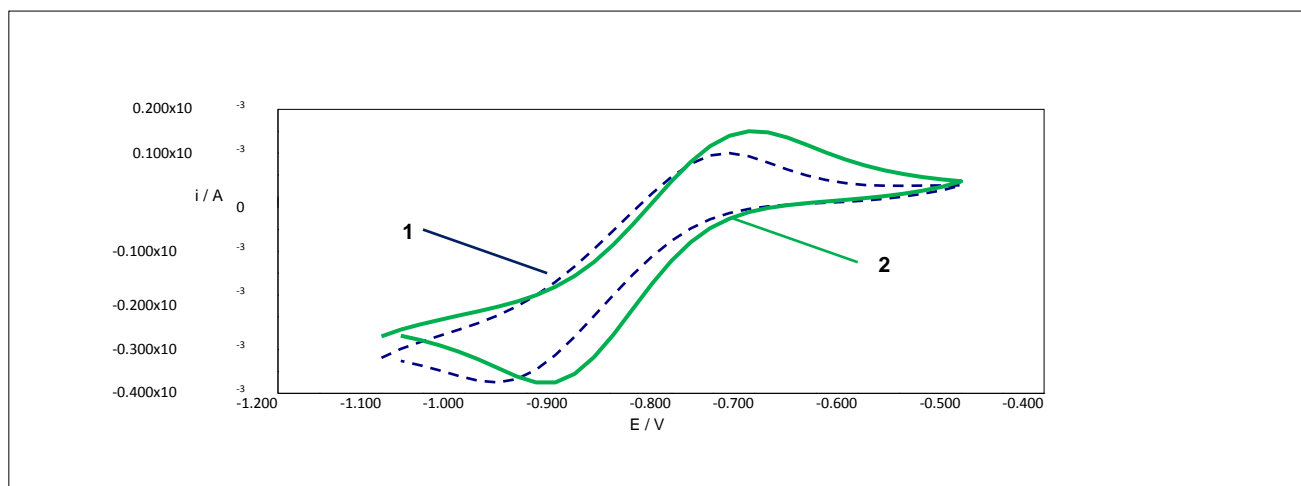


Figure 4: Cyclic voltammograms of Complex 1 (1) and Complex 2 (2) in MeCN; supporting electrolyte: Et₄NBr; potential range: -1.1 – -0.5 V; scan rate 0.2 V/s

Table 4: Characteristic potentials of Complex 1 and Complex 2 from cyclic voltammetric measurements in MeCN / Et₄NBr system

	Complex 1	Complex 2
E_{pc}/V	-0.981	-0.931
E_{pa}/V	-0.740	-0.738
$E_{1/2}/V$	-0.861	-0.835
$\Delta E/V$	0.241	0.193

All data are given vs Ag/AgCl reference electrode

CONCLUSION

New neutral complex compounds of Ru(III) with *N*-phenyl-5-*X*-salicylideneimine (where *X* = Cl or Br) and *N*-donor heterocyclic ligands (pyridine or pyrimidine) were synthesized. On the basis of mass spectra, CHN analysis, infrared and electronic spectra, the complexes were formulated as [RuCl(*N*-Ph-5-*X*-salim)₂B] where *X* = Cl for B = py and *X* = Br for B = pym. In the octahedral environment coordination of the Ru(III) to the imine nitrogen and phenolic oxygen atoms of the Schiff bases and nitrogen atom of py or pym occurred. MALDI TOF/TOF mass spectrometry confirmed existence of the neutral molecules. Redox property of complexes has been determined using cyclic voltammetry.

REFERENCES

- Akalin, E., Akyuz, S. (2008). Vibrational study on Zn(Pyrimidine)₂Cl₂, Pyrimidine-Al(OH)₃ and Pyrimidine-(Al(OH)₃)₂ complexes. *Vibrational spectroscopy*, 48,233-237.
- Bayari, S., Ataç, A., Yurdakul, Ş. (2003). Coordination behaviour of nicotinamide: an infrared spectroscopic study. *Journal of Molecular Structure*, 655, 163-170.
- Begic-Hairlahovic, S., Kahrovic, E., Turkusic, E. (2014). Synthesis, characterization and interaction with CT DNA of novel cationic complex Ru(III) with indazole and Schiff base derived from 5-chlorosalicylaldehyde. *Bulletin of the Chemists and Technologists of Bosnia and Herzegovina*, 43, 15-20.
- Blagus, A., Cincic, D., Friscic, T., Kaitner, B., Stilinovic, V. (2010). Schiff base derived from hydroxyarylaldehydes: molecular and crystal structure, tautomerism, quinoid effect, coordination compounds. *Maced. J. Chem. Chem. Eng.*, 29 (2), 117-138.
- Coluccia, M., Natile, G. (2007). *Trans-Platinum Complexes in Cancer Therapy. Anti-Cancer Agents in Medicinal Chemistry*, 111-123.
- Dholakiya, P. P., Patel M. N. (2002). Synthesis, spectroscopic studies, and antimicrobial activity of Mn(II), Co(II), Ni(II), Cu(II), and Cg(II) complexes with bidentate Schiff bases and 2,2'-bipyridylamine. *Synthesis and Reactivity in Inorganic and Metal-Organic Chemistry*, 32(4), 753-762.
- Ejidike I. P., Ajibade p. A. (2016). Synthesis, Characterization, Anticancer, and Antioxidant Studies of Ru(III) Complexes of Monobasic Tridentate Schiff Bases. *Bioinorganic Chemistry and Applications*, vol. 2016, 11 pages.
- Kahrovic, E. (2014). Ruthenium Compounds with Schiff Bases: Design and Promising Applications of Salicylideneimine Complexes. In Keeler, G. P. (Ed.), *Ruthenium: Synthesis, Physicochemical Properties and Applications*, (p.p. 269-283). NOVA Publishers.
- Kahrovic, E., Bektas, S., Turkusic, E., Zahirovic A. (2014). Evidence on antimicrobial activity of Sodium dichloro-bis[N-phenyl-5-chlorosalicylideneiminato-N,O]ruthenate(III) against gram positive bacteria. *SYLWAN*, 158(5), 482-493
- Kahrovic, E., Dehari, S., Dehari, D., Begic, S. and Ljubijankic, N. (2010). Synthesis and characterization of new Ru (III) complexes with monobasic (NO) and dibasic (ONO) Schiff bases derived from salicylaldehydes. *Technics Technologies Education Management* 5/4, 799-803.
- Kahrovic, E., Turkusic, E. (2012). New Ruthenium Complexes with Schiff Bases as Mediators for the Low Potential Amperometric Determination of Ascorbic Acid, Part II: Voltametric and Amperometric evidence of mediation with Bromo-derivative of Tetraethylammonium dichloro-bis[N-

- phenyl-5-halogeno-salicylideniminato N,O]ruthenat(III). *HealthMED*, 6/3, 1046-1049.
- Kahrovic, E., Turkusic, E., Zahirovic, A. (2014). Calf Thymus DNA Intercalation by Anionic Ru(III) Complexes Containing Tridentate Schiff Bases Derived from 5-X-Substituted Salicylaldehyde and 2-Aminophenol. *Journal of Chemistry and Chemical Engineering*, 8, 335-343.
- Kahrovic, E., Turkusic, E., Ljubijankic, N., Dehari, S., Dehari, D., Bajsman, A. (2012). New Ruthenium Complexes with Schiff Bases as Mediators for the Low Potential Amperometric Determination of Ascorbic Acid, Part I: Voltametric and Amperometric evidence of mediation with Tetraethylammonium dichloro-bis[N-phenyl-5-chloro-salicylideniminato-N,O]ruthenat(III). *HealthMED*, 6/2, 699-702.
- Keppler, B. K., Henn, M., Juhl, U. M., Berger, M. R., Niebl, R., Wagner, F. E. (1989). New ruthenium complexes for the treatment of cancer. In *Ruthenium and Other Non-Platinum Metal Complexes in Cancer Chemotherapy* (p.p. 41-69). Springer Berlin Heidelberg.
- Ljubijankic, N., Zahirovic, A., Turkusic, E., Kahrovic, E. (2013). DNA Binding Properties of Two Ruthenium (III) Complexes Containing Schiff Bases Derived from Salicylaldehyde: Spectroscopic and Electrochemical Evidence of CT DNA Intercalation. *Croatica Chemica Acta*, 86(2), 215-222.
- Turkusic, E., Kahrovic, E. (2012). Development of new low potential amperometric sensor for L-cysteine based on carbon ink modification by Tetraethylammonium dichloro-bis[N-phenyl-5-bromosalicylideniminato-N,O]ruthenat(III). *Technics Technologies Education Management*, 7/3, 1300-1303.
- Quin, L. D., Tyrell, J. A., *Fundamentals of Heterocyclic Chemistry, Importance in Nature and in the Synthesis of Pharmaceuticals*, John Wiley & Sons, 2010.

Summary / Sažetak

Sintetizirana su dva nova neutralna kompleksna spoja Ru(III) sa Schiff-ovim bazama i N-donorskim heterocikličnim ligandima. Na bazi MALDI TOF/TOF masenih spektara, CHN elementarne analize, infracrvenih i elektronskih spektara sintetizirani spojevi su formulirani kao $[\text{RuCl}(\text{N-Ph-5-X-salim})_2\text{B}]$, gdje je X = Cl za B = Py i X = Br za B = Pym. U oktaedarskom okruženju Ru(III) bidentatna Schiff-ova baza djeluje kao anionski ligand gdje se koordinacija ostvaruje preko deprotoniranog fenolnog atoma kisika i azometinskog atoma azota. Koordinacija monodentatnih N-donorskih heterocikličnih liganada se odvija preko slobodnog elektronskog para na atomu azota.

The phosphate removal efficiency electrocoagulation wastewater using iron and aluminum electrodes

Đuričić, T.^{a,*}, Malinović, B.N.^a, Bijelić, D.^b

^aUniversity of Banja Luka, Faculty of Technology, Stepe Stepanovica 73, 78000 Banja Luka,

²JP Dep-ot, Bulevar Živojina Mišića 23, 78000 Banja Luka, B&H

Article info

Received: 22/09/2016

Accepted: 21/12/2016

Keywords:

Electrode material, phosphate removal, electrolysis duration

*Corresponding author:

E-mail: tijana.malinovic@unibl.rs

Phone: +387 65 334 067

Fax: +387 51 434 351

Abstract: Effects of electrolysis duration, initial phosphate concentrations and supporting electrolyte concentrations on the phosphate removal efficiency by electrocoagulation using either aluminum or iron electrodes were investigated in this study. All experiments were performed in a batch electrochemical reactor on synthetically prepared wastewater of the initial volume 0.2 L. The results indicate that increase of initial phosphate concentration has reduced removal rate, and by increasing the electrolysis duration removal efficiency increases. It was found that the aluminum electrode has higher removal efficiency (98.9%) compared to the iron electrode (93.5%) for 40 minutes of treatment ($pH=3$, $j=1$ mA/cm², $\gamma_0=50$ mg/L P-PO₄). The addition of supporting electrolyte ($\gamma_{NaCl}=0.25$ g/L) is achieved removal efficiency of 50.2% for Fe and 52.1% fo Al electrode in only 10 minutes of treatment, respectively.

INTRODUCTION

Phosphorus is a natural nutrient, unavoidable in surface water which appears almost always as a phosphate ion (House, 2012). Although precious nutrient highly valuable for the agriculture, phosphate released in extensive quantities into the surface waters, causes eutrophication.

Removal of the phosphate from the drinking waters and also from the wastewater started to draw the attention of the scientists and professionals from the 1960s (Vasudevan, Sozhan, Ravichandran, *et. al.*, 2008). As a perspective methods have proven electrochemical methods of wastewater treatment (El-Shazly, Daous, 2013). The electrochemical technologies have attracted a great deal of attention, because of their versatility, which makes the treatment of liquids, gases and solids possible and environmental compatibility. These methods are electro dialysis, electrooxidation, electroflocculation and electrocoagulation (Miranzadeh, Rabbani, Dehqan, 2012). This research is focused on the electrocoagulation treatment of synthetic wastewater loaded with

phosphates. There are numerous studies on the removal of phosphorus from wastewater. Some of the studies related to electrochemical technology for wastewater treatment. Electrocoagulation process of wastewater, and consequently water containing phosphates, has become very attractive for research in the last two decades. Initially, the research was based on the research of feasibility and applicability of the process of electrocoagulation treatment of wastewater containing phosphates to the testing of the basic parameters such as current density, electrolysis duration, temperature, initial phosphate concentration, the type and concentration of supporting electrolyte and their optimization (Behbahani, Moghaddam, Arami, 2010; Shalaby, Nassef, Mubarak, *et. al.*, 2014; Bektas, Akbulut, Inan, *et. al.*, 2004; Irdemez, Yildiz, Tosunoglu, 2006; Irdemez, Demircioglu, Yildiz, 2006; Irdemez, Demircioglu, Yildiz, *et. al.* 2006). After that was carried studies with different types of electrodes such as mild steel, stainless steel, aluminum ore, zinc, copper, etc. and was carried to compare them (Vasudevan, *et. al.*, 2008; Vasudevan, Lakshmi, Jayaraj, *et. al.*, 2008; Vasudevan, Lakshmi, Sozhan, 2009; Hong,

Chang, Bae, *et al.*, 2013). Process performance was achieved as in the batch reactor (Attour, Tuoati, Tlili, *et al.*, 2014), in a flow reactor with recirculation (El-Shazly, Daous, 2013; Lacasa, Canizares, Saez, *et al.*, 2011), as well as in reactors which combine the electrocoagulation, electroflotation and the electrooxidation process (El-Masry, Sadek, Mekhemer, 2004).

Attour *et al.* in their research indicate that the phosphate removal efficiency from wastewater at Al electrode was 90% after 15 minutes of treatment. The highest removal of phosphate was obtained at a initial concentration of phosphate 50 mg/L, as an supporting electrolyte used is 4,5 mM NaCl and at a current density 1 mA/cm² (Attour *et al.*, 2014). A comparison between the phosphate removal efficiency by using Al and Fe electrodes are investigated Behbahani *et al.* At pH=3 are achieved maximum removal efficiency, which amounts to 100% for Al electrodes and 84.7% for Fe electrodes. This highest removal efficiency at a pH=3 was obtained at a initial phosphate concentration of 400 mg/L and at a current density of 250 A/m² for both types of electrodes. The turbidity of the solution is higher for Fe electrode. In the sludge was found a greater amount of PO₄³⁻ for Al electrode, which indicate higher removal efficiency (Behbahani *et al.*, 2010). During phosphate removal from the wastewater from the process of phosphating with zinc phosphate, pH 3 has proved as most effective. The highest phosphate removal was for 15 minutes of electrolysis. At optimal current density of 60 A/m² was removed 97.8% phosphate from wastewater (Kobya, Demirbas, Dedeli, 2010). In a series of research Irdemez *et al.* examined the impact of the initial phosphate concentration, current density and pH, as the main parameters of electrocoagulation Removal efficiency and reaction rate decreases with the increase of initial concentration of phosphate. According to their results, the removal efficiency increases with current density, therefore increasing energy consumption. It was found that the optimal initial pH-value of the wastewater is 3 (Irdemez *et al.* 2006, Irdemez *et al.* 2006, Irdemez *et al.* 2006).

EXPERIMENTAL

Experimental part of the research is contained by the application of electrocoagulation proces for removing of phosphates from simulated wastewater. Experimental setup is shown on the Figure 1. The batch electrochemical reactor of 250 cm³ capacity made from polypropylene with constant mixing was used, combined with two electrodes of the same area surface. The dimensions of the electrodes are 40x40x1 mm. The total effective area of one electrode is 17.2 cm², and the distance between 2 cm. Electrodes were connected to digital power source (Atten, APS3005SI; 30V, 5A) with the potentiostatic and galvanostatic operating options.

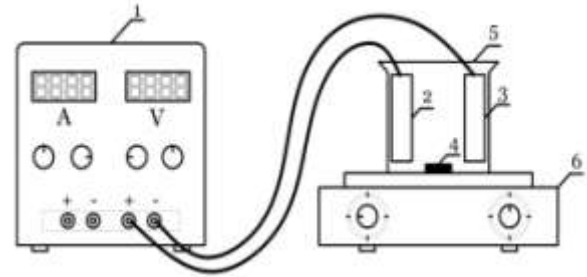


Figure 1. Schematic view of electrochemical reactor. 1 – source of electric power; 2 – anode; 3 – cathode; 4 – magnetic stir bar; 5 – electrochemical cell; 6 – magnetic stirrer

All the experiments were performed at an ambiental temperature of sample and initial volume synthetic wastewater of 200 cm³. Before each treatment electrodes were cleaned and degreased and the current density was set to a certain value. Used chemicals are of *p.a.* purity. In order to prepare synthetic wastewater of the particular concentration was used commercially available 99.3% potassium dihydrogen phosphate (KH₂PO₄), „Kemika“, Croatia. As supporting electrolyte was used 99.5% sodium chloride (NaCl), „Lachner“, Czech Republic. As an electrode material was used steel (EN 10130-91; max. 0.08% C, max. 0.12% Cr, max. 0.45% Mn, max. 0.60% Si) and aluminum (Al 99.5/EN AW-1050 A; max. 0.25% Si, max. 0.40% Fe, max. 0.05% Cu, max. 0.05% Mn, max. 0.05% Mg, max. 0.05% Ti, max. 0.07% Zn, min. 99.50% Al), which meet the required standards.

Before each experiment, in accordance to the literature data, was adjusted the optimum pH-value of the synthetic wastewater (pH=3) with HCl (Irdemez *et al.* 2006, Behbahani, *et al.*, 2010, Kobya, *et al.*, 2010). Treated synthetic wastewater after each experiment was collected and filtered through filter paper „Filtres Fioroni“, France (Ref.:0015A00007; size:125 mm; qty.: 1000). Prepared samples of synthetic wastewater before and after treatment were analyzed on the following parameters: phosphorus content (P-PO₄), total dissolved substances (TDS), pH, electrolyte resistivity (ρ) and conductivity (κ). TDS, ρ and κ are determined on the multimeter (Consort C861), and a phosphorus concentration spectrophotometrically ($\lambda_{max}=410$ nm) in the UV-VIS spectrophotometer (Perkin-Elmer, LAMBDA 25) according to a standard method (APHA, 1999). The composition of the resulting precipitate is determinate using the FTIR spectroscopy (Bruker, Tensor 27).

RESULTS AND DISCUSSION

Results for the phosphate removal by electrocoagulation are expressed by mass concentration (mg/L) and phosphate removal efficiency, E_u , in percent calculated by the followed equation:

$$E_u = \frac{\gamma_i - \gamma_f}{\gamma_i} \times 100 \% \quad (1)$$

There the γ_i and γ_f are the initial and the final concentration of the phosphate in mg/L.

Figure 2 show the influence of the electrolysis duration (2.5; 5; 10; 30; 40 min) on the reduction of phosphate concentration by using iron and aluminum electrodes, respectively. Used current density was $j=1 \text{ mA/cm}^2$ which, in accordance to the literature, was cited as the optimal current density (Attour *et al.*, 2014). Experiments were performed without the presence of supporting electrolyte and the initial concentration of phosphate $\gamma_0=50 \text{ mg/L}$. It can be seen that the aluminum electrode has a slightly greater removal efficiency (98.9%) compared to the iron electrode (93.5%), for 40 minutes of treatment, which is in accordance with previous studies (Behbahani, *et al.*, 2010).

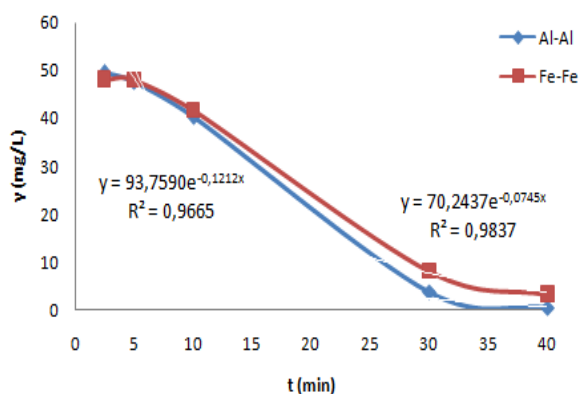


Figure 2. Phosphate concentration in relation to the electrolysis duration for iron and aluminum electrodes ($j=1 \text{ mA/cm}^2$, $t=40 \text{ min}$, $\gamma_0=50 \text{ mg/L}$, $\text{pH}=3$)

The influence of the concentration of supporting electrolyte on the phosphate removal efficiency for both electrode pairs was examined in previous research and shown in Figure 3 (Malinovic, Djuricic, Bjelajac, 2016). It was found that the optimal concentration of supporting electrolyte $\gamma_{\text{NaCl}}=0.25 \text{ g/L}$, which is significantly lower concentration compared to the previously published recommendations (Attour *et al.*, 2014; Kuokkanen, Ramo, 2014). For the case of aluminum electrodes, highest removal efficiency at a concentration of $\gamma_{\text{NaCl}}=0.25 \text{ g/L}$ was $E_u=52.1\%$, while for the iron electrode highest removal efficiency was $E_u=50.2\%$ at a same experimental conditions.

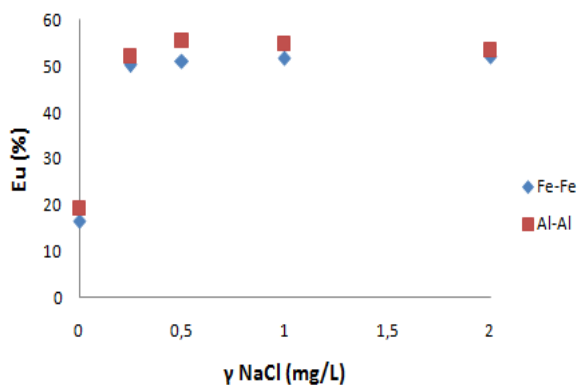


Figure 3. Removal efficiency in relation of concentration of NaCl ($j=1 \text{ mA/cm}^2$, $t=10 \text{ min}$) (Malinovic, *et al.* 2016)

By increasing the initial phosphate concentration in wastewater removal efficiency linearly decreases in the case of the both electrode pairs (Malinovic, Atlagic, Malinovic, 2016; Malinovic, Malinovic 2016) (Figures 4 and 5). At optimum current density $j=0.25 \text{ mA/cm}^2$ [19] and optimum concentration of supporting electrolyte $\gamma_{\text{NaCl}}=0.25 \text{ g/L}$ removal efficiency is increased by reducing initial phosphate concentration in wastewater (25, 50 i 100 mg/L), which is in accordance with with previous researche (Irdemez, *et al.* 2006). Efficiency was the highest at initial phosphate concentration $\gamma=25 \text{ mg/L}$ and amounts $E_u=62.6\%$ (Al), $E_u=63.4\%$ (Fe). The lowest removal efficiency was at initial phosphate concentration $\gamma=100 \text{ mg/L}$ and amounts $E_u=29.8\%$ (Al) and $E_u=30.3\%$ (Fe).

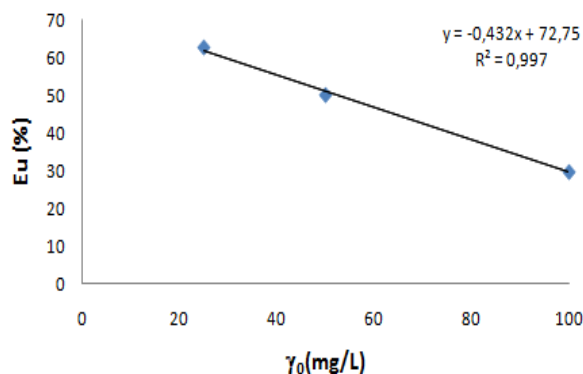


Figure 4. Removal efficiency in relation of initial phosphate concentration in wastewater, for Al electrodes ($j=0.25 \text{ mA/cm}^2$, $\gamma_{\text{NaCl}}=0.25 \text{ g/L}$, $t=10 \text{ min}$) (Malinovic, *et al.* 2016)

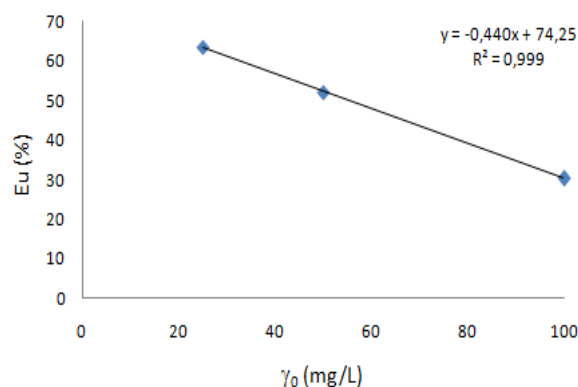


Figure 5. Removal efficiency in relation of initial phosphate concentration in wastewater, for Fe electrodes ($j=0,25 \text{ mA/cm}^2$, $\gamma_{\text{NaCl}}=0,25 \text{ g/L}$, $t=10 \text{ min}$) (Malinovic, *et al.* 2016)

In some of the previous studies electrocoagulation phosphate was researched the kinetics of the process, where concluded that the process follows a first order reaction kinetics (El-Shazly, Daous, 2013; Shalaby, Nassef, *et al.*, 2014; Zhang, Zhang, Wang, 2013). At the experimental conditions ($j=1 \text{ mA/cm}^2$, $\gamma_0=50 \text{ mg/L}$, $\text{pH}=3$), the dependence of $\ln(C_0/C)$ of the electrolysis duration (min) shows a linear relationship (Figure 6). It can be concluded that the electrocoagulation process can be described by a first order rate, which confirming the relatively high correlation coefficient for iron ($R^2=0.9837$) and aluminum electrodes ($R^2=0.9665$). Reaction rate constants of electrocoagulation phosphate

amounts $k=-0.0745 \text{ min}^{-1}$ (Fe) and $k=-0.1212 \text{ min}^{-1}$ (Al), respectively. Based on the processed data (Figure 2), equation 2 and 3 representing the dependence of the phosphate concentration variation of the electrolysis duration in electrocoagulation process using iron or aluminum electrode.

$$\gamma = 70,2437e^{-0,0745x} \quad (2)$$

$$\gamma = 93,7590e^{-0,1212x} \quad (3)$$

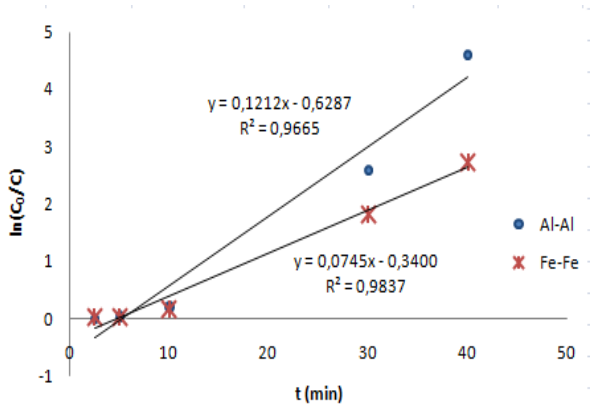


Figure 6. The dependence of $\ln(C_0/C)$ of the electrolysis duration ($j=1 \text{ mA/cm}^2$, $\gamma_0=50 \text{ mg/L P-PO}_4$, $\text{pH}=3$)

By using Fourier transform infrared spectroscopy (FTIR) method, can be determine characteristics of the obtained sediment. Using iron electrodes in the electrocoagulation process it was obtained an amorphous precipitate of iron hydroxide, and the sediment has a polymeric structure (Inan, Alaydin, 2014). For the case of aluminum electrodes, at acidic pH values, free Al^{3+} ion and $\text{Al}(\text{OH})^{2+}$ hydroxocomplex species are predominate. Precipitation of phosphate involves the dissolved cations Al^{3+} and Fe^{3+} when iron or aluminum is present in the water, $\text{FePO}_4 \cdot 2\text{H}_2\text{O}$ and $\text{AlPO}_4 \cdot 2\text{H}_2\text{O}$ or mixed $\text{Al}(\text{OH})_3\text{-AlPO}_4$ and $\text{Fe}(\text{OH})_3\text{-FePO}_4$ form (Koby, *et. al.*, 2010). In Figure 7 is shown capture FTIR spectroscopic analysis of resulting sediment after the treatment of synthetic wastewater by using aluminum electrodes.

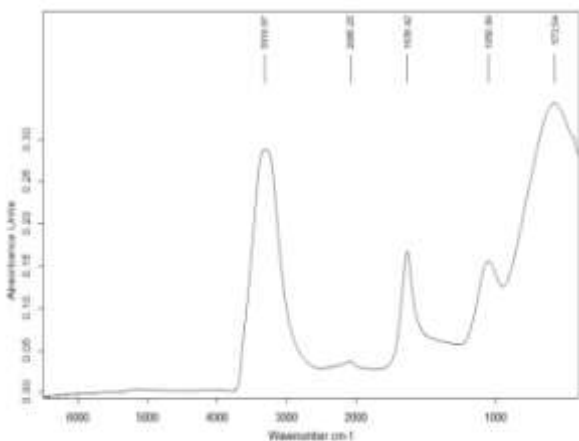


Figure 7. FTIR absorption spectrum of the resulting sediment (Al electrodes)

CONCLUSION

Using aluminum electrodes in the electrocoagulation process results a higher phosphate removal efficiency from the wastewater, in relation to the iron electrode. By increasing the electrolysis duration decreases phosphate concentration in wastewater. Based on the results, recommended concentration of the supporting electrolyte is concentration of 0.25 g/L. Increased removal efficiency is achieved with lower initial concentrations of phosphate.

REFERENCES

- APHA, (1999). *Standard Methods for Examination of Water and Wastewater*, American Public Health Association.
- Atour, A., Tuoti, M., Tlili, M., Ben Amor, M., Lapique, F., Leclerc, J.P. (2014). Influence of operating parameters on phosphate removal from water by electrocoagulation using aluminum electrodes. *Separation and purification technology*, 123, 124-129.
- Behbahani, M., Moghaddam, M.R., Arami, M. (2010). A comparison between aluminium and iron electrodes on removal of phosphate from aqueous solutions by electrocoagulation process. *International Journal of Environmental Research*, 5 (2), 403-412.
- Bektas, N., Akbulut, H., Inan, H., Dimoglo, A. (2004). Removal of phosphate from aqueous solutions by electrocoagulation. *Journal of Hazardous Materials*, 106 (2-3), 101-105.
- El-Masry, M. H., Sadek, O.M., Mekhemer, W.K. (2004). Purification of raw surface water using electrocoagulation method. *Water, Air and Soil Pollution*, 158 (1), 373-385.
- El-Shazly, A.H., Daous, M. (2013). A Kinetics and performance of phosphate removal from hot industrial effluents using a continuous flow electrocoagulation reactor. *International Journal of Electrochemical Science*, 8, 184-194.
- Hong, K., Chang, D., Bae, H., Sunwoo, S., Kim, J., Kim, D.G. (2013). Electrolytic removal of phosphorus in wastewater with noble electrode under the conditions of low current and constant voltage. *International Journal of Electrochemical Science*, 8, 8557-8571.
- House, C. D. (2012). *Standard methods for the examination of water and wastewater*, Washington: American Public Health Association Publisher.
- Inan, H., Alaydin, E. (2014). Phosphate and nitrogen removal by iron produced in electrocoagulation reactor. *Desalination and water treatment*, 52 (7-9), 1396-1403.
- Irdemez, S., Yildiz, Y., Tosunoglu, V. (2006). Optimization of phosphate from wastewater by electrocoagulation with aluminium plate electrodes. *Separation and Purification Technology*, 52 (2), 394-401.
- Irdemez, S., Demircioglu, N., Yildiz, Y.S. (2006). The effects of pH on phosphate removal from wastewater by electrocoagulation with iron plate electrodes. *Journal of Hazardous Materials*, 137 (2), 1231-1235.

- Irdemez, S., Demircioglu, N., Yildiz, Y.S., Bingul, Z. (2006). The effects of current density and phosphate concentration on phosphate removal from wastewater by electrocoagulation using aluminium and iron plate electrodes. *Separation and Purification Technology*, 52, 218-223.
- Koby, M., Demirbas, E., Dedeli, A., Sensoy, M.T. (2010). Treatment of rinse water from zinc phosphate coating by batch and continuous electrocoagulation processes. *Journal of Hazardous Materials*, 173 (1-3), 326-334.
- Kuokkanen, V., Kuokkanen, T., Ramo, J., Lassi, U., Roininen, J. (2015). Removal of phosphate from wastewaters for further utilization using electrocoagulation with hybrid electrodes - Techno-economic studies. *Journal of Water Process Engineering*, 8, e50-e57.
- Lacasa, E., Canizares, P., Saez, C., Fernandez, F.J., Rodrigo, M.A. (2011). Electrochemical phosphates removal using iron and aluminium electrodes. *Chemical Engineering Journal*, 172 (1), 137-143.
- Malinovic, B.N., Djuricic, T., Bjelajac, N. *Influence of certain process parameters on phosphate removal by electrocoagulation*, in Proceedings of IX International scientific conference contemporary materials 2016., Banja Luka. (in press).
- Malinovic, B.N., Gotovac-Atlagic, S., Malinovic, T., Bjelajac, N., Milovanovic, A. *Phosphate removal from wastewater by electrocoagulation process using aluminum electrode*, in Proceedings of 53rd Meeting of the Serbian Chemical Society, Kragujevac 2016.
- Malinovic, B.N., Malinovic, T. *Phosphate removal from wastewater by electrocoagulation process using aluminum electrode*, in Proceedings of 13th International Conference on Fundamental and Applied Aspects of Physical Chemistry, Physical Chemistry 2016, Beograd. (in press).
- Miranzadeh, M.B., Rabbani, D., Dehqan, S. (2012). Electrocoagulation process for removal of adenosine-5'-monophosphate and sodium hexamethaphosphate from synthetic wastewater. *International Journal of Physical Science*, 7 (10), 1571-1577.
- Shalaby, A., Nassef, E., Mubarak, A., Hussein, M. (2014). Phosphate removal from wastewater by electrocoagulation using aluminium electrode. *American Journal of Environmental Engineering and Science*, 1 (5), 90-98.
- Vasudevan, S., Lakshmi, J., Jayara, J., Sozhan, G. (2008). Remediation of phosphate-contaminated water by electrocoagulation with aluminium, aluminium alloy and mild steel anodes. *Journal of Hazardous Materials*, 164, 1480-1486.
- Vasudevan, S., Lakshmi, J., Sozhan, G. (2009). Optimization of the process parameters for removal of phosphate from drinking water by electrocoagulation. *Desalination and Water Treatment*, 12 (1-3), 407-414.
- Vasudevan, S., Sozhan, G., Ravichandran, S., Jayaraj, J., Lakshmi, J., Sheela, S.M. (2008). Studies on the removal of phosphate from drinking water by electrocoagulation process. *Industrial & Engineering Chemistry Research*, 47, 2018-2023.
- Zhang, S., Zhang, J., Wang, W., Li, F., Cheng, X. (2013). Removal of phosphate from landscape water using and electrocoagulation process powered directly by photovoltaic solar modules. *Solar Energy Materials and Solar Cells*, 117, 73-80.

Summary/Sažetak

U ovom radu ispitan je uticaj vremena trajanja elektrolize, početne koncentracije fosfata i koncentracije pomoćnog elektrolita na efikasnost uklanjanja fosfata elektrokoagulacijom, primjenom aluminijskih ili željeznih elektroda. Svi eksperimenti su izvedeni u šaržnom elektrohemijskom reaktoru na sintetički pripremljenoj otpadnoj vodi početnog volumena 0.2 L. Rezultati pokazuju da sa porastom početne koncentracije fosfata smanjuje se efikasnost uklanjanja, a sa porastom vremena trajanja elektrolize raste i efikasnost uklanjanja fosfata. Aluminijske elektrode pokazuju veću efikasnost uklanjanja (98.9%) u poređenju sa željeznim elektrodama (93.5%) u toku 40 minuta tretmana ($pH=3$, $j=1$ mA/cm², $\gamma_0=50$ mg/L P-PO₄). Dodatkom pomoćnog elektrolita ($\gamma_{NaCl}=0.25$ g/L) postignuta je efikasnost uklanjanja od 50.2% za Fe, odnosno 52.1% za Al, za samo 10 minuta tretmana.



Mathematical modeling and simulation of the composting process in a pilot reactor

Papračanin, E. *, Petric, I.

*Department of Chemical Engineering, Faculty of Technology Tuzla, University of Tuzla, Univerzitetska 8, 75000 Tuzla,
Bosnia & Herzegovina*

Article info

Received: 28/10/2016
Accepted: 20/12/2016

Keywords:

mathematical modeling
simulation
composting process
kinetics
pilot reactor

*Corresponding author:

E-mail: enisa.avdihodzic@untz.ba
Phone: 00-387-35-320-806

Abstract: In this paper, a mathematical model for composting process with an engineering approach was presented. The model describes the n -th order kinetics of composting process (mesophilic-thermophilic phase) with mass and heat balances in the process. Verification of the model was performed using experimental data obtained from a pilot reactor. Measured dynamic state variables used for a verification of the model were: organic matter mass, water mass in a mixture, amount of oxygen and carbon dioxide, temperature of mixture and the temperature of gas phase. The developed mathematical model was implemented in numerical software package MATLAB. Three kinetic parameters were estimated using the Marquardt method. Global sensitivity analysis and statistical F-test showed that the model is valid for predicting the change in five dynamic state variables. The advantage of the model is that it can be applied to the composting process with mixtures of different compositions in reactors with different volumes.

INTRODUCTION

Waste as a result of human activities which in the modern age, as cities developed, is a serious problem. Waste collection and disposal is necessary, as for hygiene and space reasons, because large quantities of solid waste cover huge areas (Atalia *et al.*, 2015). Waste management is a critical area in practice with regard to increase of pollution. Management techniques for organic waste are carried out in many ways: waste disposal in landfills, incineration, pyrolysis and gasification, composting and anaerobic digestion (Taiwo, 2011). According to the environmental laws of the European Union, organic waste in landfills will have to be reduced to a certain extent, it implies a choice of one of several methods for the treatment of the organic portion of municipal solid waste, of which the cheapest and most effective is composting process.

Composting is a complex biological process, in which the heterogeneous organic waste is converted into humus (compost), under the influence of mixed microbial populations in controlled conditions of moisture, temperature and aeration. The composting process can be characterized as a way of sustainable waste management (Bonoli *et al.*, 2012), and the resulting

compost can be used to improve soil quality, and can be used for fertilization and soil conditioning (Zaha *et al.*, 2011; Zorpas *et al.*, 2000).

In order to develop a process that would lead to a more efficient degradation of organic matter and reduce the negative impact of waste on the environment, mathematical modeling provides great opportunities for simulation and optimization of processes. Mathematical modeling provides the understanding of dynamic interaction between the mechanisms and provides the basis for a rational design process (Higgins and Walker, 2001). By the literature review, it can be said that most of the so far published models based on solving equations of heat balance (Bach *et al.*, 1987; Kishimoto *et al.*, 1987; Nakasaki *et al.*, 1987; Haug, 1993; Van Lier *et al.*, 1994; Kaiser, 1996; Stombaugh and Nokes, 1996; Das and Keener, 1997; Mohee *et al.*, 1998; Seki, 2000; Scholwin and Bidlingmaier, 2003; Xi *et al.*, 2005) and mass balance (Keener *et al.*, 1993; Kaiser, 1996; Stombaugh and Nokes, 1996; Das and Keener, 1997; Mohee *et al.*, 1998; Higgins and Walker, 2001). Most of the researchers observed a system for composting at the macro level, with the emphasis on reactor system

(Nakasaki *et al.*, 1987; Hogan *et al.*, 1989; Keener *et al.*, 1993; Van Lier *et al.*, 1994; Richard *et al.*, 1999; Robinzon *et al.*, 2000; Barrena *et al.*, 2005; Nakayama *et al.*, 2007; Mason, 2008). Physical modeling of processes which helps identifying process in many aspects in laboratory and pilot scale. Opposite the physical modeling, mathematical modeling enables prediction of characteristics of the process, based on the knowledge of independent data on the measured variables and process conditions. Verified mathematical model predicts, within certain limits, the characteristics of the process in the laboratory, pilot and full scale (Mason, 2007). The authors who have applied engineering approach, set the reactor in the focus of research, during which they modeled the process that involves mass balance, heat balance, as well as other processes occurring *in vivo*. Some of the authors who applied engineering approach are: Nakasaki *et al.*, (1987), Hogan *et al.*, (1989), Keener *et al.*, (1993), Van Lier *et al.*, (1994), Richard *et al.*, (1999), Robinzon *et al.*, (2000), Themelis and Kim (2002), Cronje *et al.* (2004), Barrena *et al.*, (2005), Mudhoo and Mohee (2006, 2007), Nakayama *et al.*, (2007), Mason (2008), Kumar *et al.*, (2009), Zhanget *al.*, (2010), Baptista *et al.*, (2010), Petric *et al.*, (2015), Shishido and Seki (2015). The thing that the researchers dealt with the last thirty years, is corrective functions for temperature, free space for air, moisture content and oxygen concentration. During literature review, the most important and most modeled corrective function is related to temperature. General review of corrective function for temperature, can be found in Mason (2007). A large number of the researchers modeled composting process with first order kinetics. However, models with first order kinetics are greatly simplified and the results do not agree very well with the data from the experiment, especially in the case of very heterogeneous systems. Very few of researchers described the degradation of the substrate, with kinetics *n*-th order kinetics: Briški *et al.*, (2003a, 2003b, 2007); Petric and Selimbašić (2008); Barneto *et al.*, (2010); Avdihodžić *et al.*, (2011). In their work Barneto *et al.*, (2010), gave an explanation why the composting process can not be predicted first order kinetics. The objectives of this study are related to possibilities of performing process of aerobic composting of municipal solid waste in pilot reactors, development of an integrated kinetic and reactor mathematical model to describe the decomposition of organic matter, mass transfer and heat, based on existing models, then optimization of kinetic parameters of the proposed model based on experimental data for several dynamic state variables obtained from the pilot reactor and at the end verification and validation of the developed mathematical model, with independent data and testing the sensivity of the model.

MATERIALS AND METHODS

In the experiments have been used a specially designed pilot reactors (volume 57 dm³). Pilot reactors are made of high density polyethylene, following dimensions: height 686 mm, outer diameter 330 mm, wall thickness 4.8 mm. Reactors are thermally insulated with a layer of

foamed polyethylene thickness of 10 mm. The reactors were equipped with two air inlets and a few aperture for the taking samples. Two taps are attached on the cover of reactors, one tap is used for the continuous exit gas mixture, and the second tap is used for measuring the concentration of carbon dioxide and oxygen in the reactor outlet.

Composting material

Organic fraction of municipal solid waste (OFMSW) were used in the experiment, also with poultry manure, wood chips, waste yeast from the beer industry. Basic physical and chemical characteristics of the material are shown in Table 1. The basic material used in the experiment were OFMSW, which is synthesized by mixing the food waste (42.1 mass.%), paper and cardboard (31.6 mass.%) and garden waste (26.3 mass.%)

Table 1. Basic physical and chemical characteristics of OFMSW, poultry manure, wood chips, waste yeast

Material	Moisture content (% w.b.)	Organic Matter (% d.b.)	pH	Electrical conductivity (dS m ⁻¹)	C/N ratio
OFMSW	72.44	88.17	6.70	1.790	52.73
Poultry manure	77.03	75.13	7.53	2.317	5.83
Wood chips	10.03	99.90	5.31	0.240	77.19
Waste yeast	95.61	91.55	6.46	2.795	21.19

w.b. – wet base, d.b. – drybase

Food waste is collected from restaurants in the Student Center of the University of Tuzla and the main city market in Tuzla. Garden waste which is used in the experiment collected from the city's parks and home gardens in Tuzla. The paper that was used in the experiment, consisting mainly used office paper collected at the Faculty of Technology in Tuzla. Cardboard that was used in the experiment, collected from several shopping centers in Tuzla. The role of poultry manure is to adjust the ratio of C/N, and to act as inoculum. Sawdust is added to increase aeration of mixture in reactors. Table 2 shows the percentage composition of the initial mixtures used in the reactors, and Table 3 shows the physical-chemical composition of the mixture for composting.

Table 2. Percentage composition of the starting mixture (mass.%) in the reactors

Reactor	OFMSW	Poultry manure	Wood chips	Waste yeast
1	67.6	10.8	10.8	10.8
2	77.8	5.5	11.1	5.5
3	82.0	5.1	10.3	2.6

Table 3. Basic physical and chemical characteristics of starting mixtures in reactors

Reactor	Moisture content (% w.b.)	Organic matter (% d.b.)	pH	Electrical Conductivity (dS m ⁻¹)	C/N ratio
1	71.09	90.00	6.72	1.299	71.09
2	63.09	92.96	6.80	1.303	63.09
3	65.65	89.27	6.98	1.280	65.65

Sampling and analysis

After daily mixing of the composting mixtures, samples were taken from different places in the mass (top, middle and bottom, three samples from each places) in order to obtain a representative sample. Moisture content was analyzed by dry oven method at 105°C for 24 h (APHA, 1995). The organic matter (OM) content (volatile solids) was determined after burning in an oven at 550°C for 6 h (APHA, 1995). Conversion of organic matter (%) was calculated from the initial and final organic matter mass, according to the following equation:

$$K = \frac{(m_{OTP} - m_{OTK})}{m_{OTP}} \cdot 100 \quad 1$$

m_{OTP} – mass of organic matter at the beginning of the process (kg),

m_{OTK} – mass of organic matter at the end of the process (kg).

Determination of nitrogen is carried out by the Kjeldahl method (Austrian Standard, 2001). The mass percentage of carbon (%C) is calculated according to the following equation (Haug, 1993):

$$\%C = \frac{\%OM}{1.8} \quad 2$$

Concentrations of carbon dioxide and oxygen Infrared Gas Analyzer MGA5, VarioPlus Industrial (MRU GmbH, Germany) was used. The electrochemical cell of the analyzer is used to measure the concentration of oxygen in the range of 0 to 21.0% by volume, where the accuracy of ± 0.2 vol.%.

Mathematical modeling

All details about the mathematical model (description; assumptions and simplifications; mass balances equations for water, carbon dioxide, oxygen, ammonia and nitrogen; heat balances equations for solid–liquid and gas phases; other supporting algebraic equations, explanations) can be found in the previous paper (Petric *et. al.*, 2015).

The focus in this paper will be on n -th order kinetics and on effect of temperature on reaction rate. The n -th order kinetics was applied, where the reaction rate is equal to the rate of organic matter degradation:

$$\frac{dm_{OT}}{dt} = -k \cdot m_{OT}^n \quad 3$$

Reaction rate constant is the function of temperature, oxygen concentration, pH, moisture content and free air space:

$$k = k_T \cdot k_{O_2} \cdot k_{pH} \cdot k_{H_2O} \cdot k_{SPZ} \quad 4$$

As a basis for the description of the effect of temperature on reaction rate constants, modified Arrhenius expression were used, (Fogler, 2005; Sheridan *et al.*, 2012):

$$k_T = A \cdot e^{\frac{E}{R} \left(\frac{1}{293} - \frac{1}{T} \right)} \quad 5$$

wherein:

A – frequency factor (units depending on the order of reaction),

T – thermodynamic temperature of the substrate (K),

E – activation energy (J/kmol),

R – universal gas constant (J/kmol·K).

This model has been proposed a modified form of the expression (5):

$$k_T = \alpha \cdot e^{\beta \left(\frac{1}{293} - \frac{1}{T} \right)} \quad 6$$

wherein:

$\alpha = A$ $\beta = E/R$ kinetic constants that need to be determined, together with the reaction order n in the expression (3). Other equations for correction factors in equation (4) and constants used in model are given in previous paper (Petric *et. al.*, 2015). Stoichiometric coefficient are determined later in the paper.

Mathematical model consists of twelve nonlinear ordinary differential equations with twelve dynamic state variables (mass of organic matter, mass of dissolved oxygen, mass of dissolved carbon dioxide, mass of dissolved ammonia, mass of water in the composting mixture, mass of oxygen in gas phase, mass of carbon dioxide in gas phase, mass of ammonia in gas phase, mass of water vapor in gas phase, mass of nitrogen in gas phase, temperature of gas phase, temperature of solid–liquid phase) and corresponding algebraic equations. All differential equations and algebraic equations are mutually connected and nonlinear and therefore, they have to be solved simultaneously both for the purpose of model calibration and numerical simulation.

Four different categories of data are required in the model: initial values of the dynamic state variables, constants (physical, thermodynamic and stoichiometric), kinetic parameters and operational conditions. Calculation of initial mass values for dissolved oxygen, carbon dioxide and ammonia in interstitial water was based on solubility data from literature (Perry and Green, 1997). Initial mole values of gases were calculated using the initial values of molar flows of gases, airflow rate and volume of gas phase.

Applied numerical methods and software

Algorithms for parameter estimation and numerical simulation were implemented in numerical software packages Matlab and Polymath. For numerical solution of system of differential equations, ODE23s solver, modified Rosenbrock method (Shampine and Reichelt,

1997). In order to determine the kinetic parameters, Marquardt method (Marquardt, 1963) was used with application of experimental data. As a criterion of agreement between values obtained by model and experimental data, the following target function F was taken as:

$$F = \sum_{j=1}^m \sum_{i=1}^n W_j (Y_{ij,model} - Y_{ij,eksp})^2 \quad (7)$$

wherein:

W_j – weight coefficient,

$Y_{ij,model}$ – value of dynamic state variables obtained by the model,

$Y_{ij,eksp}$ – value of dynamic state variables obtained by experiment.

After optimization of the kinetic parameters and the order of reaction, stoichiometric coefficients for oxygen, carbon dioxide and water and amount of loss of conductive-convective heat were adjusted. Experimental data used for verification of the model are: substrate temperature, temperature of the gas phase, carbon dioxide and oxygen concentration, mass of organic matter, mass of water in the substrate. The program consists a main file and three sub-routines and one file with experimental values of the dynamic state variables. The main program is used to call experimental data required for optimization, then vector of initial conditions for independent and dependent variables, as a vector of initial assumptions of parameters that need to be optimized. The main program also performs a statistical analysis by calling one of the routines for Statistics and the output is the optimization results numerically and graphically. Linear, multiple linear and nonlinear regression was performed in the software package *Polymath*. Regression is performed in order to obtain of approximate values for the initial vector parameters which are optimized using known values for corrective function of temperature and the experimental data. Sensitivity analysis was performed with the aim of evaluation relative importance of selected model parameters. Global sensitivity analysis was performed by determination the absolute and relative sensitivity of parameters. Details can be found in the previous paper (Petric *et al.*, 2015). F-statistical test, as an indicator of the sensitivity of the model was performed.

RESULTS AND DISCUSSION

Optimization of kinetic parameters

Numerical optimization presents a serious challenge in systems, such as the composting process. Problems that occur during optimization of these "live" system usually related to problems of initial conditions. First of all it is necessary to select an appropriate numerical method that would successfully solve a system of several differential equations and then even further to optimize the unknown parameters. As initial values for the of dynamic state variables in the model, experimental values are used for one of the reactors (reactor 1). The complex biochemical systems and their modeling represent the systems that is basically very difficult to simulate and optimize. The

problem of initial conditions for the parameters is solved so that the used data from previous research Avdihodžić (2011). Table 4 shows optimized values of kinetic parameters together with the mean-square deviation. Comparing the value of the standard deviation with the previous work (Petric *et al.*, 2015), valued at 0.4958, we can conclude that the selected corrective function of temperature gives significantly better results in the optimization of parameters.

Table 4. Optimized values of kinetic parameters in the mathematical model

Parameter	Value	Unit
α	$9.6595 \cdot 10^{-5}$	$\text{kg}^{1-n} \cdot \text{h}^{-1}$
β	$4.9140 \cdot 10^3$	K
n	1.5526	-

*SD² = 0.1020

Experimental data which has been used to evaluate the model parameters, are shown in Figure 1. Swedish chemist Arrhenius first proposed the dependence of the reaction rate constant of temperature, which was later confirmed through empirical and experimental data for a large number of reactions, including reactions in biological systems (Fogler, 2005). Several authors have used the Arrhenius model for temperature correction, which is a function of the reaction rate constants for the processes of degradation: Benefield and Randall (1980), Haug (1993), Mashauri and Kayombo (2002), Rousseau *et al.*, (2004), Marsili-Libelli and Checchi (2005), Nitorisavut and Klomjek (2005), Andreottola *et al.*, (2007), Kadlec (2009). Most of the authors used the mentioned corrective function for the first order kinetics, while in this study is used a model of n -th order. Model of n -th order, is proposed based on the fact that the organic waste consists many different organic compounds which decompose with different rates and different kinetics of reaction order obtained value of the activation energy is correlated with literature values. Adjusted values for stoichiometric coefficients are: Value for conductive-convective heat loss is $2650 \text{ J} \cdot \text{h}^{-1}$.

Sensitivity analysis

With the aim of testing the sensitivity of the model, values of the absolute and relative sensitivity of model parameters were calculated. Absolute and relative sensitivity of the parameters is shown in Table 5. The positive values of APS indicate that all three parameters lead to an increase in the difference between the experimental and simulation results. Sensitivity analysis was performed for a small deviation of model parameters from their optimal values (+1%). Based on the RPS values it can be concluded that the most sensitive parameter is reaction order and it has the greatest impact on the formulation of the entire model. Also, it is necessary to perform the validation of the model from the point of view of data analysis. For this purpose F-test was performed. F-test was performed

with the significance level $\alpha = 0.05$. Table 6 shows the results of the F-distribution data.

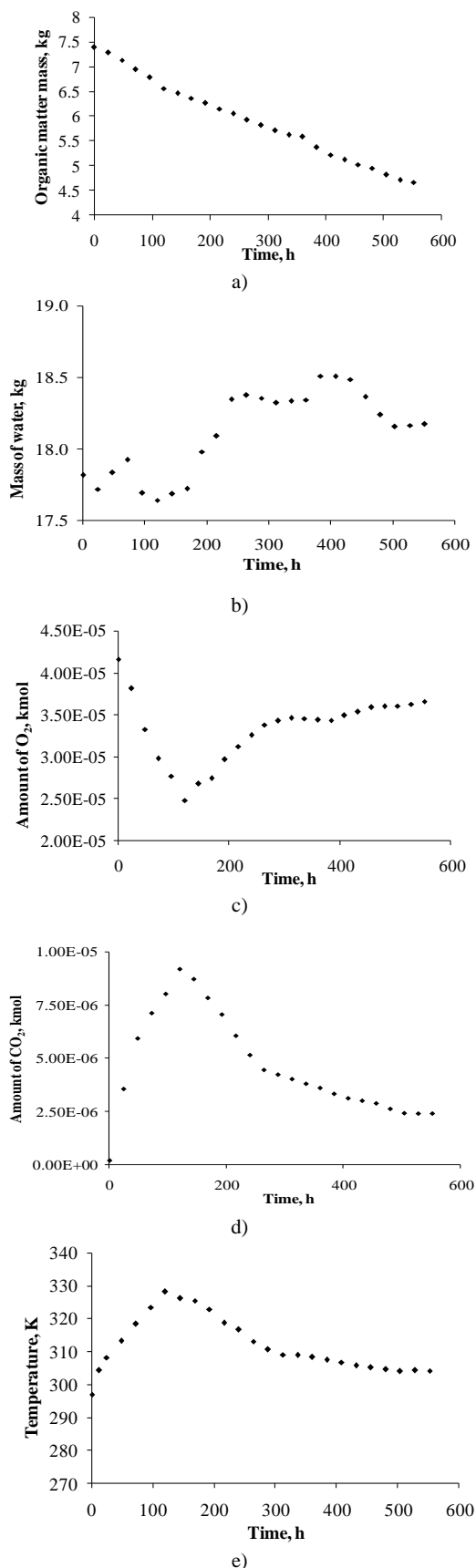


Figure 1. Experimental data from reactor 1: a) mass of organic matter, b) mass of water in substrate, c) amount of O_2 , d) amount of CO_2 , e) temperature of substrate.

The results of F-distribution show that the model is acceptable for given conditions for the four dynamic state variables. Only for the mass of water, the null hypothesis is rejected. Performing a sensitivity analysis, in terms of data for the mass of water in the substrate, similar results get Neves *et al.* (2007). In the future, it is necessary to perform a sensitivity analysis before the optimization of kinetic parameters in order to obtain more reliable simulation results.

Table 5. Parameters of the model and values of the sensitivity analysis

Parameter of the model	Value	APS	RPS
α	$9.65 \cdot 10^{-5}$	1147578	0.08932
β	4914.0	0.037635	0.14070
n	1.5526	22647.63	23.7114

^aAPS-eng. absolute parameter sensitivity

^bRPS-eng. relative parameter sensitivity

Table 6. Results of the statistical analysis of data

Dynamic state variable	σ_{exp}^a	σ_{sim}^b	Value of F-test	Testing the hypothesis
Mass of organic matter	0.7047	0.7422	1.0532	$1.0532 \leq 2.0144$
Mass of water	0.0866	0.9848	11.366	$11.366 > 2.0144$
Amount of O_2	$1.57 \cdot 10^{11}$	$2.24 \cdot 10^{11}$	1.4290	$1.4290 \leq 2.0144$
Amount of CO_2	$5.52 \cdot 10^{12}$	$6.29 \cdot 10^{12}$	1.1385	$1.1385 \leq 2.0144$
Temperature of gas phase	71.94	65.25	1.1026	$1.1026 \leq 2.0144$
Temperature of substrate	71.94	65.62	1.0962	$1.0962 \leq 2.0144$

a- variance of experimental data

b- variance of simulation data

Verification of the model

Predictive simulation models are approximate imitation of real systems, which can never accurately describe the actual system. Verification of the model was performed with data from two different reactors for five dynamic variables of state (subsection 2.5). Verification of the model with experimental data for the mass of organic matter are shown in Figure 2, mass of the water in substrate are shown in Figure 3, the amount of gases (CO_2 i O_2) are shown in Figure 4 and results for the temperature of the substrate (measured values are the same and the values calculated by model differ in the maximum $0.5^\circ C$) are shown in Figure 5. A comparison of experimental results and the numerical simulation showed good agreement throughout the entire process except when it comes to the mass of water in the substrate, where they observed certain deviations. The model shows a normal trend but experimental data shows an unusual distribution. One of the reasons why there is an unusual trend of experimental data, is the

possibility of generation of air pockets in which there has been a condensation of water vapor with the samples were taken.

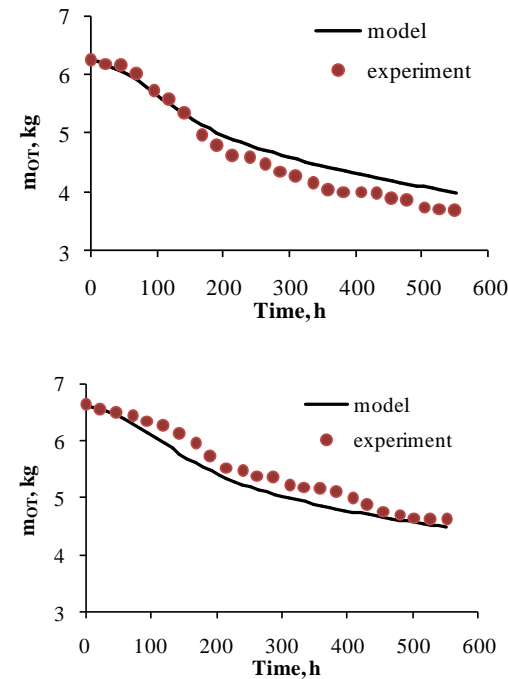


Figure 2. Verification of the model for the mass of OM: a) data from reactor 2, b) data from reactor 3.

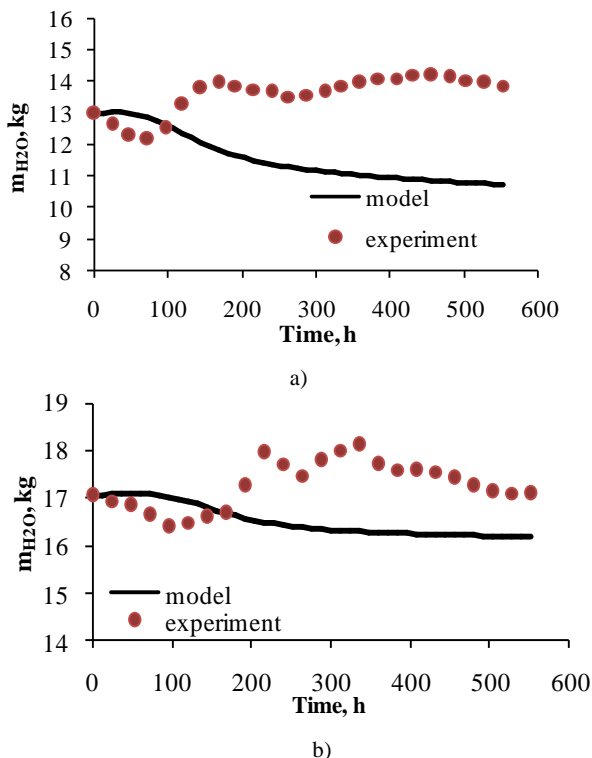


Figure 3. Verification of the model for the mass of water in the substrate: a) data from reactor 2, b) data from reactor 3.

Reaching the maximum temperature is the basis for the efficiency of the composting process (Finstein i Morris, 1975; Finstein *et al.*, 1986b) and during the period of thermophilic degradation leads to the destroying largest number of pathogens (Diaz, 2007). Temperature profiles in pilot reactors can reliably predict the temperature profiles in the processes taking place in full scale. This

fact is one of the advantages of this model. The fact that the model well described experimental data confirms that the model is valid for use on different experimental conditions, which is one of the goals of mathematical modeling. With small modifications, referring to the initial conditions, this model can successfully simulate the process of decomposition of organic solid waste with different additions. No matter what kind of substrate is used in the composting process, this model can well predict the degradation process, especially in the active stage of the process.

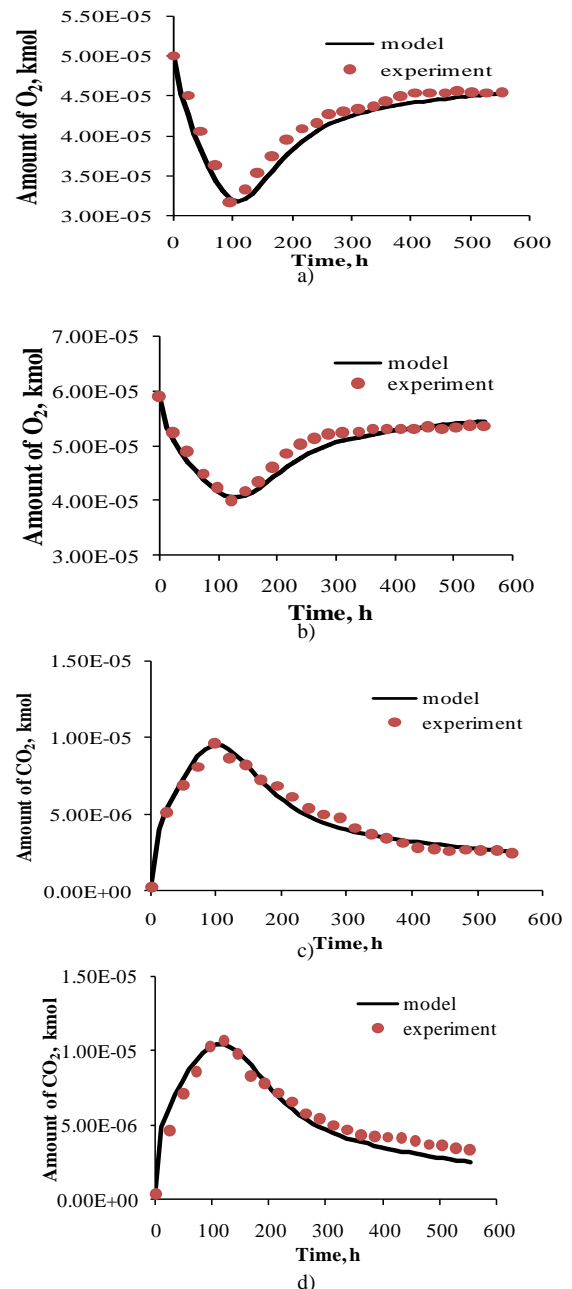


Figure 4. Model verification of the amount of gases: a) and b) verification for amount of O_2 for data from reactor 2 and 3. c) and d) verification for amount of CO_2 for data from reactor 2 and 3.

This conclusion can be justified by modeling the process kinetics of n -th reaction order. Modeling the process of n -th order kinetics, gives significantly better results when it comes to degradation of organic matter from the

standpoint of biochemical processes that occur. This was confirmed by Zhang *et al.*, (2012) and Kulcu (2015).

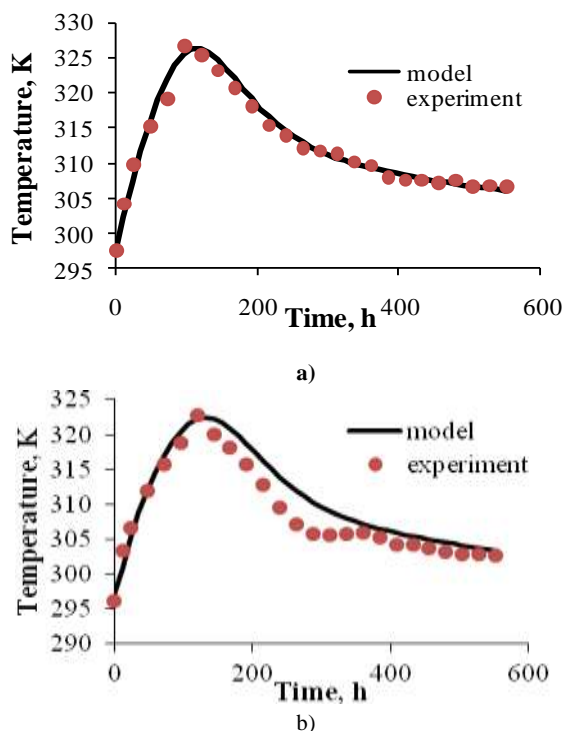


Figure 5. Verification of the model for the temperature of the substrate: a) data from reactor 2, b) data from reactor 3.

CONCLUSIONS

In this paper, the biggest problems related to mathematical modeling of the process, during the initiation of the developed mathematical model. The problem of initial conditions is solved by using data from previous studies. In the developed mathematical model the activation energy for the degradation process of waste were determinate (40855 kJ/kmol). Besides the activation energy, frequency factor is estimated ($9.6595 \cdot 10^{-5} \text{ kg}^{-1.55} \text{ h}^{-1}$) and reaction order (1.55). Global sensitivity analysis showed that variations of all three parameters affect the increase in the difference in the agreement between the model and experimental data. Reaction order is most sensitive parameter. Results of the F-distribution show that the model is acceptable for given conditions with the level of significance $\alpha = 0.05$, except of mass of water in the substrate. Verification of the model was performed for five measured dynamic state variables. The variety of initial conditions in two reactors is important for the verification of the model. The fact that the model very well describes experimental data shows that the model is valid for use on different experimental conditions. Advantage of this model is reflected in the fact that with small changes, referring to the initial conditions, can successfully simulate the composting process of organic solid waste with different additions. Heterogeneous systems, such as the material used in this study are difficult to describe with constant values stoichiometric coefficients for entire process in the future should pay attention just to the values of stoichiometric coefficients and their changes during the

process. In the future, should collect data from the plant in full scale with the aim of checking the validity of the proposed model.

REFERENCES

- Andreottola, G., Oliveira, E., Foladori, P., Zigliio, R. (2007). Respiriometric techniques for assessment of biological kinetics in constructed wetlands. *Water Science and Technology*, 56 (3) 255-261.
- APHA (American Public Health Association), *Standard Methods for the Examination of Water and Wastewater*, APHA, Washington, DC, 1995.
- Atalia, K.R., Buha, D.M., Bhavsar, K.A., Shah, N.K. (2015): A Review on Composting of Municipal Solid Waste, *IOSR Journal of Environmental Science, Toxicology and Food Technology* (IOSR-JESTFT) e-ISSN, 2319-2402.
- Avdihodžić, E. (2011). *Laboratorijska i numerička simulacija procesa kompostiranja komunalnog krutog otpada sa prisilnom aeracijom u reaktoru*, Univerzitet u Tuzli, Tehnološki fakultet Tuzla, Magistarski rad, UDK 631.879.4:519.876.5.
- Austrian Standard FLG Nr. 292/2001, Analytical Methods and Quality Control for Waste Compost (2001) Austrian Standardization Institute, Vienna.
- Bach, P.D., Nakasaki, K., Shoda, M., Kubota, H. (1987). Thermal Balance in Composting *Operations. Journal of Fermentation Technology*, 65(2), 199-209.
- Baptista, M., Antunes, F., Gonçalves, M. S., Morvan, B., Silveira, A. (2010). Composting kinetics in full-scale mechanical-biological treatment plants. *Waste Management*, 30, 1908-1921.
- Barrena R., Vázquez F., Gordillo M.A., Gea T., Sánchez A. (2005): Respiriometric assays at fixed and process temperatures to monitor composting process. *Bio-resource Technology*, 96, 1153-1159
- Barneto, A.G., Carmona, J.A., Ferrer, J.A.C., Blanco, M.J.D. (2010). Kinetic study on the thermal degradation of a biomass and its compost: Composting effect on hydrogen production. *Fuel*, 89(2), 462-473.
- Benefield, L.D., Randall, C.W. (1980). *Biological Design for Wastewater Treatment*, Prentice Hall, Englewood Cliffs.
- Bonoli, A., Dall'Ara, A. (2012). A bioremediation case of an ex-quarry area restored by paper sludge. *Journal of Biotechnology*, 157(4), 499-504.
- Briški, F., Horgas, N., Vuković, M., Gomzi, Z. (2003). Aerobic composting of tobacco industry solid waste – simulation of the process. *Clean Technologies and Environmental Policy*, 5, 295-301.
- Briški, F., Gomzi, Z., Hublin, A., Vuković, M. (2003a): Aerobno kompostiranje otpadaka voća i povrća: modeliranje procesa. *Kemija u industriji* 52 (3), 95-102.
- Briški F., Gomzi Z., Horgas N., Vuković M. (2003b): Aerobic composting of tobacco solid waste. *Acta Chim. Slov.* 50, 715-729.

- Briški, F., Vuković, M., Papa, K., Gomzi, Z., Domanovac, T. (2007): Modelling of Composting of Food Waste in a Column Reactor. *Chemical Papers*, 61(1), 24-29.
- Cronje, A.L., Turner, C., Williams, A.G., Barker, A.J., Guy, S., (2004): Composting under controlled conditions. *Environmental Science and Technology*, 24, 1221-1234.
- Das, K., Keener, H.M. (1997): Numerical Model for the Dynamic Simulation of a Large Scale Composting System. *Transactions of the ASAE*, 40(4), 1179-1189.
- Diaz, L. F., & Savage, G. M. (2007): Factors that affect the process. *Waste Management Series*, 8, 49-65.
- Fogler, H.S. (2005). *Elements of Chemical Reaction Engineering*. Prentice Hall, USA. Haug, R.T. (1993). *The practical handbook of compost engineering*. Lewis Publishers. Boca Raton, 385-436.
- Finstein, M.S., Morris, M.L. (1975): Microbiology of Municipal Solid Waste Composting. *Advances in Applied Microbiology* 19, 113-151.
- Finstein, M.S., Miller, F.C., Strom, P.F. (1986b): Monitoring and evaluating composting process performance. *Journal Water Pollution Control*, Vol. 58, No. 4, 271-278.
- Higgins, C.W., Walker, L.P. (2001). Validation of a new model for aerobic organic solids decomposition: simulations with substrate specific kinetics. *Process Biochemistry*, 36, 875-884
- Hogan, J.A., Miller, F.C., Finstein, M.S. (1989): Physical Modeling of the Composting Ecosystem. *Applied and Environmental Microbiology*, 55(5), 1082-1092.
- Kadlec, R.H. (2009): Comparison of free water and horizontal subsurface treatment wetlands. *Ecological Engineering*, 35 159-174.
- Kaiser, J. (1996). Modelling composting as a microbial ecosystem: A simulation approach. *Ecological Modelling*, 91, 25-37.
- Keener, H.M., Marugg, C., Hansen, R.C. Hoitink, H.A.J. (1993): *Optimizing the efficiency of the composting process*, in H.A.J. Hoitink, and H. Keener (Eds.), Proceedings of the International Composting Research Symposium, Renaissance Publications, Columbus, OH, 59-94.
- Kishimoto, M., Preechapan, C., Yoshida, T., Taguchi, H. (1987): Simulation of an aerobic composting of activated sludge using a statistical procedure. *MIRCEN Journal* 3, 113-124.
- Kumar, S., Sakhale, A., Mukherjee, S. (2009): Simplified Kinetic Analysis for Composting of Municipal Solid Waste. *Practice Periodical of Hazardous, Toxic, and Radioactive Waste Management*, 13(3), 179-186.
- Marquardt, D.W. (1963): An Algorithm for least Squares Estimation of Nonlinear Parameters. *Journal of the Society for Industrial and Applied Mathematics*, 11, 431.
- Marsili-Libelli S., Checchi N. (2005): Identification of dynamic models for horizontal subsurface constructed wetlands. *Ecological Modelling*, 187 201-218.
- Mashauri, D.A., Kayombo, S. (2002): Application of the two coupled models for water quality management: facultative pond cum constructed wetland models. *Physics and Chemistry of the Earth, Parts A/B/C*, 27(11), 773-781.
- Mason, I.G. (2007): *A Study of Power, Kinetics, and Modelling in the Composting Process* (PhD Thesis). University of Canterbury, New Zealand, 2007, 1-436.
- Mason, I.G. (2008): An evaluation of substrate degradation patterns in the composting process. Temperature-corrected profiles. *Waste Management*, 28, 1751-1765.
- MathWorks *Matlab*, Version 7.6.0.324, 2008, USA.
- Mohee, R., White, R.K., Das, K.C. (1998): Simulation Model for Composting Cellulosic (Bagasse) Substrates. *Compost Science and Utilization*, 6(2), 82-92.
- Mudhoo, A., Mohee, R. (2006): Sensitivity Analysis and Parameter Optimization of a Heat Loss Model for a Composting System. *Journal of Environmental Informatics*, 8(2), 100-110.
- Mudhoo, A., Mohee, R. (2007): Overall Heat Transfer Coefficients in Organic Substrates Composting. *Journal of Environmental Informatics*, 9(2), 87-99.
- Nakasaki, K., Kato, J., Akiyama, T., Kubota, H. (1987): A New Composting Model and Assessment of Optimum Operation for Effective Drying of Composting Material. *Journal of Fermentation Technology*, 65(4), 441-447.
- Nakayama, A., Nakasaki, K., Kuwahara, K., Sano, Y. (2007): A Lumped Parameter Heat Transfer Analysis for Composting Processes with Aeration. *Journal of Heat Transfer*, 129(7), 902-906.
- Neves, D.S.F., Gomes, A.P.D., Tarelho, L.A.C., Matos, M.A.A. (2007): Application of a Dynamic Model to the Simulation of the Composting Process. Proceedings Sardinia 2007, Eleventh International Waste Management and Landfill Symposium, S. Margherita di Pula, Cagliari, Italy, 1-5 October 2007, CISA, Environmental Sanitary Engineering Centre, Italy, 1-10.
- Nitorisavut, S., Klomjek, P. (2005). Inhibition kinetics of salt-affected wetland for municipal wastewater treatment. *Water Research*, 39 4413-4419.
- Perry, R.H., Green D.W. (1997). *Perry's Chemical Engineers' Handbook*, McGraw-Hill, New York.
- Petric, I., Avdihodžić, E., Ibrić, N. (2015). Numerical simulation of composting process for mixture of organic fraction of municipal solid waste and poultry manure. *Ecological Engineering*, 75, 242-249.
- Petric, I., Selimbašić, V. (2008). Development and validation of mathematical model for aerobic composting process. *Chemical Engineering Journal*, 139(2), 304-317.
- Polymath*, Educational Version 6.0, Michael Elly, (2004). The CACHE Corporation USA.
- Richard, T.L., Walker, L.P., Gossett, J.M. (1999). The Effects of Oxygen on Solid-State Biodegradation Kinetics. *Proceedings of the Institute of Biological Engineering*, 2, 10-30.

- Robinson, R., Kimmel, E., Avnimelech, Y. (2000). Energy and mass balances of windrow composting system Published by the American Society of Agricultural and Biological Engineers, St. Joseph, Michigan, *Transactions of the ASABE*, 43(5), 1253-1259.
- Rousseau, R., Schreiner, E., Kohlmeyer, A., Marx, D. (2004). Temperature-dependent conformational transitions and hydrogen-bond dynamics of the elastin-like octapeptide GVG (VPGVG): a molecular-dynamics study. *Biophysical Journal*, 86(3), 1393-1407.
- Scholwin, F., Bidlingmaier, W. (2003). *Fuzzyfying the composting process: a new model based control strategy as a device for achieving a high grade and consistent product quality*. In: Proceedings of the Fourth International Conference of ORBIT Association on Biological Processing of Organics: Advances for a Sustainable Society, 30th April-2 May, 2003, Perth, Australia. ORBIT Association, Weimar, Germany, 739-751.
- Seki, H. (2000). Stochastic Modeling of Composting Processes with Batch Operation by the Fokker-Planck Equation. *Transaction of the ASAE*, 43(1), 169-179.
- Shampine, L.F., Reichelt, M.W. (1997). The Matlab ODE Suite. *SIAM Journal on Scientific Computing*, 18, 1-22.
- Sheridan, C., Petersen, J., Rohwer, J. (2012). On modifying the Arrhenius equation to compensate for temperature changes for reactions within biological systems. *Water SA*, 38(1), 149-151.
- Shishido, T., Seki, H. (2015). Laboratory-scale Experiment for an Active-stage Composting Process under the Same Material and Operating Conditions, *Journal of Agricultural Meteorology*, 71(2), 111-123.
- Stombaugh, D.P., Nokes, S.E. (1996). Development of a biologically based aerobic composting simulation model. *Transactions of the ASAE*, 39(1), 239-250.
- Taiwo, A.M. (2011). Composting as a sustainable waste management technique in developing countries, *Journal of Environmental Science and Technology*, 4(2), 93-102.
- Themelis, N.J., Kim, Y.H. (2002). Material and energy balances in a large-scale aerobic bioconversion cell. *Waste Management and Research*, 20, 234-242.
- Van Lier, J.J.C., Van Ginkel, J.T., Straatsma, G., Gerrits, J.P.G., Van Griensven, L.J.L.D. (1994). Composting of mushroom substrate in a fermentation tunnel: compost parameters and a mathematical model. *Netherlands Journal of Agricultural Science*, 42(4), 271-292.
- Xi, B., Wei, Z., Liu, H. (2005). Dynamic Simulation for Domestic Solid Waste Composting Processes. *The Journal of American Science*, 1(1), 34-45.
- Zah, C., Saucius, A., Dumitrescu, L., Manciulea, I. (2011). Aspects regarding recycling sludge by composting. *Environmental Engineering and Management Journal*, 10, 219-224.
- Zhang, J., Gao, D., Chen, T.B., Zheng, G.D., Che, J., Ma, C., Guo, S.L., Du, W. (2010). Simulation of substrate degradation in composting of sewage sludge. *Waste Management*, 30, 1931-1938.
- Zorpas, A.A., Kapetanios, E., Zorpas, G.A., Karlis, P., Vlyssides, A., Haralambous, I., Loizidou, M. (2000). Compost produced from organic fraction of municipal solid waste, primary stabilized sewage sludge and natural zeolite. *Journal of Hazardous Materials*, 77, 149-159.

Summary/Sažetak

U ovom radu je predstavljen matematički model procesa kompostiranja sa inženjerskim pristupom. Model je opisan kinetikom n -tog reda (mezofilno-termofilna faza) zajedno sa bilansom mase i topline u procesu. Verifikacija modela je izvedena korištenjem eksperimentalnih podataka dobijenih iz pilot reaktora. Mjerene dinamičke varijable, korištene za verifikaciju modela su: masa organskih tvari, masa vode u supstratu, količina kisika i ugljičnog dioksida, temperatura smjese i temperature gasne faze. Razvijeni matematički model implementiran je u numerički softverski paket MATLAB, pri čemu su određena su tri kinetička parametra korištenjem Marquardt metode. Globalna analiza osjetljivosti i F -statistički test su pokazali da je model validan za predviđanje pet dinamičkih varijabli stanja. Prednost ovog modela se ogleda u činjenici da se ovaj model može primijeniti na proces kompostiranja smjese različitog sastava u reaktorima različitih volumena.



Development and validation of the mathematical model for synthesis of maleic anhydride from *n*-butane in a fixed bed reactor

Petric, I., Karić E.*

Department of Chemical Engineering, Faculty of Technology, University of Tuzla,
Univerzitetska 8, 75000 Tuzla, Bosnia and Herzegovina

Article info

Received: 14/10/2016
Accepted: 28/12/2016

Keywords:

modeling
n-butane
maleic anhydride
fixed bed reactor
simulation
kinetic models

Corresponding author: Ervin Karić

E-mail: ervin.karic@untz.ba

Phone: +387 60 321-5468

Fax: +387 35 320-741

Abstract: The aims of this study were the following: development of the mathematical model for numerical simulation of partial oxidation of *n*-butane to maleic anhydride in a fixed bed reactor and validation of developed mathematical model with real process data from industrial reactor located in the Global Ispat Coke Industry Lukavac. Mathematical model is consisted of differential equations that describe mass balances of each species, energy balance, stoichiometry of reactions, pressure drop, kinetic model. Numerical software package Polymath with Runge-Kutta-Fehlberg method was used for numerical solution of differential equations. The developed mathematical model was validated with three process data sets of five measured variables (temperature, pressure, concentration of *n*-butane, concentration of carbon dioxide, concentration of carbon monoxide) and with application of ten kinetic models from literature. Comparison of simulation results and measured data showed a good agreement for three kinetic models. For the chosen kinetic model, profiles of temperature, molar flows, conversion of *n*-butane and selectivity of maleic anhydride were also presented.

INTRODUCTION

Maleic anhydride is a chemical compound with multiple applications in the chemical industry. It is used for the production of polyester and alkyd resins, additives for lubricating oil, as the acid in the food industry, polymeric materials etc. When *n*-butane replaced benzene as a raw material for the production of maleic anhydride, it has enabled the development of highly active and selective catalyst. New process for the production of maleic anhydride enabled higher yields with lower investments. Higher yields of maleic anhydride are achieved with oxygen concentration lower than its stoichiometric amount. Among many industrial processes, partial oxidation of *n*-butane to maleic anhydride has received a special attention because of its economic profitability as well as a high demand for maleic anhydride as chemical product. Modern commercial processes for the production of the maleic anhydride are based on a selective oxidation of *n*-butane over a vanadium-phosphorus oxide catalyst in

fixed bed reactors and fluidized bed reactors (Dente *et al.*, 2003). Fixed bed reactor is well known technology, whose improvement is based on the modification of catalyst rather than design of a reactor. Cruz-Lopez *et al.* (2005) investigated the selective oxidation of *n*-butane in a membrane reactor. They used a high concentration of *n*-butane. Fixed bed reactor is limited to processes with a low concentration of *n*-butane (below 2%), while a fluid bed reactor can operate with a higher concentration of *n*-butane. Gascón *et al.* (2006) investigated the kinetics of oxidation of *n*-butane to maleic anhydride over a vanadium catalyst of commercial phosphorus under aerobic and anaerobic conditions in the temperature range from 400 to 435°C. Fluid bed reactor has higher efficiency for heat removal, better temperature control and a lower yield of maleic anhydride compared to fixed bed reactor. Diedenhoven *et al.* (2012) developed a model for dynamics of phosphoric oxidation of *n*-butane to

maleic anhydride with a vanadium-phosphorus-oxide catalyst. The model showed that reverse sorption processes determine the content of phosphorus in the catalyst which is based on a vanadium-phosphorus oxide. With addition of certain phosphorus concentration, the loss can be compensated, while exceed of phosphorus concentration can cause a complete deactivation of the catalyst. Trifirò and Grasefi (2014) analyzed the key aspects for oxidation of *n*-butane to maleic anhydride using a mixture of a vanadium-phosphorus oxide catalyst, in order to determine relevant parameters required for optimization of the catalyst.

Mathematical models provide a powerful tool for simulation and design of process equipment in chemical/process industry, as well as for determination of the conditions of optimal performance. Results of these studies can serve as useful guidelines for improving the design and operation of the plants well as for improving the performance of the whole process without a need for expensive tests on the plant.

The aims of this study were the following: development of the mathematical model for numerical simulation of partial oxidation of *n*-butane to maleic anhydride in a fixed bed reactor and validation of developed mathematical model with real process data from industrial reactor located in the Global Ispat Coke Industry Lukavac.

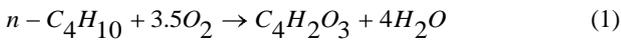
MATHEMATICAL MODEL

The following assumptions and simplifications were taken into account while developing the model:

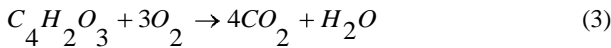
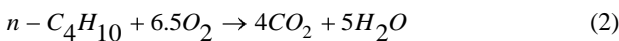
- there are no radial gradients of temperature and concentration in the reactor,
- a reactor operates in a steady-state,
- pseudo one-dimensional model is used,
- pressure drop coefficient is assumed,
- overall heat transfer coefficient is taken from the reference Sharma *et al.* (1991).

The mechanism of reaction set I (in the case of application of the kinetics models (12) and (13)).

The main reaction:

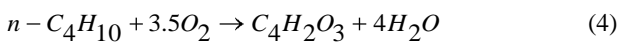


Side reactions:

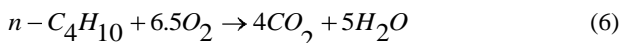
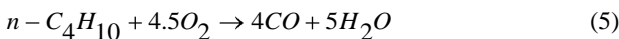


The mechanism of reaction set II (in the case of application of the kinetics models (7), (8), (9), (10), (11), (14), (15) and (16)).

The main reaction:



Side reactions:



The investigated kinetic models are:

Alonso *et al.* (2001):

$$r_1 = \left\{ 1.96 \cdot e^{\left[\frac{-125000}{R} \left(\frac{1}{T} - \frac{1}{653} \right) \right]} \right\} \cdot \frac{C_B}{\left[1 + \frac{59 \cdot C_B}{C_O} + \frac{26 \cdot C_M}{C_O} \right]}$$

$$r_2 = \left\{ 0.86 \cdot e^{\left[\frac{-145000}{R} \left(\frac{1}{T} - \frac{1}{653} \right) \right]} \right\} \cdot \frac{C_B}{\left[1 + \frac{59 \cdot C_B}{C_O} + \frac{26 \cdot C_M}{C_O} \right]}$$

$$r_3 = \left\{ 0.07 \cdot e^{\left[\frac{-180000}{R} \left(\frac{1}{T} - \frac{1}{653} \right) \right]} \right\} \cdot \frac{C_M}{\left[1 + \frac{59 \cdot C_B}{C_O} + \frac{26 \cdot C_M}{C_O} \right]} \quad (7)$$

$$r_1 = \left\{ 0.61 \cdot e^{\left[\frac{-116000}{R} \left(\frac{1}{T} - \frac{1}{653} \right) \right]} \right\} \cdot \frac{C_B}{\left[1 + \frac{20 \cdot C_B}{C_O} + \frac{12 \cdot C_M}{C_O} \right]}$$

$$r_2 = \left\{ 0.3 \cdot e^{\left[\frac{-130000}{R} \left(\frac{1}{T} - \frac{1}{653} \right) \right]} \right\} \cdot \frac{C_B}{\left[1 + \frac{20 \cdot C_B}{C_O} + \frac{12 \cdot C_M}{C_O} \right]}$$

$$r_3 = \left\{ 0.04 \cdot e^{\left[\frac{-138000}{R} \left(\frac{1}{T} - \frac{1}{653} \right) \right]} \right\} \cdot \frac{C_M}{\left[1 + \frac{20 \cdot C_B}{C_O} + \frac{12 \cdot C_M}{C_O} \right]} \quad (8)$$

$$r_1 = \left\{ 0.86 \cdot e^{\left[\frac{-80000}{R} \left(\frac{1}{T} - \frac{1}{653} \right) \right]} \right\} \cdot \frac{C_B}{\left[1 + \frac{20 \cdot C_B}{C_O} + \frac{12 \cdot C_M}{C_O} \right]}$$

$$r_2 = \left\{ 0.11 \cdot e^{\left[\frac{-80000}{R} \left(\frac{1}{T} - \frac{1}{653} \right) \right]} \right\} \cdot \frac{C_B}{\left[1 + \frac{20 \cdot C_B}{C_O} + \frac{12 \cdot C_M}{C_O} \right]}$$

$$r_3 = \left\{ 0.19 \cdot e^{\left[\frac{-98000}{R} \left(\frac{1}{T} - \frac{1}{653} \right) \right]} \right\} \cdot \frac{C_M}{\left[1 + \frac{20 \cdot C_B}{C_O} + \frac{12 \cdot C_M}{C_O} \right]} \quad (9)$$

$$\left[\frac{\text{kmol}}{\text{kgcat} \cdot \text{s}} \right]$$

Buchanan and Sundaresan (1986):

$$r_1 = \left[1.96 \cdot 10^{10} \cdot e^{\frac{-125000}{R-T}} \right] \cdot \frac{C_B}{\left[1 + \frac{59 \cdot C_B}{C_O} + \frac{26 \cdot C_M}{C_O} \right]}$$

$$r_2 = \left[3.40 \cdot 10^{11} \cdot e^{\frac{-145000}{R-T}} \right] \cdot \frac{C_B}{\left[1 + \frac{59 \cdot C_B}{C_O} + \frac{26 \cdot C_M}{C_O} \right]}$$

$$r_3 = \left[1.70 \cdot 10^{13} \cdot e^{\frac{-180000}{R-T}} \right] \cdot \frac{C_M}{\left[1 + \frac{59 \cdot C_B}{C_O} + \frac{26 \cdot C_M}{C_O} \right]} \quad (10)$$

$$r_1 = \left[1.16 \cdot 10^9 \cdot e^{-\frac{116000}{RT}} \right] \cdot \frac{C_B}{\left[1 + \frac{20 \cdot C_B}{C_O} + \frac{12 \cdot C_M}{C_O} \right]}$$

$$r_2 = \left[7.50 \cdot 10^9 \cdot e^{-\frac{130000}{RT}} \right] \cdot \frac{C_B}{\left[1 + \frac{20 \cdot C_B}{C_O} + \frac{12 \cdot C_M}{C_O} \right]}$$

$$r_3 = \left[4.80 \cdot 10^9 \cdot e^{-\frac{138000}{RT}} \right] \cdot \frac{C_M}{\left[1 + \frac{20 \cdot C_B}{C_O} + \frac{12 \cdot C_M}{C_O} \right]} \quad (11)$$

$$\left[\frac{\text{kmol}}{\text{kgcat} \cdot \text{s}} \right]$$

Centi *et al.* (1985):

$$r_1 = \frac{2.191 \cdot 10^{-4} \cdot 2616 \cdot C_B \cdot C_O^{0.2298}}{1 + 2616 \cdot C_B}$$

$$r_2 = 7.028 \cdot 10^{-5} \cdot C_O^{0.2298}$$

$$r_3 = 4.989 \cdot 10^{-6} \cdot C_M \cdot \left(\frac{C_O^{0.6345}}{C_B^{1.151}} \right) \quad (12)$$

$$\left[\frac{\text{mol}}{\text{kgcat} \cdot \text{s}} \right]$$

Marín *et al.* (2010):

$$r_1 = \left\{ 3.73 \cdot 10^{-4} \cdot e^{-\left[\frac{86515.5}{R} \left(\frac{1}{T} - \frac{1}{613} \right) \right]} \right\} \cdot \frac{C_B}{\left[1 + \frac{0.08 \cdot C_B}{C_O} + \frac{124.24 \cdot C_M}{C_O} \right]}$$

$$r_2 = \left\{ 8.76 \cdot 10^{-5} \cdot e^{-\left[\frac{103293.1}{R} \left(\frac{1}{T} - \frac{1}{613} \right) \right]} \right\} \cdot \frac{C_B}{\left[1 + \frac{0.08 \cdot C_B}{C_O} + \frac{124.24 \cdot C_M}{C_O} \right]}$$

$$r_3 = \left\{ 1.65 \cdot 10^{-4} \cdot e^{-\left[\frac{146052}{R} \left(\frac{1}{T} - \frac{1}{613} \right) \right]} \right\} \cdot \frac{C_M}{\left[1 + \frac{0.08 \cdot C_B}{C_O} + \frac{124.24 \cdot C_M}{C_O} \right]} \quad (13)$$

$$\left[\frac{\text{mol}}{\text{kgcat} \cdot \text{s}} \right]$$

Lorences *et al.* (2003):

$$r_1 = \left\{ 2.17 \cdot e^{-\left[\frac{54418}{R} \left(\frac{1}{T} - \frac{1}{653} \right) \right]} \right\} \cdot \frac{C_B}{\left[1 + \frac{14 \cdot C_B}{C_O} + \frac{208 \cdot C_M}{C_O} \right]}$$

$$r_2 = \left\{ 1.34 \cdot e^{-\left[\frac{104650}{R} \left(\frac{1}{T} - \frac{1}{653} \right) \right]} \right\} \cdot \frac{C_B}{\left[1 + \frac{14 \cdot C_B}{C_O} + \frac{208 \cdot C_M}{C_O} \right]}$$

$$r_3 = \left\{ 0.19 \cdot e^{-\left[\frac{66976}{R} \left(\frac{1}{T} - \frac{1}{653} \right) \right]} \right\} \cdot \frac{C_M}{\left[1 + \frac{14 \cdot C_B}{C_O} + \frac{208 \cdot C_M}{C_O} \right]} \quad (14)$$

$$\left[\frac{\text{kmol}}{\text{kgcat} \cdot \text{s}} \right]$$

Schneider *et al.* (1987):

$$r_1 = 9.66 \cdot 10^{-5} \cdot \frac{0.11 \cdot 10^{-5} \cdot p_O^{\frac{1}{2}}}{1 + 0.11 \cdot 10^{-5} \cdot p_O^{\frac{1}{2}}} \cdot p_B$$

$$r_2 = 1.72 \cdot 10^{-5} \cdot \frac{4.2 \cdot 10^{-5} \cdot p_O}{1 + 4.2 \cdot 10^{-5} \cdot p_O} \cdot p_B$$

$$r_3 = 2.21 \cdot 10^{-5} \cdot \frac{4.2 \cdot 10^{-5} \cdot p_O}{1 + 4.2 \cdot 10^{-5} \cdot p_O} \cdot p_B \quad \text{atm} \quad (15)$$

Sharma *et al.* (1991):

$$r_1 = \left\{ 0.96 \cdot 10^{-6} \cdot e^{-\left[\frac{93100}{R} \left(\frac{1}{T} - \frac{1}{673} \right) \right]} \right\} \cdot p_B^{0.54} \cdot (1 + 310 \cdot p_M)^{-1}$$

$$r_2 = \left\{ 0.15 \cdot 10^{-6} \cdot e^{-\left[\frac{93100}{R} \left(\frac{1}{T} - \frac{1}{673} \right) \right]} \right\} \cdot p_B^{0.54}$$

$$r_3 = \left\{ 0.29 \cdot 10^{-5} \cdot e^{-\left[\frac{155000}{R} \left(\frac{1}{T} - \frac{1}{673} \right) \right]} \right\} \cdot p_M \cdot (1 + 310 \cdot p_M)^{-2} \quad \text{atm} \quad (16)$$

A – n-C₄H₁₀, B – O₂, C – C₄H₂O₃, D – CO₂, E – H₂O, F – CO

The molar balance of components is given by the equation:

$$\frac{dF_i}{dW} = r_i \quad (17)$$

where: *i* – component, *F_i* – molar flow of component *i* (kmol/h), *r_i* – reaction rate for component *i* (kmol/(kg·h)), *W* – mass of catalyst (kg).

The heat balance is given by the equation:

$$\frac{dT}{dW} = \frac{U \cdot a \cdot (T_a - T) + \sum_{j=1}^m r_{ji} \cdot \Delta H_{Rji}}{\sum_{i=1}^n F_i \cdot C_{pi}} \quad (18)$$

where: *i* – component, *j* – reaction, *U* – overall heat transfer coefficient (kJ/(m²·h·K)), *a* – area of heat exchange A per unit volume of reactor *V* (1/m), *A* – surface of heat exchange (m²), *V* – volume of reactor (m³), *C_{pi}* – specific heat capacity of component *i* (kJ/(kmol·K)), *T_a* – ambient temperature (K), *T* – temperature of the reaction mixture in reactor (K), *r_{ji}* – rate of the *j* reaction for the *i* component (kmol/(kg·h)), *ΔH_{Rji}* – heat of the *j* reaction for the *i* component (kJ/kmol).

Concentrations of components *C_i* in the reactions are given by the equation:

$$C_i = C_{T0} \cdot \left(\frac{F_i}{F_T} \right) \cdot \left(\frac{T_0}{T} \right) \cdot \left(\frac{P}{P_0} \right) \quad (19)$$

where: *i* – number of component, *C_{T0}* – total concentration of reaction mixture (kmol/m³), *F_T* – total molar flow of reaction mixture (kmol/h), *F_i* – molar flow

of component i (kmol/h), T_0 – inlet temperature of the reaction mixture (K), T – temperature of the reaction mixture in reactor (K), P_0 – inlet pressure of the reaction mixture (bar), P – pressure of the reaction mixture in reactor (bar).

The total inlet concentration of reaction mixture C_{T0} :

$$C_{T0} = \frac{P_0}{R \cdot T_0} \quad (20)$$

where: R – universal gas constant, (J/(mol·K)).

The total molar flow of reaction mixture F_T :

$$F_T = \sum_{i=1}^n F_i \quad (21)$$

Relative rates of reaction in reaction j in compact notation:

$$\frac{r_{ji}}{v_{ji}} = \frac{r_{jk}}{v_{jk}} \quad (22)$$

where: j – reaction; i, k – component, v – stoichiometric coefficient, r – reaction rate.

The pressure drop is given by the equation:

$$\frac{dP}{dW} = -\frac{\alpha}{2} \cdot \frac{T}{T_0} \cdot \frac{P_0}{\left(\frac{P}{P_0}\right)} \cdot \frac{F_T}{F_{T0}} \quad (23)$$

where: α – pressure drop parameter (1/kg).

The conversion of n -butane is given by the equation:

$$X_A = \frac{F_{A0} - F_A}{F_{A0}} \quad (24)$$

where: F_{A0} – inlet molar flow of n -butane (kmol/h), F_A – outlet molar flow of n -butane (kmol/h).

The yield of maleic anhydride is given by the equation:

$$\tilde{Y}_C = \frac{F_C}{F_{A0} - F_A} \quad (25)$$

where: F_C – outlet molar flow of maleic anhydride (kmol/h).

The selectivity of maleic anhydride is given by the equation:

$$\tilde{S}_{CE} = \frac{F_C}{F_E} \quad (26)$$

where: F_E – outlet molar flow of water (kmol/h).

Input data for mathematical model are: $T_0=431.15$ K, $P_0=134000$ Pa, $F_{A0}=20.98$ kmol/h, $F_{B0}=262.1$ kmol/h, $F_{D0}=0.4$ kmol/h, $F_{E0}=6.72$ kmol/h, $T_a=683.15$ K, $W=0.6359$ kg, $U=107$ W/(m²·K), $\alpha=0.8$ kg⁻¹, $A=0.00035$ m², $V=0.0013$ m³, $a=0.26923$ m⁻¹, $R=8.314$ J/(mol·K).

$$\Delta\hat{H}_R^{(I)} = -1242655.575 + 8.039 \cdot T + 0.0124025 \cdot T^2 - (J/mol) \quad (27)$$

$$-0.00004 \cdot T^3 + 1.85255 \cdot 10^{-8} \cdot T^4$$

$$\Delta\hat{H}_R^{(II)} = -2646628.37 + 48.939 \cdot T + 0.013971 \cdot T^2 - (J/mol) \quad (28)$$

$$-0.0000517 \cdot T^3 + 3.07003 \cdot 10^{-8} \cdot T^4$$

$$\Delta\hat{H}_R^{(III)} = -1428408 + 40.9 \cdot T - 0.026385 \cdot T^2 - (J/mol) \quad (29)$$

$$C_{PA} = 9.487 + 0.3313 \cdot T - 1.108 \cdot 10^{-4} \cdot T^2 - (J/(mol·K)) \quad (30)$$

$$-2.2821 \cdot 10^{-9} \cdot T^3$$

$$C_{PB} = 28.106 - 3.68 \cdot 10^{-6} \cdot T + 1.475 \cdot 10^{-5} \cdot T^2 - (J/(mol·K)) \quad (31)$$

$$-1.065 \cdot 10^{-8} \cdot T^3$$

$$C_{PC} = -13.075 + 0.3484 \cdot T - 2.184 \cdot 10^{-4} \cdot T^2 + (J/(mol·K)) \quad (32)$$

$$+ 4.839 \cdot 10^{-8} \cdot T^3$$

$$C_{PD} = 19.975 + 7.343 \cdot 10^{-2} \cdot T - 5.601 \cdot 10^{-5} \cdot T^2 + (J/(mol·K)) \quad (33)$$

$$+ 1.715 \cdot 10^{-8} \cdot T^3$$

$$C_{PE} = 32.243 + 1.923 \cdot 10^{-3} \cdot T + 1.055 \cdot 10^{-5} \cdot T^2 - (J/(mol·K)) \quad (34)$$

$$- 3.596 \cdot 10^{-9} \cdot T^3$$

$$C_{PF} = 30.896 - 1.285 \cdot 10^{-2} \cdot T + 2.789 \cdot 10^{-5} \cdot T^2 - (J/(mol·K)) \quad (35)$$

$$- 1.271 \cdot 10^{-8} \cdot T^3$$

Numerical software package Polymath with Runge-Kutta-Fehlberg method was used for a numerical solution of differential equations.

RESULTS AND DISCUSSION

Tables 1-3 show comparisons of the results of numerical simulations with measured values of outlet process parameters, differences between numerical simulations results and measured values of outlet process parameters, and percentage deviations of the numerical simulations results from measured values of outlet reactor process parameters. From October 2015, the reactor in the Global Ispat Coke Industry Lukavac operates with a new catalyst Polycat MAC 4 ML (manufacturer POLYNT, Italy). The measured outlet process parameters are: temperature, pressure, volume percentages of n -butane, carbon dioxide and carbon monoxide. The best agreement of simulation results and measured values was achieved with application of the kinetic model (15) by Schneider *et al.* (1987) for December 2015 and February 2016, while the best agreement for January 2016 was achieved with application of the kinetic model (16) by Sharma *et al.* (1991).

Table 1: Comparisons of results of numerical simulation and measured values of outlet process parameters.

Kinetic model	T_{out} (K)	P_{out} (bar)	% butane			
			n -butane	CO ₂	CO	
Measured value	A	682.74	0.664	0.29	1.05	1.03
	B	678.9	0.672	0.28	1.08	1.06
	C	683.15	0.662	0.30	1.30	1.06
	(7)	650.12	0.644	0.48	3.43	4.58
	(8)	657.04	0.622	0.40	3.08	2.01
	(9)	640.69	0.659	0.47	2.72	5.42
	(10)	650.32	0.644	0.49	3.43	142
	(11)	651.97	0.643	0.37	2.89	2.89
	(12)	674.09	0.610	0.86	0.91	-
	(13)	673.03	0.615	0.43	2.19	-
	(14)	628.99	0.689	0.55	4.26	2.12
	(15)	682.75	0.601	0.79	0.84	1.21
	(16)	678.51	0.603	0.82	0.87	1.05

Legend: A - average values for December 2015, B - average values for January 2016, C - average values for February 2016, T_{out} – outlet temperature of the reaction mixture (K), P_{out} – outlet pressure of the reaction mixture (bar), %butane - outlet volume percentage of n -butane, %CO₂ - outlet volume percentage of carbon dioxide, %CO - outlet volume percentage of carbon monoxide.

Table 2: Differences between results of numerical simulation and measured values of outlet process parameters.

Kinetic model	T_{out} (%)	P_{out} (%)	% n -butane (%)	% CO_2 (%)	% CO (%)
(7)	4.78	3.01	-65.52	-226.67	-344.66
	4.24	4.17	-71.43	-217.59	-332.08
	4.84	2.72	-60.00	-163.85	-332.08
(8)	3.76	6.33	-37.93	-193.33	-95.15
	3.22	7.44	-42.86	-185.19	-89.62
	3.82	6.04	-33.33	-136.92	-89.62
	6.16	0.75	-62.07	-159.05	-426.21
(9)	5.67	1.93	-67.86	-151.85	-411.32
	6.21	0.45	-56.67	-109.23	-411.32
(10)	4.75	3.01	-68.97	-226.67	-37.86
	4.21	4.17	-75.00	-217.59	-33.96
	4.8	2.72	-63.33	-163.85	-33.96
	4.51	3.16	-27.59	-175.24	-180.58
(11)	3.97	4.32	-32.14	-167.59	-172.64
	4.56	2.87	-23.33	-122.31	-172.64
	1.27	8.13	-196.55	13.33	-
(12)	0.71	9.23	-207.14	15.74	-
	1.33	7.85	-186.67	30.00	-
	1.42	7.38	-48.28	-108.57	-
(13)	0.86	8.48	-53.57	-102.78	-
	1.48	7.10	-43.33	-68.46	-
(14)	7.87	-3.77	-89.66	-305.71	-105.83
	7.35	-2.53	-96.43	-294.44	-100.00
	7.93	-4.08	-83.33	-227.69	-100.00
(15)	0.001	9.49	-172.41	20.00	-17.48
	-0.57	10.57	-182.14	22.22	-14.15
	0.059	9.21	-163.33	35.38	-14.15
(16)	0.62	9.19	-182.76	17.14	-1.94
	0.057	10.27	-192.86	19.44	0.94
	0.68	8.91	-173.33	33.08	0.94

The best agreement of simulation values for outlet pressure and measured values was achieved with application of the kinetic model (9) by Alonso *et al.* (2001). The best agreement of simulation values for volume percentage of *n*-butane and measured values was achieved with application of the kinetic model (11) by Buchanan and Sundaresan (1986). The best agreement of simulation values for outlet volume percentage of carbon dioxide and measured values was achieved with application of the kinetic model (12) by Centi *et al.* (1985).

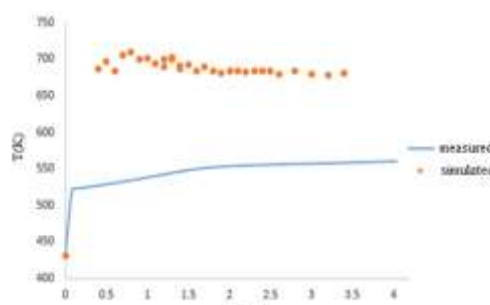
The best agreement of simulation values for outlet volume percentage of carbon monoxide and measured values was achieved with application of the kinetic model (16) by Sharma *et al.* (1991). Larger deviations of simulation values of outlet volume percentages *n*-butane, carbon dioxide and carbon monoxide, for some kinetic models, probably occurred due to the simplified reaction schemes and simplified reactor model. The largest and the least deviations for the outlet temperature of reaction mixture were observed with application of the kinetic model (14) by Lorences *et al.* (2003), and with application of the kinetic model (15) by Schneider *et al.* (1987). The largest and the least deviations for the outlet pressure of reaction mixture were observed with application of the kinetic model (15) by Schneider *et al.* (1987) and with application of the kinetic model (9) by Alonso *et al.* (2001). The largest and the least deviations for the outlet volume percent of *n*-butane were observed with application of the kinetic model (16) by Sharma *et al.*

(1991) and with application of the kinetic model (11) by Buchanan and Sundaresan (1986). The largest and the least deviations for the outlet volume percent of carbon dioxide were observed with application of the kinetic model (14) by Lorences *et al.* (2003) and with application of the kinetic model (12) by Centi *et al.* (1985). The largest and the least deviations for the outlet percent of reaction mixture were observed with application of the kinetic model (9) by Alonso *et al.* (1991) and with application of the kinetic model (16) by Sharma *et al.* (1991).

Table 3: Percentage deviations of results of numerical simulation from measured values of outlet reactor process parameters.

Kinetic model	T_{out} (K)	P_{out} (bar)	% n -butane	% CO_2	% CO
(7)	32.62	0.02	-0.19	-2.38	-3.55
	28.78	0.028	-0.2	-2.35	-3.52
	33.03	0.018	-0.18	-2.13	-3.52
(8)	25.7	0.042	-0.11	-2.03	-0.98
	21.86	0.05	-0.12	-2.00	-0.95
	26.11	0.04	-0.1	-1.78	-0.95
(9)	42.05	0.005	-0.18	-1.67	-4.39
	38.21	0.013	-0.19	-1.64	-4.36
	42.46	0.003	-0.17	-1.42	-4.36
(10)	32.42	0.02	-0.2	-2.38	-0.39
	28.58	0.028	-0.21	-2.35	-0.36
	32.83	0.018	-0.19	-2.13	-0.36
(11)	30.77	0.021	-0.08	-1.84	-1.86
	26.93	0.029	-0.09	-1.81	-1.83
	31.18	0.019	-0.07	-1.59	-1.83
(12)	8.65	0.054	-0.57	0.14	-
	4.81	0.062	-0.58	0.17	-
	9.06	0.052	-0.56	0.39	-
(13)	9.71	0.049	-0.14	-1.14	-
	5.87	0.057	-0.15	-1.11	-
	10.12	0.047	-0.13	-0.89	-
(14)	53.75	-0.025	-0.26	-3.21	-1.09
	49.91	-0.017	-0.017	-3.18	-1.06
	54.16	-0.027	-0.027	-2.96	-1.06
(15)	-0.01	0.063	0.063	0.21	-0.18
	-3.85	0.071	0.071	0.24	-0.15
	-0.4	0.061	0.061	0.46	-0.15
(16)	4.23	0.061	0.061	0.18	-0.02
	0.39	0.069	0.069	0.21	0.01
	4.64	0.059	0.059	0.43	0.01

Figures 1-10 show a comparison of simulated and measured values for temperatures of the reaction mixture along reactor length for different kinetic models that were used in the simulation.

**Figure 1:** Comparison of simulation and measured values for temperature of reaction mixture reactor length, in the kinetic model (7) by Alonso *et al.* (2001)

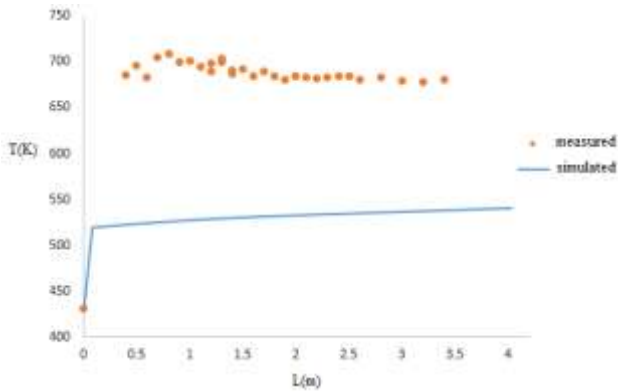


Figure 2: Comparison of simulation and measured values for temperature of reaction mixture along reactor length, in the kinetic model (8) by Alonso *et al.* (2001).

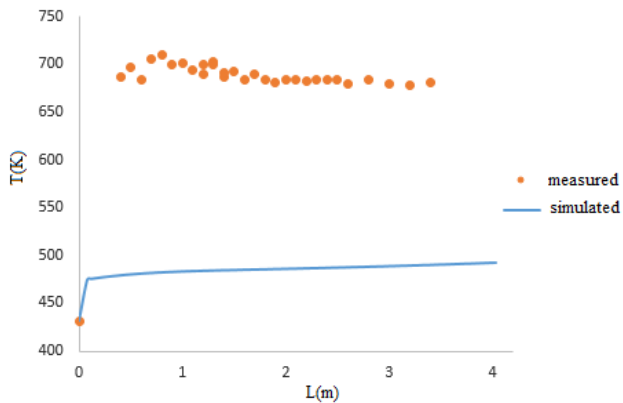


Figure 3: Comparison of simulation and measured values for temperature of reaction mixture along reactor length, in the kinetic model (9) by Alonso *et al.* (2001).

Alonso *et al.* (2001) investigated the kinetics (kinetic models (7), (8) and (9)) in a pilot membrane reactor with fluid bed of catalyst (located inside the porous membrane). The application of kinetics obtained from a fluidized bed reactor on industrial fixed bed reactor is the main reason for a poor agreement of simulation results and measured values.

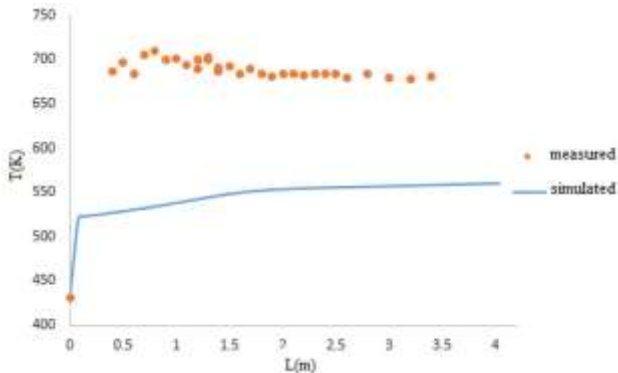


Figure 4: Comparison of simulation and measured values for temperature of reaction mixture along reactor length, in the kinetic model (10) by Buchanan and Sundaresan (2001).

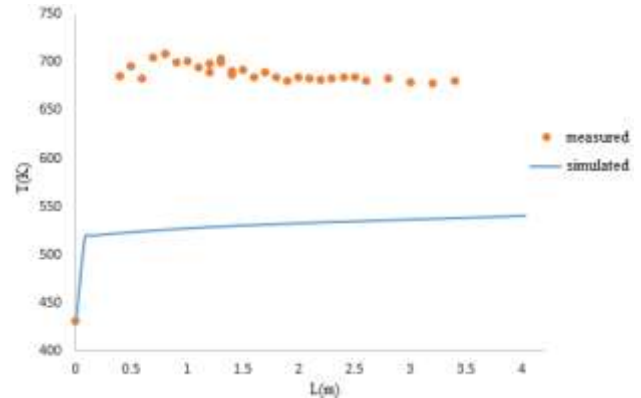


Figure 5: Comparison of simulation and measured values for temperature of reaction mixture along reactor length, in the kinetic model (11) by Buchanan and Sundaresan (2001).

Buchanan and Sundaresan (1986) investigated the kinetic models (10) and (11) and determined the kinetics for partial oxidation of *n*-butane over a vanadium phosphate catalyst. They also determine the effect of phosphorus on the kinetics of the oxidation of *n*-butane. They used a tubular reactor with internal tube diameter of 7 mm and catalyst diameter of 4 mm. These values significantly differ from the values in the industrial plant of Global Ispat Coke Industry Lukavac (internal diameter tubes 21 mm, catalyst diameter 2 mm) and this fact had a major impact on a poor agreement of simulation results and measured values in the present study.

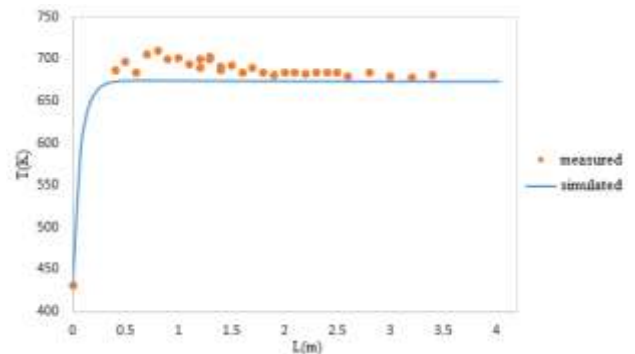


Figure 6: Comparison of simulation and measured values for temperature of reaction mixture along reactor length, in the kinetic model (12) by Centi *et al.* (1985).

Centi *et al.* (1985) investigated the kinetic model (12) and they used a fixed bed reactor based on a vanadium-phosphorus oxide. Inlet temperature was between 370 and 410°C. Simulated temperatures of the reaction mixture along reactor length with kinetic model (6) show good agreement with measured values in the present study, due to the use of similar type of reactor and the same type of catalyst. The kinetic model (14) uses the concentrations of *n*-butane, oxygen, and maleic acid.

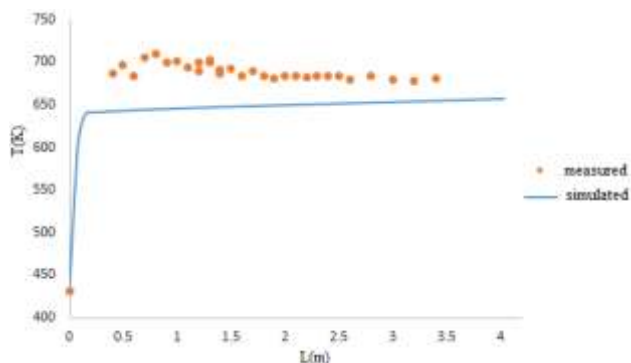


Figure 7: Comparison of simulation and measured values for temperature of reaction mixture along reactor length, in the kinetic model (13) by Marín *et al.* (2010).

Marín *et al.* (2010) investigated the kinetic model for partial oxidation of *n*-butane to maleic anhydride in a membrane reactor with enhanced heat transfer through the membrane walls. They also investigated the influence of the reactor length, flow rate of gas phase, inlet temperature of reaction mixture and inlet concentration of *n*-butane on *n*-butane conversion and selectivity of maleic anhydride. They used fixed bed reactor with the catalyst tubes (inner diameter of 34 mm, length of 0.5 m). In the industrial plant of Global Ispat Coke Industry Lukavac, a reactor tube with inner diameter 21 mm and length of 3.7 m was used. Therefore, the differences in the main dimensions of reactor (laboratory reactor versus industrial reactor) were possible cause of a poor agreement of simulation results and measured values in the present study. The kinetic model (13) uses the concentration of *n*-butane, oxygen, and maleic acid.

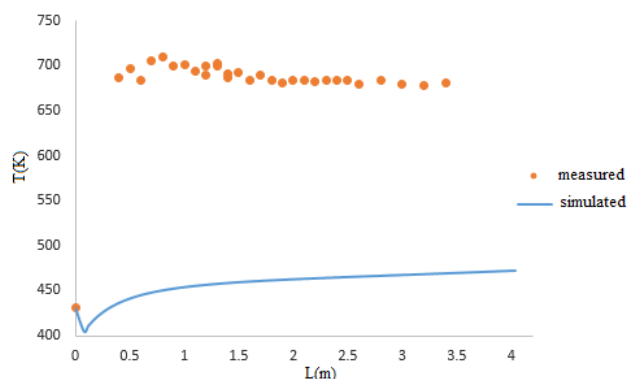


Figure 8: Comparison of simulation and measured values for temperature of reaction mixture along reactor length, in the kinetic model (14) by Lorences *et al.* (2003).

Lorences *et al.* (2003) investigated the kinetic model (14) with a wide range of operating conditions in order to assess their impacts on environmental pollution, the selectivity of maleic anhydride, bio-based products, productivity and reaction rate. The experiment was performed with a catalyst based on a vanadium-phosphorus oxide in a fluid bed reactor (inner diameter 0.04 m, height of 0.79 m). Volume percentages of *n*-butane at reactor inlet were 2, 5 and 9%. In the industrial reactor of Global Ispat Coke Industry Lukavac, volume percentage of *n*-butane at reactor inlet is 1.65%. The differences in the inlet volume percentages of *n*-butane is probably the main reason for a poor agreement of simulation and measured values in the present study.

Moreover, kinetic model (14) uses the concentrations of *n*-butane, oxygen, and maleic acid.

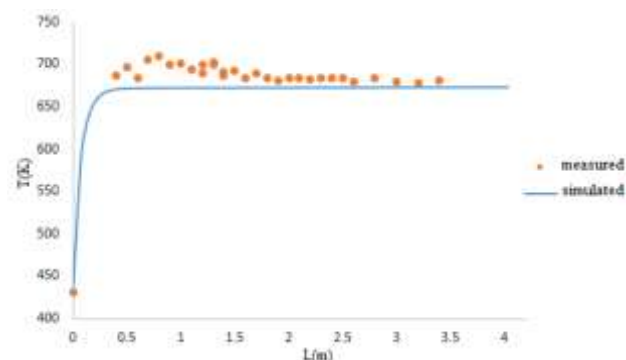


Figure 9: Comparison of simulation and measured values for temperature of reaction mixture along reactor length, in the kinetic model (15) by Schneider *et al.* (1987).

Schneider *et al.* (1987) investigated the kinetics (kinetic model (15)) of the oxidation of *n*-butane over a catalyst based on a vanadium-phosphorus oxide (reactor length of 6.5 m, internal diameter of tube 1.15 cm). Simulation values of temperatures of the reaction mixture along reactor length for the kinetic model (15) show a good agreement with measured values (Figure 9) in the present study. The kinetic model (15) uses the partial pressures of *n*-butane, oxygen, and maleic acid.

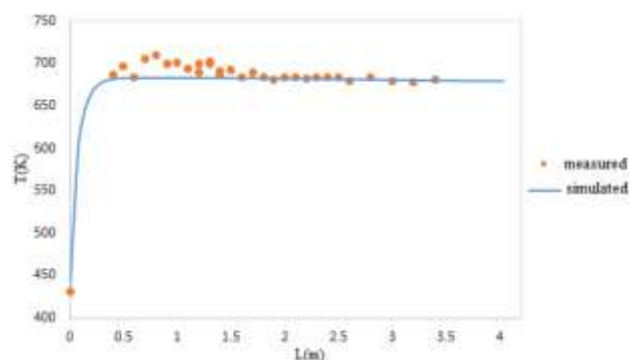


Figure 10: Comparison of simulation and measured values for temperature of reaction mixture along reactor length, in the kinetic model (16) by Sharma *et al.* (1991).

Sharma *et al.* (1991) investigated the kinetic model of selective oxidation of *n*-butane to maleic anhydride (kinetic model (16)). They used data from commercial fixed bed reactor with a catalyst based on a vanadium-phosphorus oxide. The volume percentage of butane at the reactor was 1.81%. The kinetic model used the partial pressures of *n*-butane, oxygen, and maleic acid. Simulation values of temperature of reaction mixture along reactor length show good agreement with measured values (Figure 10) in the present study. The same type of reactor and similar type of catalyst was used in industrial plant of Global Ispat Coke Industry Lukavac. Figures 11-16 show the conversion of *n*-butane, the yield of maleic anhydride, the selectivity of maleic anhydride, the molar flow rate of *n*-butane, the molar flow rate of maleic anhydride, the molar flow rate of oxygen, all along reactor length (the application of kinetic model by Sharma *et al.* (1991)).

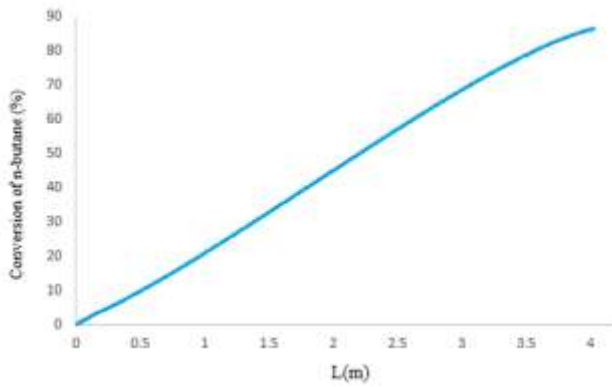


Figure 11: Conversion of *n*-butane along reactor length.

Centi *et al.* (1985) investigated the dependence of the conversion of *n*-butane as a function of space time from the physical inputs of the reaction mixture in the reactor to the exit of the reaction mixture from the reactor. Space time is correspondent with length of the reactor tube. The conversion of *n*-butane is increased by the space-time reactor, as shown in the present study.

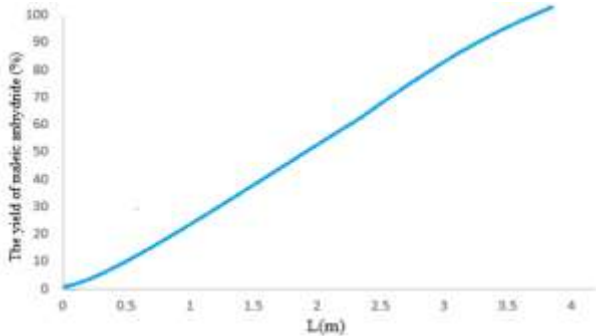


Figure 12: Yield of maleic anhydride along reactor length.

Alonso *et al.* (2001) investigated the yield of maleic anhydride by the length of the reactor tube. They found that the yield of maleic anhydride along reactor length, which has been shown in this study.

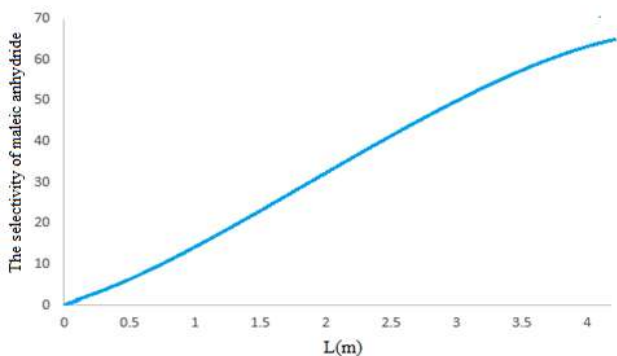


Figure 13: Selectivity of maleic anhydride along reactor length.

Moser and Schrader (1984) investigated the selectivity of maleic anhydride in a function of space time from the inlet of reaction mixture in a reactor to the outlet of reaction mixture from the reactor. The selectivity of maleic anhydride was increased with increase of space time, as it was shown in the present study.

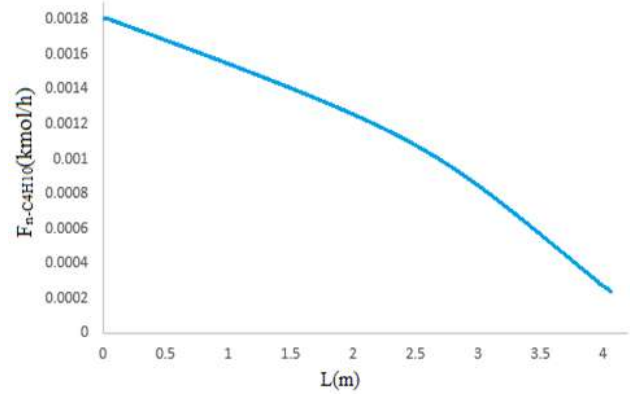


Figure 14: Molar flow rate of *n*-butane along reactor length.

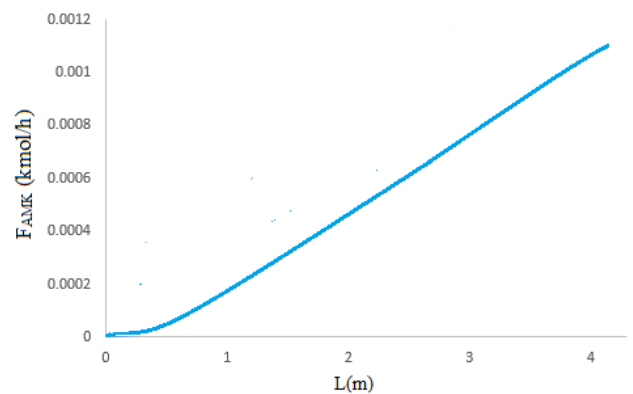


Figure 15: Molar flow rate of maleic anhydride along reactor length.

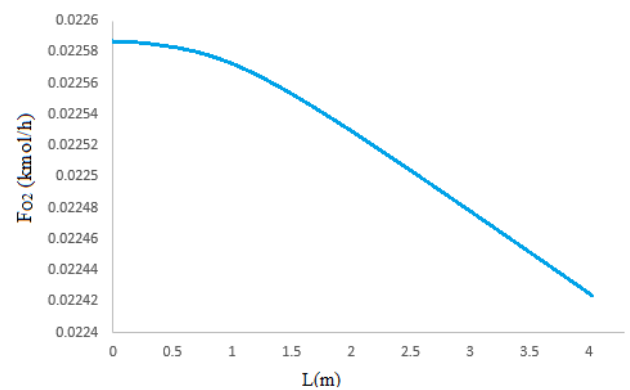


Figure 16: Molar flow rate of oxygen along reactor length.

CONCLUSIONS

The mathematical model for numerical simulation of partial oxidation of *n*-butane to maleic anhydride in a fixed bed reactor was developed. Validation of developed mathematical model was performed with real process data from industrial reactor. The mathematical model was validated with three process data sets of five measured variables (temperature, pressure, concentration of *n*-butane, concentration of carbon dioxide, concentration of carbon monoxide) and with application of ten kinetic models from literature. Comparison of simulation results and measured data showed a good agreement with application of three kinetic models: (12) (by Centi *et al.*, 1985), (15) (by Schneider *et al.*, 1987) and (16) (by Sharma *et al.*, 1991). The profiles along reactor length for the main process parameters (conversion of *n*-butane, the yield of maleic anhydride, the selectivity of maleic

anhydride, the molar flow rate of *n*-butane, the molar flow rate of maleic anhydride, the molar flow rate of oxygen) were also analyzed. Future work is directed to improvement of the model, further validation of the model and optimization of the process performance.

REFERENCES

- Alonso, M., Lorences, M.J., Pina, M.P., Patience, G.S. (2001). Butane partial oxidation in an externally fluidized bed-membrane reactor. *Catalysis Today*, 67(1-3), 151-157.
- Buchanan, J.S., Sundaresan, S. (1986). Kinetics and Redox Properties of Vanadium Phosphate Catalysts for Butane Oxidation. *Applied Catalysis*, 26, 211-226.
- Centi, G., Fornasari, G., Trifirò, F. (1985). *n*-butane oxidation to maleic anhydride on vanadium-phosphorus oxides: Kinetic analysis with a tubular flow stacked-pellet reactor. *Industrial & Engineering Chemistry Research Development*, 24, 32-37.
- Cruz-Lopez, A., Guilhaume, N., Miachon, S., Dalmon, J.A. (2005). Selective oxidation of butane to maleic anhydride in a catalytic membrane reactor adapted to rich butane feed. *Catalysis Today*, 107-108, 949-956.
- Dente, M., Pierucci, S., Tronconi, E., Cecchini, Mr., Ghelfi, F. (2003). Selective oxidation of *n*-butane to maleic anhydride in fluid bed reactors: detailed kinetic investigation and reactor modelling. *Chemical Engineering Science*, 58, 643-648.
- Diedenhoven, J., Reitzmann, A., Mestl, G., Turek, T. (2012). A Model for the Phosphorus Dynamics of VPO Catalysts during the Selective Oxidation of *n*-Butane to Maleic Anhydride in a Tubular Reactor. *Chemie Ingenieur Technik*, 84(4), 1-8.
- Gascón, J., Valenciano, R., Téllez, C., Herguido, J., Menéndez, M. (2006). A generalized kinetic model for the partial oxidation of *n*-butane to maleic anhydride under aerobic and anaerobic conditions. *Chemical Engineering Science*, 61, 6385-6394.
- Lorences, M.J., Patience, G.S., Diez, F.V., Coca, J. (2003). Butane Oxidation to Maleic Anhydride: Kinetic Modeling and Byproducts. *Industrial & Engineering Chemistry Research*, 42, 6730-6742.
- Marín, P., Hamel, C., Ordóñez, S., Diez, F.V., Tsotsas, E., Seidel-Morgenstern, A. (2010). Analysis of a fluidized bed membrane reactor for butane partial oxidation to maleic anhydride: 2D modelling. *Chemical Engineering Science*, 65, 3538-3548.
- Moser, T.P., Schrader, G.L., 1985. Selective Oxidation of *n*-Butane to Maleic Anhydride by Model V-P-O Catalysis. *Journal of Catalysis*, 92, 216-231.
- Schneider, P., Emig, G., Hofmann, H. (1987). Kinetic investigation and reactor simulation for the catalytic gas-phase oxidation of *n*-butane to maleic anhydride. *Industrial & Engineering Chemistry Research*, 26, 2326-2241.
- Sharma, R.K., Cresswell, D.L., Newson, E.J. (1991). Kinetics and fixed-bed reactor modelling of butane oxidation to maleic anhydride. *American Institute of Chemical Engineers Journal*, 37(1), 39-47.
- Trifirò, F., Grasselli, R. K. (2014). How the Yield of Maleic Anhydride in *n*-Butane Oxidation, Using VPO Catalysts, was Improved Over the Years. *Topics in Catalysis*, 57(14-16), 1188-1195.

Summary/Sažetak

Ciljevi ove studije su bili: razvoj matematičkog modela za numeričku simulaciju oksidacije *n*-butana u anhidrid maleinske kiseline u industrijskom cijevnom reaktoru sa nepokretnim slojem katalizatora i verifikacija razvijenog matematičkog modela sa stvarnim procesnim veličinama sa industrijskog reaktora koji se nalazi Global Ispat Koksna Industrija d.o.o. Lukavac. Matematički model se sastoji od diferencijalnih jednačina koje opisuju materijalni bilans svake komponente, energetske bilans, stehiometriju reakcija, pad pritiska, kinetički model. Za rješavanje diferencijalnih jednačina korišten je numerički softverski paket Polymath sa Runge-Kutta-Fehlberg metodom. Razvijeni matematički model je verificiran sa tri seta procesnih podataka od pet mjerenih varijabli (temperatura, pritisak, koncentracija *n*-butana, koncentracija ugljikovog dioksida, koncentracija ugljikovog monoksida) i sa primjenom deset kinetičkih modela preuzetih iz literature. Usporedba simulacijskih rezultata i mjerenih podataka je pokazala dobro slaganje za tri kinetička modela. Za odabrani kinetički model, prikazani su profili temperature, molarnih protoka, konverzije *n*-butana i selektivnosti anhidrida maleinske kiseline.



Nanosensors applications in agriculture and food industry

Enisa Omanović-Miklićanin^a, Mirjana Maksimović^b

^aFaculty of Agriculture and Food Sciences, University of Sarajevo, Zmaja od Bosne 8, 71 000 Sarajevo, B&H

^bFaculty of Electrical Engineering, University of East Sarajevo, Vuka Karadžića 30, 71123 East Sarajevo, B&H

Abstract info

Received: 25/10/2016
Accepted: 21/12/2016

Keywords:

Nanotechnology
Nanosensors
Agriculture
Food
Food Industry

Corresponding author:

Enisa Omanović-Miklićanin
enisa.omanovic.miklicanin@gmail.com
+387 33 225 727
+387 33 667 427

Abstract: Food safety is very important issue in food industry and agriculture because it is directly related to the influence of food on the human health. Recent food safety incidents (such as the melamine affair in 2007 and 2008) and public health concerns about synthetic food additives and chemical residues in food have driven the need to develop rapid, sensitive, and reliable methods to detect those food hazards. An alternative is given in the rapid development of nanosensors which have advantage to detect food components in an easy and quick manner. Linking nanosensors with modern Information and Communication Technologies (ICTs) enables novel and online ways for different components detection accompanied with high accuracy. Various types of nanosensors are being developed to meet the different requirements in food inspection (nanosensors for detection of external and internal conditions in food packaging, carbon nanotubes based electrochemical sensors for detection of cations, anions and organic compounds in food, various aptamers for detection of pesticides, antibiotics, heavy metals, microbial cells and toxins).

The work reviews development and application of the most present nanosensors in agriculture and food industry.

INTRODUCTION

Food safety is a prime concern of human life. With increased globalization of food this implies the importance of food quality assessment in all steps of agri-food supply chain. The chain includes all steps “from the

farm to the table” production, distribution, processing, and marketing of agricultural food products to the final consumers (Fig. 1) (Ahumada and Villalobos 2009).

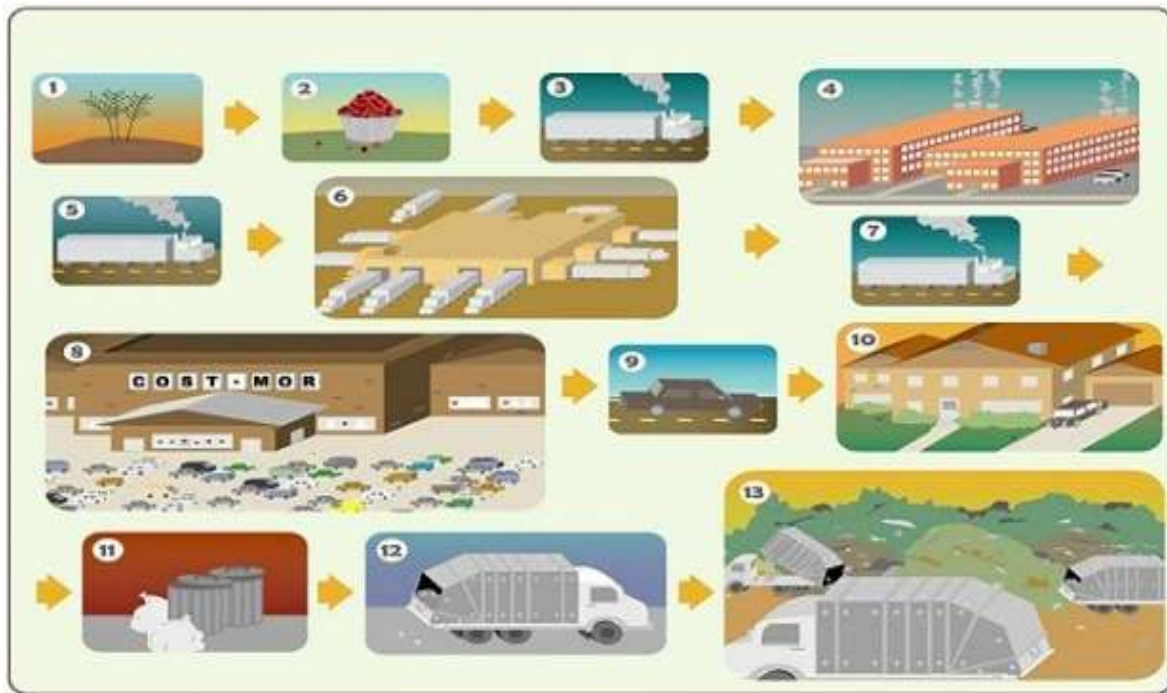


Fig.1 Agri-food supply chain (QS Article 2012)

Globalization of food production along with consumer concerns related to food quality and safety have resulted in interconnected and global systems for the production and distribution of food, followed by significant increase in food standards (Sharma et al. 2015). This approach required a move from the former end-of-line product inspection approach to a new environment in which quality assurance is required at every step of food production chain to ensure safe food and to show compliance with regulatory and customer requirements. As a result, upcoming quality and food safety assessment procedures will require additional essential elements such as low detection limits, high sensitivity and specificity, miniaturization of instrumentation for portable use, simple sample preparation steps (Craig et al. 2013).

At laboratory level, food safety can be quantitatively assessed by various methods, including cell culture and fine instrumental analysis. The main disadvantage of these methods is long analysis time ranging from several hours to days, usually with different pretreatment steps. However, food safety is nowadays threatened by contaminants which cannot be detected with standard analytical methods e.g. formaldehyde, plant pathogens, excessive pesticide residues, (Li and Sheng 2014). The inadequacy of conventional methods to solve new challenges in food safety, leads to the development of new, miniaturized and fast analytical techniques with low detection limits. Nanotechnology aspects integrated with analytical tools present one of the key solutions for development of new devices.

In addition, nanotechnology, as one of the exciting new fields of research, has great promise in addressing many of the pressing needs in the food and agriculture sectors by opening new avenues of food production, manufacturing and packaging, plant cropping and animal feeding. In the food sector, this technology has great potential to improve food functionality and quality. Unfortunately, many of the nanotechnological tools for food and agriculture field are still on a research level. Only practical applications of nanotechnology are in food packaging and in nanosensors for detection of food contaminants. Nanotechnology, nanominerals and nanosensors in the agri-food sector, including feed and nutrient components, intelligent packaging and quick-detection systems, can be seen as new source of key improvements in the agrarian sector (Fig. 2).

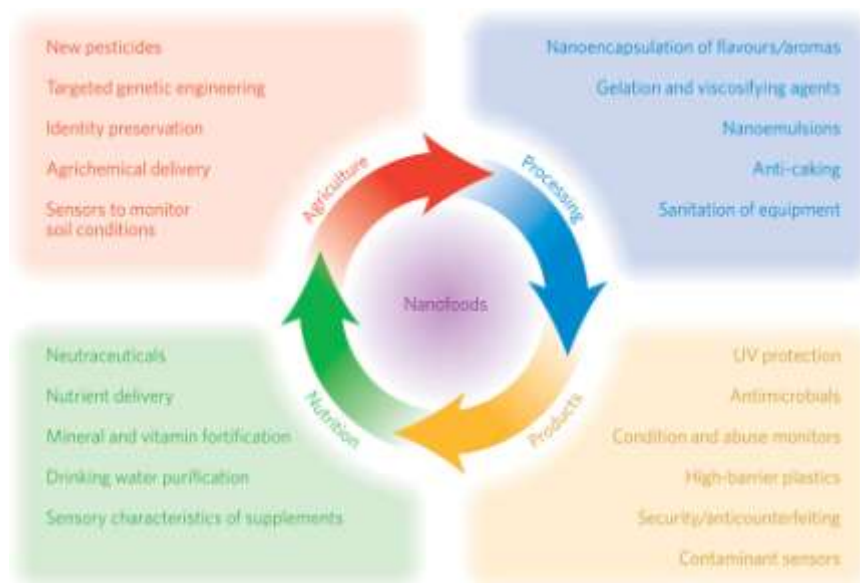


Fig.2 Nanotechnology's potential benefits to many areas of the food industry (Duncan, 2011)

Innovative enhancements for the molecular treatment of diseases, rapid disease detection, successful dealing with viruses and crop pathogens, enhancing the power of plants to absorb nutrients as well as lowering usage doses of pesticides and herbicides proved that nanotechnology has the potential to revolutionize the agricultural and food industry (Joseph and Morrison 2006). To understand and address the importance of nanotechnology in the agri-food sector, this paper represents a review of types and applications of the most present nanosensors in agriculture and food industry. Even there is a belief that nanotechnology will also protect the environment indirectly through the use of renewable energy supplies, and filters or catalysts to reduce pollution and clean-up existing pollutants (Joseph and Morrison 2006), there are still many concerns regarding nanomaterials toxicity and possible negative impact on the surroundings. Alongside the potential advantages of nanotechnology applications in the agri-food supply chain, concerns regarding nanotoxicology and safety will be discussed as well.

Nanosensors

Nanosensors are emerging as a promising tools for the applications in the agriculture and food production. They offer significant improvements in selectivity, speed and sensitivity compared to traditional chemical and biological methods. Nanosensors can be used for determination of microbes, contaminants, pollutants and food freshness (Joyner and Kumar 2015).

The nanosensors used in food analyses combine knowledge of biology, chemistry and nanotechnology and may also be called nanobiosensors.

Need for nanosensors

The part of food production where the need for the nanosensors is the most visible is food packaging and food transport.

Food packaging prevent sensory exposure from the foods thus consumers must rely on expiry dates provided by producers based on a set of idealized assumptions about the way that the food is stored or transported. If the transport or storage conditions are violated for any period of time, the quality of food might be deteriorated which might not be known to the consumer unless the food package is opened, or even consumed (Joyner and Kumar 2015).

Nanosensors can improve the disadvantages of food packaging through their unique chemical and electro-optical properties. They are able to detect the presence of gasses, aromas, chemical contaminants, pathogens, and even changes in environmental conditions. Nanosensors ensure that consumers purchase fresh and tasty products and reduce the frequency of food-borne illnesses which improve food safety.

Development of nanosensors in agri-food sector

Nanosensors have the arrangement like ordinary sensors, but their production is at the nanoscale. Therefore, nanosensor can be defined as an extremely small device than can bind to whatever is wanted to be detected and send back a signal. These tiny sensors are capable of detecting and responding to physicochemical (sensors) and biological signal (biosensors), transferring that response into a signal or output that can be used by humans.

Compared with traditional sensors and their shortcomings, nanosensors have several advantageous properties, such as high sensitivity and selectivity, near real-time detection, low cost and portability and other necessary attributes which are improved by using nanomaterials in their construction (Lu and Bowles 2013). There are many techniques for development of nanosensors which involves top-down lithography, molecular self-assembly and bottom-up assembly approaches. Current nanosensors devices can be divided into (Liu 2003):

- Nanostructured materials - e.g. porous silicon,
- Nanoparticles based sensors,
- Nanoprobes,
- Nanowire nanosensors,
- Nanosystems: cantilevers, Nano-electromechanical systems (NEMS).

Based on applications in food analysis, nanosensors can be divided on:

- Nanoparticle based nanosensors
- Electrochemical nanosensors
- Optical nanosensors

Aptasensors

Aptasensors are biosensors consisting of aptamers (the target-recognition element) and nanomaterial (the signal transducers and/or signal enhancers). Aptamers are single stranded nucleic acid or peptide molecules of size less than 25 kDa with natural or synthetic origin. They are highly specific and selective towards their target compound (ions, proteins, toxins, microbes, viruses) due to their precise and well defined three-dimensional structures. Aptamers are named as synthetic antibodies due to their selection and generation through an *in vitro* combinatorial molecular technique called SELEX. Dissociation constants of aptamers are in nanomolar or picomolar range. Aptamers are extensively used as recognition elements in the fabrication of aptasensors (Sharma et al. 2015). There are a wide variety of nanomaterials, which can be used in aptasensors (metal nanoparticles and nanoclusters, semiconductor nanoparticles, carbon nanoparticles, magnetic nanoparticles etc) (Sharma et al. 2015). Also, a wide variety of transducing systems have been employed in aptasensors for food quality assessment and safety. The principles of aptasensors are based on the property of the nanoparticle being used. Based on the detection systems, aptamers can be classified into optical and electrochemical systems.

Nanosensors applications

Numerous nanosensors are developed for various applications in agricultural and food industry either to quickly identify threats in the case of suspected food poisoning, or integrated into packaging as nanotracers to show the history of the food product and whether it is of acceptable quality at any given time. For instance, the use of nanosensors in food packaging to detect growth of microorganisms and change color when a threshold level

is reached, as well as nanosensors applied in on-line process control, for monitoring of storage conditions are useful for preventing food poisoning (Augustin and Sanguansri 2009). As another example, scientists are making the gold nanoparticles and coat them with molecules that can bind to substances like pesticides. Farmers could spray these nanoparticles on their fields to detect a chemical like a pesticide (Rathbun 2013).

Furthermore, nanosensors employing Raman spectroscopy are ideally suited for food forensic. Food forensics is investigation of food origin, adulteration and contamination. Nanosensors application in this contributes to the specificity of the method and allows application of various analytes which can be probed; ranging from the macro-food, lipids, proteins and carbohydrates, to the minor components, dyes, pigments, preservatives.

More examples of nanosensors and their development for agriculture and food applications are depicted in (Augustin and Sanguansri 2009; Rai et al. 2012; Parisi et al. 2014). According to Fig. 2 and performed surveys of research articles (Joseph and Morrison 2006; Valdes et al. 2009; Lu and Bowles 2013; Prasad et al. 2014; Nanowerk 2014; Sekhon 2014; Berekaa 2015; Rai et al. 2015), the list of potential applications of nanosensors in agri-food supply chain can be summarized, as it is shown in Table 1.

It can be highlighted that nanosensors are useful for sensing and reporting real time information regarding the product from production through to delivery to the consumer. Nanosensors are far from being simply a passive, information-receiving device. They can get information from immediate and remote contexts and can analyze, record and report data. They can be designed to manage this at critical control points in the supply chain - from the point food is produced or packaged, through to the time it is consumed.

The latest developments have resulted in nanosensors which are quite near commercialization: nanosensors and nanoscale coatings to replace thicker, more wasteful polymer coatings for preventing corrosion, nanosensors for detection of aquatic toxins, nanoscale biopolymers for improved decontamination and recycling of heavy metals, nanosensors able to provide quality assurance by tracking microbes, toxins and contaminants through the food processing chain by using data capture for automatic control functions and documentation, among others (Prasad et al 2014; Lu and Bowles 2013).

Gold nanoparticles functionalized with cyanuric acid groups selectively bind to melamine, an adulterant used to artificially inflate the measured proteins content of pet foods and infant formulas (Ai et. al, 2009).

A promising photoactivated indicator ink for in-package oxygen detection based upon nanosized TiO₂ or SnO₂ particles and a redox-dye (methylene blue) has been developed (Mills, 2005) (Fig. 3).

Nanosensors based on nanoparticles have also been developed to detect the presence of moisture content inside a food packaging (Luechinger et al., 2007) (Fig. 4).

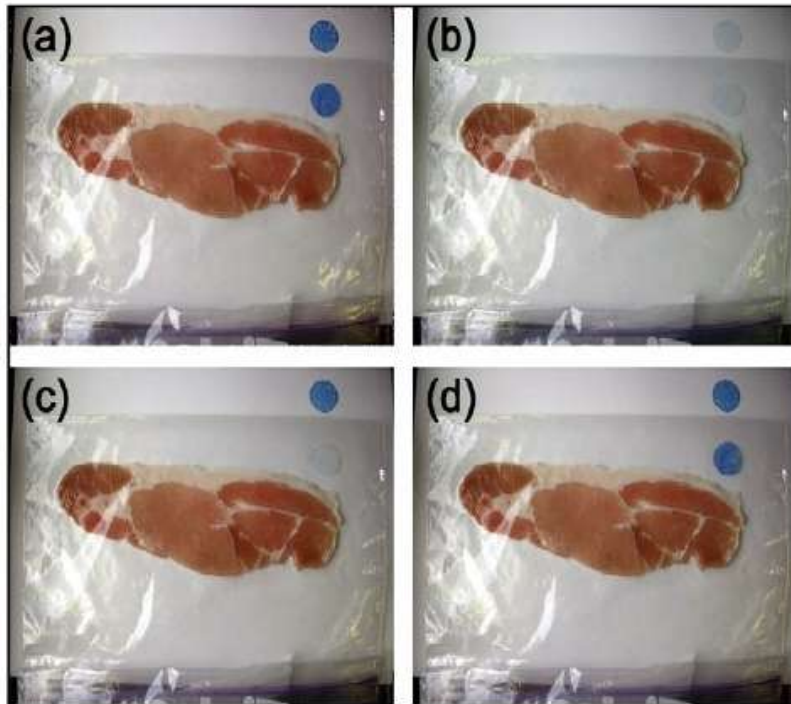


Fig.3 Photographs of O₂ sensors which utilize UV-activated TiO₂ nanoparticles and methylene blue indicator dye, one placed inside of a food package flushed with CO₂ and one placed outside. In (a) the package is freshly sealed and both indicators are blue. The photograph in (b) shows the indicators immediately after activation with UVA light. After a few minutes, the indicator outside of the package returns to a blue color, whereas the indicator in an oxygen-free atmosphere remains white (c) until the package is opened, in which case the influx of oxygen causes it to change back to blue (d). This system could be used to easily and noninvasively detect the presence of leaks in every package immediately after production and at retail sites (Adapted from: Mills, 2005)

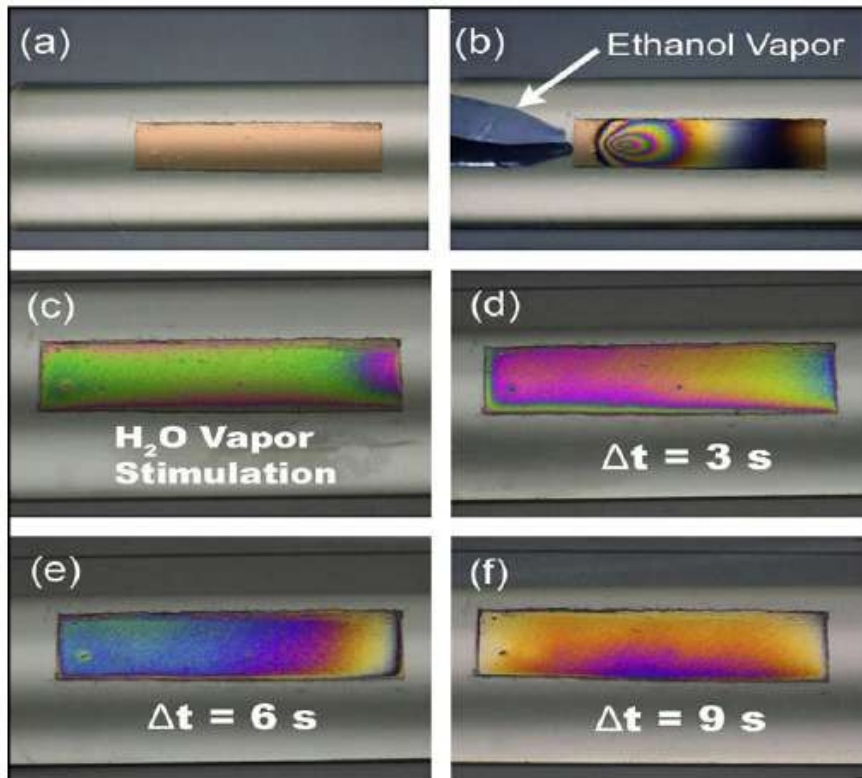


Fig.4 Moisture sensor which utilizes carbon-coated copper nanoparticles dispersed in a polymer matrix (a). Ethanol vapor exposure results in rapid and reversible iridescent coloration (b). Water vapor exposure swells the polymer, which causes the nanoparticles to exhibit larger interparticle separation distances and thus different observable optical behavior (c). As moisture dissipates (d-f), the sensor reverts back to its native state and appearance (Adapted from: Luechinger et al., 2007)

Table 1: Nanosensors potential applications in agri-food sector

Agriculture	Food processing	Food packaging	Food transport	Nutrition
<ul style="list-style-type: none"> • Nanosensors for monitoring soil conditions (e.g. moisture, soil pH), a wide variety of pesticides, herbicides, fertilizers, insecticides, pathogens and crop growth as well • Nanosensors for detection of food-borne contaminants or for monitoring environmental conditions at the farm • Nanochips for identity preservation and tracking • Nanocapsules for delivery of pesticides, herbicides, fertilizers and vaccines • Nanosensors and nano-based smart delivery systems for efficient use of agricultural natural resources (e.g. water), nutrients and chemicals through precision farming • Nanoparticles to deliver growth hormones or DNA to plants in controlled manner • Nanoparticles used as smart nanosensors for early warning of changing conditions that are able to respond to different conditions • Aptasensors for determination of pesticides and insecticides (e.g. phorate, acetamiprid, isocarbophos) • Aptasensors for determination of antibiotics, drugs and their residues (e.g. cocaine, oxytetracycline, tetracycline, kanamycin). • Aptasensors for determination of heavy metals (e.g. Hg^{2+}, As^{3+}, Cu^{2+}) 	<ul style="list-style-type: none"> • Nanoencapsulated flavor enhancers • Nanotubes and nanoparticles as gelation and viscosifying agents • Nanocapsule infusion of plant based steroids to replace a meat's cholesterol • Nanoparticles to selectively bind and remove chemicals or pathogens from food • Aptasensors for determination of microbial toxins (e.g. OTA, Fumonisin B1) 	<ul style="list-style-type: none"> • Portable nanosensors to detect chemicals, pathogens and toxins in food • DNA biochips to detect pathogens and to determine the presence of different kind of harmful bacteria in meat or fish, or fungi affecting fruit • Nanosensors incorporated into packaging materials for detection of chemicals released during food spoilage and serve as electronic tongue (e.g. bitter, sweet, salty, umami, and sour detection), or nose (e.g. wine characterization) • Electromechanical nanosensors to detect ethylene • Nanosensors applied as labels or coating to add an intelligent function to food packaging in terms of ensuring the integrity of the package through indication of time-temperature variations and microbial safety • Aptasensors for determination of microbial cells (e.g. Salmonella typhimurium, Escherichia Coli, Listeria monocytogenes) • Aptasensors for determination of antibiotics, drugs and their residues (e.g. cocaine, oxytetracycline, tetracycline, kanamycin). • Aptasensors for determination of heavy metals (e.g. Hg^{2+}, As^{3+}, Cu^{2+}) 	<ul style="list-style-type: none"> • Nanosensors for monitoring environmental conditions during distribution and storage • Nanosensors for traceability and monitoring product conditions during transport and storage, what is crucial for products which have a limited shelf-life • Smart-sensor technology for monitoring the quality of grain, dairy products, fruit and vegetables in a storage environment in order to detect the source and the type of spoilage • Aptasensors for determination of microbial cells (e.g. Salmonella typhimurium, Escherichia Coli, Listeria monocytogenes) 	<ul style="list-style-type: none"> • Nanocapsules incorporated into food to deliver nutrients • Nanocochleates (50 nm coiled nanoparticles) for delivering nutrients (e.g. vitamins, lycopene, and omega fatty acids) more efficiently to cells, without affecting the color or taste of food

Toxicology and safety aspects of nanosensors utilization in agricultural and food industry

Despite the tremendous benefits of nanosensors in the agriculture and food industry, there is a huge public concern regarding toxicity and environmental effect. There is very limited knowledge about its long term adverse effect on soil, plants and ultimately on human (Dubey and Mailapalli 2016). Preliminary studies on animal have shown potential toxicity of nanomaterials for liver, kidneys, and immune system. Additionally, the effects of exposure to engineered nanoparticles may be dissimilar from the effects induced by naturally occurring nanoparticles (Rai and Ingle 2012). Therefore, risk assessment studies to show adverse effects of nanoparticles on human health and the environment should be standardized and their number should be increased while at the same time the field of nanotoxicology emerges to international level. Obviously, the necessity of awareness of the nanoparticles presence in the environment and their detection, the measurement of nanoparticles emissions, life-cycle, toxicity and impact to human health and environment are crucial in achieving all the benefits nanotechnologies has to offer.

The toxicity of nanoparticles in the environment depends on their size, type, charge, etc. Additionally, the influence of nanoparticles on the environment depends also of the environmental factors (humidity, temperature, wind flow rate, the nature of light, etc). However, properties of nanomaterials, small size and large surface allow easy dispersion and bonding in the environment and with human tissues.

One way in which nanomaterials enter the environment and humans is through agriculture sector (Rico 2015). Nanoparticles strongly interact with soils. Nanomaterials enhanced plant foods and pesticides are able to disperse into soil, water and atmosphere, to bond more strongly with pollutants and carry them through soil and water (Sastry 2012). Exposure to nanofertilizers and pesticides, can contribute to health hazards (Sastry 2012). Migration of nanoparticle incorporated in food material to human is also high risk (Berekaa 2015). In other words, direct exposure of consumers to nanomaterials poses a serious problem to human health. Nanoparticles can enter the human body through the skin, respiratory system or digestive system (Fig. 5). However, as long as the nanoparticles remain bound, exposure is limited or very low. Health impact and safety regarding the application of nanomaterials was reported in detail by Teow et. al (2011).

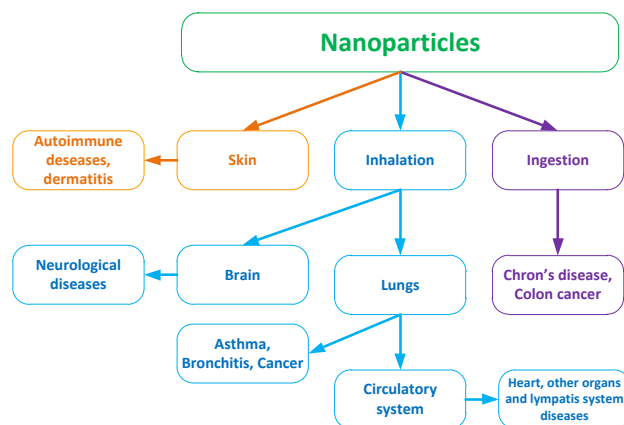


Fig. 5. Potential harmful effects of nanoparticles to human health

Modern techniques revealed that nanomaterials with higher reactivity and ability to cross membrane barriers can lead to different toxico-kinetic and toxico-dynamic properties. Some nanomaterials interact with proteins and enzymes leading to oxidative stress and generation of ROS, which cause destruction of mitochondria and produce apoptosis.

Over the last few years there have been numerous publications reporting a variety of biological and toxicological interactions of nanomaterials in *in vitro* and *in vivo* experimental systems. A wide range of biochemical and toxicological endpoints within each system have been reported. Most have been directed to proinflammatory and inflammatory markers since existing knowledge on the health effects of ambient fine particulates and nanomaterials has identified a central role for oxidative stress and inflammation in the toxicological mode of action of nanoparticles.

Therefore, the understanding of the biological and toxicological effects of nanomaterials has significantly advanced in the last few years. Much of this has been in relation to what type of physical characterization and toxicological data is required for hazard and risk assessment, and how to go about obtaining it. Serious adverse effects have not been observed in limited applications to nanomaterials of "traditional" tests for assessing the acute toxicity of chemicals. The toxicological data sets available for nanomaterials remain rudimentary, for example long term inhalation studies, reproductive or developmental studies are not available. The fact that, if nanoparticles are absorbed into the systemic circulation, they may be retained within cells for long periods, makes it imperative that chronic studies be undertaken for hazard and risk assessment of nanomaterials.

One of the potential solutions to make nanotechnology applications as safe as possible is moving towards green nanotechnology. Safe and energy efficient nanomaterials, nanoproducts and processes, reduced waste, lessen greenhouse gas emissions and usages of renewable materials are the benefits green nanotechnology concept offers. Even this concept is still in the lab/start-up phase, it is anticipated that by greening nanotechnology, environmental, health and societal benefits of nanoparticle production and nanoparticle application in various fields will be maximized (Dahl et al. 2007, OECD 2013, Goel and Bhatnagar 2014).

Nanosensors in the realization of smart agri-food sector

Nanotechnology is recognized by the European Commission as one of its six “Key Enabling Technologies” that have potential to significantly improve various industrial sectors. Even nanotechnology application to the agriculture and food sectors is at the nascent stage compared with some other sectors, like drug delivery and pharmaceuticals, the current challenges of sustainability, food security and climate change implicate enhanced researchers' interest in exploring the role and significance of nanotechnology in the improvement processes of the agrarian sector (Parisi et al. 2015). Nanotechnology holds the potential to revolutionize the global food system, and there are a lot more applications in agriculture and food system that can be expected in the years to come (Prasad et al. 2014). Novel agricultural and food safety systems, disease-treatment delivery methods, tools for molecular and cellular biology, sensors for detecting pathogens and pesticides, intelligent packaging materials, environmental protection, and education of the public and future workforce are some of examples of the important impact that nanotechnology could have in agrarian sector (Garcia et al. 2010).

Inexpensive sensors, cloud computing and intelligent software together can revolutionize the whole agri-food sector. Thanks to the computers, global satellite positioning systems and remote sensing devices, precise farming becomes reality. Monitoring and measuring of environmental variables, and making appropriate and on-time decisions and performing targeted action according to collected data in order to maximize output (i.e. crop yields) with optimal use of resources (i.e. fertilizers, pesticides, herbicides, etc.) are the main characteristics of precise farming vision (Rai and Ingle 2012).

It is important to highlight various micro-nano bio systems, developed as projects of European Commission (2015) and used to realize smart agri-food systems. Technology development, particularly Internet of Things (IoT), as an emerging reality where more and more devices are connected to users and other devices via the Internet, significantly contribute to the realization of the smart agriculture by increasing the quality, quantity, sustainability and cost effectiveness of agricultural production. The innovative application of nanotechnology in IoT creates a new paradigm, namely the Internet of Nano Things (IoNT). Nanosensors, because of their small dimensions, can collect information from numerous different points. Nanosensors made from non-biological materials, such as carbon nanotubes, have ability to sense and signal, acting as wireless nanoantennas (Garcia-Martinez 2016).

External devices can then integrate the data to automatically generate incredibly detailed report and respond to potentially devastating changes in their environment. There are numerous intelligent nanosystems, used in the smart agriculture for the crop monitoring, immobilization of nutrients and their release in soil, analysis of pesticides, moisture and soil pH. Networks of connected nanosensors for monitoring soil or plant conditions have ability to alert automatically according to conditions detected by sensors and therefore influence more efficient usage of the water, fertilizers, herbicide, pesticide, insecticide, etc. In this way, a real time and comprehensive monitoring of the crop growth, lead to accurate and on-time decisions, reduced costs and waste, improved quality of production and above all, to sustainable agriculture.

As food safety is a main concern nowadays, it is essential to have manners and systems which enable foodstuffs traceability and monitoring during the whole food chain process (Maksimovic et al. 2015). Nanosensors can be applied along the entire food supply chain, in order to detect different targets in quickly, sensitive, and cost-effective manners. This is necessary in the process of ensuring food quality, safety, freshness, authenticity, and traceability (Fraceto et al. 2016). For instance, involving nanosensors in the design of smart or intelligent packaging, spoilage or harmful contaminants during distribution or storage can be detected alongside enabled transfer of information regarding product conditions. In this way food producers, transportation and hospitality/retail companies become connected as never before.

The response generated due to changes related to internal or external environmental factor, are recorded through specific sensors (Berekaa 2015), stored in the database and via Internet 24/7 available insight into soil and crop health, food contaminations, quality, etc (Fig. 6). In this way, rapid response and reactions to detections of abnormally parameters' values, are enabled and lead to more quality and safe food, what direct influence to human health. However, to achieve the full potential IoNT has to offer in agriculture and food industry, many concerns, regarding data security and privacy as well as nanomaterial's toxicity and impact to the environment and human must be considered.

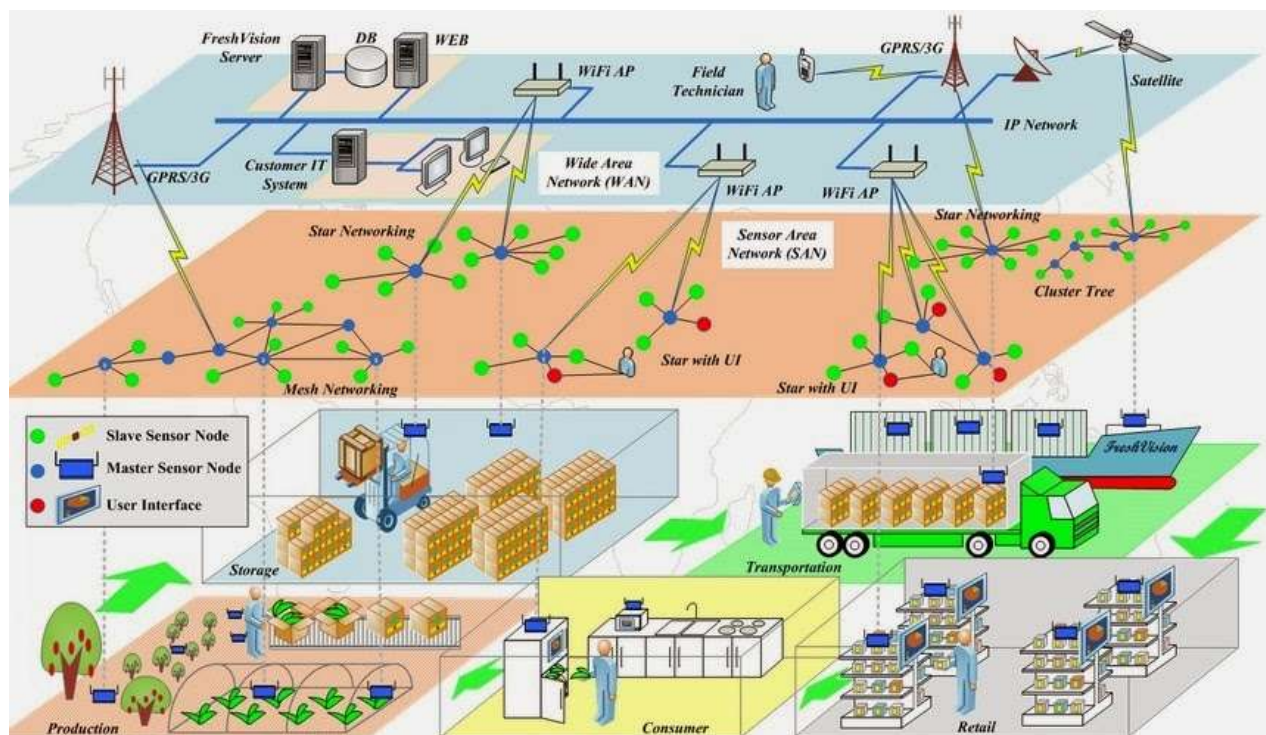


Fig.6 IoT architecture for the agri-food sector (Gannon 2016)

CONCLUSION

Recent advancements in nanotechnology, embraced with intense research at both academic and industrial levels and advancements in ICTs, show its potential to positively influence the agri-food sector. Improved quality of the soil, increased productivity, stimulation of plant growth, the use of precise farming, monitoring food quality and freshness during production, processing, distribution and storage, are just some of the many benefits nanotechnology, nanomaterials and nanosensors have to offer in agricultural and food industry. The excellent specificity of the nanosensors and aptamers allows an analysis of wide variety analytes, including heavy metal ions, toxins, pathogens, small molecules, nucleic acids and proteins. Nanoparticles add on to the selectivity and convenience of the diagnostics, by the providing larger surface area for aptamer immobilization as well as by conferring their own opto-physical and electrochemical properties to the sensor. Some obstacles still exist in the development of field-applicable nanosensor techniques (sample pretreatment technique, specificity, expenses). It can be hoped that further insight into the probable solutions to these problems and in the development of novel nanomaterials will boost designing of affordable and easily operable nanomaterial based sensing system. However, the full potential of nanotechnology in agriculture and food sector is yet to be realized and can be achieved only with improved awareness and knowledge of the potential harm from nano-enabled products, and the long-term impacts of nanomaterials to the environment and human health. The future researches will be focused in the development of

novel reliable material, methods and smart devices on the nano-scale, to the realization of IoNT vision, as well as to the evaluation of their impact on the human and environment. Moving towards green nanotechnology and green IoT will lead to a whole new world of safe nanoproducts and their widespread applications with little or no hazards to human health and the environment.

REFERENCES

- Ahumada, O., Villalobos, J.R. (2009). Application of planning models in the agri-food supply chain: A review, *European Journal of Operational Research* 195:1–20
- Ai, K., Liu, Y., Lu, L. (2009). Hydrogen bonding recognition-induced color change of gold nanoparticles for visual detection of melamine in raw milk and infant formula, *Journal of the American Chemical Society*, Vol. 131 (27), 9496-9497
- Augustin, M.A., Sanguansri, P. (2009). Nanostructured Materials in the Food Industry, *Advances in Food and Nutrition Research*, Vol. 58, pp.183-213
- Berekaa, M. (2015). Nanotechnology in Food Industry; Advances in Food processing, Packaging and Food Safety, *Int.J.Curr.Microbiol.App.Sci* 4(5): 345-357
- Craig, A.P., Franca, A.S., Irudayaraj, J. (2013). Surface-enhanced Raman spectroscopy applied to food safety, *Annu Rev Food Sci Technol.* 2013; 4: 369-380

- Dahl, J. A. et al. (2007). Toward Greener Nanosynthesis, *Chem. Rev.*, 107, 2228–2269
- Dubey, A., Mailapalli, D.R. (2016). Nanofertilisers, Nanopesticides, Nanosensors of Pest and Nanotoxicity in Agriculture, E. Lichtfouse (ed.), Sustainable Agriculture Reviews 19, Sustainable Agriculture Reviews, Springer International Publishing Switzerland 2016
- Duncan, T.V. (2011). The communication challenges presented by nanofoods, *Nature Nanotechnology*, Vol. 6, pp. 683-688
- European Commission (2015). Projects on Smart Agri-Food systems. ec.europa.eu/newsroom/horizon2020/document.cfm?doc_id=18158 (4/12/2016).
- Fraceto et al. (2016). Nanotechnology in Agriculture: Which Innovation Potential Does It Have?. *Front. Environ. Sci.*
- Gannon, M. (2016). Personal website, http://mark_gannon_cdsr.workfolio.com/
- García, M., Forbe, T., Gonzalez, E. (2010) Potential applications of nanotechnology in the agro-food sector. *Food Science and Technology* (Campinas) ISSN 0101-2061 Ciênc. Tecnol. Aliment. Vol.30 no.3.
- Garcia-Martinez, J. (2016) The Internet of Things Goes Nano, <http://www.scientificamerican.com/article/the-internet-of-things-goes-nano/>, (4/10/2016).
- Goel, A. and Bhatnagar, S. (2014). Green Nanotechnology, *BioEvolution*, pp. 3-4
- Joyner, J.R., Kumar, D.V. (2015). Nanosensors and their applications in food analysis: a review, Vol. 1, Issue 4, 80-90
- Joseph, T., Morrison, M. (2006). Nanotechnology in Agriculture and Food, ftp://ftp.cordis.europa.eu/pub/nanotechnology/docs/nanotechnology_in_agriculture_and_food.pdf (1/10/2016).
- Li, Z., Sheng, C. (2014). Nanosensors for food safety, *J Nanosci Nanotechnol.* Jan;14(1):905-12.
- Liu, Y. (2003) Nanosensors, <http://www.slideserve.com/kim-johnston/nanosensors>, (3/10/2016).
- Lu, J. and Bowles, M. (2013) How Will Nanotechnology Affect Agricultural Supply Chains?, *International Food and Agribusiness Management Review*, Vol. 16, Issue 2.
- Luechinger, N.A., Loher, S., Athanassiou, E.K., Grass, R.N., Stark, W.J. (2007). Highly sensitive optical detection of humidity on polymer/metal nanoparticle hybrid films. *Langmuir*, 23(6), 3473-3477
- Maksimovic, M. et al. (2015). Application of Internet of Things in food packaging and transportation. *Int. J. Sustainable Agricultural Management and Informatics*, Vol. 1, No. 4, pp. 333-350
- Mills, A. (2005). Oxygen indicators and intelligent inks for packaging food. *Chemical Society Reviews*, 34(12), 1003-1011
- Nanowerk, (2014). Nanotechnology in agriculture, <http://www.nanowerk.com/spotlight/spotid=37064.php> (1/10/2016).
- OECD (2013). Nanotechnology for Green Innovation, OECD Science, Technology and Industry Policy Papers, No. 5, OECD Publishing.
- QS Article (2012). Agri-Food Supply Chain (ASC) affects the Cost Price for Customers, <http://www.qsarticle.com/agri-food-supply-chain-asc-affects-the-cost-price-for-customers/>, (18/9/2016).
- Parisi, C., Vigani, M., Rodríguez-Cerezo, E. (2014). Proceedings of a workshop on “Nanotechnology for the agricultural sector: from research to the field”, Joint Research Centre
- Parisi, C., Vigani, M., Rodríguez-Cerezo, E. (2015). Agricultural Nanotechnologies: What are the current possibilities? *Nanotoday*, Science Direct, Volume 10, Issue 2, Pages 124–127
- Prasad, R., Kumar, V., Prasad, K. S. (2014). Nanotechnology in sustainable agriculture: Present concerns and future aspects. *African Journal of Biotechnology*. Vol. 13(6), pp. 705-713
- Rai, M., Ingle, A. (2012). Role of nanotechnology in agriculture with special reference to management of insect pests. *Appl Microbiol Biotechnol* 94:287–293
- Rai, M., Ribeiro, C., Mattoso, L., Duran, N. (2015). *Nanotechnologies in Agriculture and Food*, Springer International Publishing Switzerland
- Rai, V., Acharya, S., Dey, N. (2012). Implications of Nanobiosensors in Agriculture, *Journal of Biomaterials and Nanobiotechnology*, 3, 315-324
- Rico, C. (2015). Nanomaterial Implications for Agricultural Productivity and Food Safety. <http://www.azonano.com/article.aspx?ArticleID=4076> , (20/12/2016).
- Rathbun, L. C. (2013). Nanosensors and the Food Supply, <http://www.nanooze.org/nanosensors-and-the-food-supply-2/>, (2/10/2016).
- Sastry, R.K. (2012). Potential Economic Impacts of Agri-Nanotechnology. “International Symposium on Assessing the Economic Impact of Nanotechnology”, Washington DC
- Sekhon, B. S. (2014). Nanotechnology in agri-food production: an overview, *Nanotechnol Sci Appl.* 7: 31–53.
- Sharma, R., Ragavan, K.V., Thakur, M.S. Raghavaro, K.S.M.S. (2015). Recent advances in nanoparticle based aptasensors for food contaminants, *Biosensors and Bioelectronics* 74, 612-627
- Teow, Y., Asharani, P.V., Hand, M.P., Valiyaveetil, S. (2011). Health impact and safety of engineered nanomaterials. *Chem Commun.* 47, 7025-7038
- Valdes, M.G. et al. (2009). Analytical nanotechnology for food analysis, *Microchim Acta* 166:1–19

Summary/Sažetak

Sigurnost hrane je vrlo važan aspekt u prehrambenoj industriji i poljoprivredi, jer je u direktnoj vezi sa uticajem hrane na zdravlje ljudi. Nedavni incidenti povezani sa sigurnošću hrane (kao što su afere melamina u 2007. i 2008.) i zabrinutost javnosti zbog sintetičkih aditiva i hemijskih ostataka u hrani istakli su važnost razvoja brzih, osjetljivih i pouzdanih metoda za otkrivanje kontaminanata u hrani. Značajan doprinos sigurnosti hrane daju nanosenzori koji određuju komponente i kontaminante hrane na brz i jednostavan način i u malim koncentracijama. Povezivanje nanosenzora sa modernim informacijskim i komunikacijskim tehnologijama (IKT) omogućava nove i online načine za detekciju različitih komponenti uz visok procenat tačnosti. Postoje različite vrste nanosenzora koji odgovaraju na zahtjeve u inspekciji hrane (nanosenzori integrisani u pakovanju za detekciju vanjskih i unutrašnjih parametara, elektrohemijski senzori na bazi ugljeničnih nanocijevi za detekciju kationa, aniona i organskih spojeva u hrani, razni aptameri za detekciju pesticida, antibiotika, teških metala, ćelijskih mikroba i toksina). Ovaj rad predstavlja pregled razvoja i aplikacija najprisutnijih nanosenzora u poljoprivredi i prehrambenoj industriji.

INSTRUCTIONS FOR AUTHORS

GENERAL INFORMATION

Bulletin of the Chemists and Technologists of Bosnia and Herzegovina (Glasnik hemičara i tehnologa Bosne i Hercegovine) is a semiannual international journal publishing papers from all fields of chemistry and related disciplines.

Categories of Contributions

1. *Original Scientific Papers* – (about 10 typewritten pages) report original research which has not been published previously, except in a preliminary form. The paper should contain all the necessary information to enable reproducibility of the described work.
2. *Short Communications* – (about 5 typewritten pages) describing work that may be of a preliminary nature but which merits immediate publication.
3. *Notes* – (about 3 typewritten pages) report unpublished results of short, but complete, original research or describe original laboratory techniques.
4. *Reviews* – (about 30 typewritten pages) present a concise and critical survey of a specific research area. Generally, these are prepared by the invitation of the Editor.
5. *Book and Web Site Reviews* – (about 2 typewritten pages).
6. *Extended Abstracts* – (about 2 typewritten pages) of Lectures given at international meetings.
7. *Technical Papers* – (about 10 typewritten pages) report on applications of an already described innovation. Typically, technical articles are not based on new experiments.

Reviewing the Manuscript

All contributors are evaluated according to the criteria of originality and quality of their scientific content, and only those deemed worthy will be accepted for publication. To facilitate the reviewing process, authors are encouraged to suggest three persons competent to review their manuscript. Such suggestions will be taken into consideration but not always accepted.

The Editor-In-Chief and Editors have the right to decline formal review of a manuscript when it is deemed that the manuscript is:

1. on a topic outside the scope of the Journal;
 2. lacking technical merit;
 3. of insufficient novelty for a wide international readership;
 4. fragmentary and providing marginally incremental results; or
 5. is poorly written.
-

Proofs

When a manuscript is ready for printing, the corresponding author will receive a PDF-formatted manuscript for proof reading, which should be returned to the journal within one week. Failure to do so will be taken as the authors are in agreement with any alteration which may have occurred during the preparation of the manuscript.

Copyright

Subscribers may reproduce tables of contents or prepare lists of articles including abstracts for internal circulation within their institutions. Permission of the Publisher is required for resale or distribution outside the institution and for all other derivative works, including compilations and translations.

Professional Ethics and Publication Policy

The journal expects the Editors, Referees and authors to adhere to the well-known standards of professional ethics. Authors are responsible for the factual accuracy of their contributions. Submission of the paper commits the author not to submit the same material elsewhere. Referees should act promptly. If certain circumstances preclude prompt attention to the manuscript at the time it is received, the non-received manuscript should be returned immediately to the Editor or the Referee should contact the Editor for possible delay of the report submission date. The Editor accepts full responsibility for his decisions on the manuscripts.

PREPARATION AND SUBMISSION OF MANUSCRIPT**Cover Letter**

Manuscripts must be accompanied by a cover letter in which the type of the submitted manuscript. It should contain:

1. full name(s) of the author(s),
2. mailing address (address, phone and fax numbers, e-mail) of the author to whom correspondence should be addressed,
3. title of the paper (concise, without any abbreviations),
4. type of contribution,
5. a statement that the article is original and is currently not under consideration by any other journal or any other medium, including preprints, electronic journals and computer databases in the public domain, and
6. the names, full affiliation (department, institution, city and country), and
7. e-mail addresses of three potential Referees.

Contributors from Bosnia and Herzegovina should provide the name and full affiliation of at least one Referee from abroad.

Authors are fully encouraged to use ***Cover Letter Template***.

Manuscript preparation

The submitted articles must be prepared with Word for Windows. Manuscripts should be typed in English (either standard British or American English, but consistent throughout) with 1.5 spacing (12 points Times New Roman; Greek letters in the character font Symbol) in A4 format leaving 2.5 cm for margins. Authors are fully encouraged to use **Manuscript Template**.

All contributions should be written in a style that addresses a wider audience than papers in more specialized journals. Manuscripts with grammar or vocabulary deficiencies are disadvantaged during the scientific review process and, even if accepted, may be returned to the author to be rewritten in idiomatic English. The authors are requested to seek the assistance of competent English language expert, if necessary, to ensure their English is of a reasonable standard. The journal maintains its policy and takes the liberty of correcting the English of manuscripts scientifically accepted for publication.

Tables and figures and/or schemes should not be embedded in the manuscript but their position in the text indicated. In electronic version (Word.doc document) tables and figures and/or schemes should follow the text, each on a separate page. Please number all pages of the manuscript including separate lists of references, tables and figures with their captions.

IUPAC and International Union of Biochemistry and Molecular Biology recommendations for the naming of compounds should be followed.

SI units, or other permissible units, should be employed. The designation of physical quantities should be in Times New Roman font. In text, graphs, and tables, brackets should be used to separate the designation of a physical quantity from the unit. Please do not use the axes of graphs for additional explanations; these should be mentioned in the figure captions and/or the manuscript (example: "pressure at the inlet of the system, kPa" should be avoided).

Percents and per mills, although not being units in the same sense as the units of dimensioned quantities, can be treated as such. Unit symbols should never be modified (for instance: w/w %, vol.%, mol.%) but the quantity measured has to be named, *e.g.* mass fraction, $w=95\%$; amount (mole) fraction, $x=20\%$.

Latin words, as well as the names of species, should be in *italic*, as for example: *i.e.*, *e.g.*, *in vivo*, *ibid*, *Artemisia annua* L., *etc.* The branching of organic compound should also be indicated in *italic*, for example, *n*-butanol, *tert*-butanol, *etc.*

Decimal numbers must have decimal points and not commas in the text (except in the Bosnian/Croatian/Serbian abstract), tables and axis labels in graphical presentations of results. Thousands are separated, if at all, by a comma and not a point.

Structure of the Manuscript

The manuscript must contain, each on a separate page, the title page, abstract in English, (abstract in Bosnian/Croatian/Serbian), graphical abstract (optional), main text,

list of references, tables (each table separately), illustrations (each separately), and legends to illustrations (all on the same page).

1. **Title page** must contain: the title of the paper (bold letters), full name(s) of the author(s), full mailing addresses of all authors (italic), keywords (up to 6), the phone and fax numbers and the e-mail address of the corresponding author.
 2. A one-paragraph **abstract** written of 150–200 words in an impersonal form indicating the aims of the work, the main results and conclusions should be given and clearly set off from the text. Domestic authors should also submit, on a separate page, a Summary/Sažetak. For authors outside Bosnia and Herzegovina, the Editorial Board will provide a Bosnian/Croatian/Serbian translation of their English abstract.
 3. Authors are encouraged to submit a **graphical abstract** that describes the subject matter of the paper. It should contain the title of the paper, full name(s) of the author(s), and graphic that should be no larger than 11 cm wide by 5 cm tall. Authors are fully encouraged to use **Graphical Abstract Template**.
 4. **Main text** should have the following form:
 - **Introduction** should include the aim of the research and a concise description of background information and related studies directly connected to the paper.
 - **Experimental** section should give the purity and source of all employed materials, as well as details of the instruments used. The employed methods should be described in sufficient detail to enable experienced persons to repeat them. Standard procedures should be referenced and only modifications described in detail.
 - **Results and Discussion** should include concisely presented results and their significance discussed and compared to relevant literature data. The results and discussion may be combined or kept separate.
 - The inclusion of a **Conclusion** section, which briefly summarizes the principal conclusions, is highly recommended.
 - **Acknowledgement** (optional).
 - Please ensure that every **reference** cited in the text is also present in the reference list (and *vice versa*). Unpublished results and personal communications are not recommended in the reference list, but may be mentioned in the text. If these references are included in the reference list they should follow the standard reference style of the journal and should include a substitution of the publication date with either "Unpublished results" or "Personal communication" Citation of a reference as "in press" implies that the item has been accepted for publication. As a minimum, the full URL should be given and the date when the reference was last accessed. Any further information, if known (DOI, author names, dates, reference to a source publication, etc.), should also be given. No more than 30 references should be cited in your manuscript.
In the text refer to the author's name (without initials) and year of publication (e.g. "Steventon, Donald and Gladden (1994) studied the effects..." or "...similar to values reported by others (Anderson, Douglas, Morrison, *et al.*, 1990)..."). Type the names of the first three authors at first citation. At subsequent citations use
-

first author *et al.* The list of references should be arranged alphabetically by authors' names and should be as full as possible, listing all authors, the full title of articles and journals, publisher and year.

Examples of **reference style**:

a) Reference to a journal publication:

Warren, J. J., Tronic, T. A., Mayer, J. M. (2010). Thermochemistry of proton-coupled electron transfer reagents and its implications. *Chemical Reviews*, 110 (12), 6961-7001.

b) Reference to a book:

Corey, E. J., Kurti, L. (2010). *Enantioselective chemical synthesis*. (1st Ed.) Direct Book Publishing, LLC.

c) Reference to a chapter in an edited book:

Moody, J. R., Beck II, C. M. (1997). Sample preparation in analytical chemistry. In Settle, F. A. (Ed.), *Handbook of instrumental techniques for analytical chemistry*. (p.p. 55-72). Prentice Hall.

d) Reference to a proceeding:

Seliskar, C. J., Heineman, W.R., Shi, Y., Slaterbeck, A.F., Aryal, S., Ridgway, T.H., Nevin, J.H. (1997). *New spectroelectrochemical sensor*, in Proceedings of 37th Conference of Analytical Chemistry in Energy and Technology, Gatlinburg, Tennessee, USA, p.p. 8-11.

e) Patents:

Healey, P.J., Wright, S.M., Viltro, L.J., (2004). *Method and apparatus for the selection of oral care chemistry*, The Procter & Gamble Company Intellectual Property Division, (No.US 2004/0018475 A1).

f) Chemical Abstracts:

Habeger, C. F., Linhart, R. V., Adair, J. H. (1995). Adhesion to model surfaces in a flow through system. *Chemical Abstracts*, CA 124:25135.

g) Standards:

ISO 4790:1992. (2008). *Glass-to-glass sealings - Determination of stresses*.

h) Websites:

Chemical Abstract Service, www.cas.org, (18/12/2010).

- **Tables** are part of the text but must be given on separate pages, together with their captions. The tables should be numbered consequently in Latin numbers. Quantities should be separated from units by brackets. Footnotes to tables, in size 10 font, are to be indicated consequently (line-by-line) in superscript letters. Tables should be prepared with the aid of the Word table function, without vertical lines. Table columns must not be formatted using multiple spaces. Table rows must not be formatted using Carriage returns (enter key; ↵ key). Tables should not be incorporated as graphical objects.
- **Figures and/or Schemes** (in high resolution) should follow the captions, each on a separate page of the manuscript. High resolution illustrations in TIF or EPS format (JPG format is acceptable for colour and greyscale photos, only) must be uploaded as a separate archived (.zip or .rar) file.

Figures and/or Schemes should be prepared according to the artwork instructions.

- **Mathematical and chemical equations** must be numbered, Arabic numbers, consecutively in parenthesis at the end of the line. All equations should be embedded in the text except when they contain graphical elements (tables, figures, schemes and formulae). Complex equations (fractions, integrals, matrix...) should be prepared with the aid of the Word Equation editor.

Artwork Instructions

Journal accepts only TIF or EPS formats, as well as JPEG format (only for colour and greyscale photographs) for electronic artwork and graphic files. MS files (Word, PowerPoint, Excel, Visio) are NOT acceptable. Generally, scanned instrument data sheets should be avoided. Authors are responsible for the quality of their submitted artwork.

Image quality: keep figures as simple as possible for clarity - avoid unnecessary complexity, colouring and excessive detail. Images should be of sufficient quality for the printed version, i.e. 300 dpi minimum.

Image size: illustrations should be submitted at its *final size* (8 cm for single column width or 17 cm for double column width) so that neither reduction nor enlargement is required.

Photographs: please provide either high quality digital images (250 dpi resolution) or original prints. Computer print-outs or photocopies will not reproduce well enough for publication. Colour photographs rarely reproduce satisfactorily in black and white.

The facility exist for color reproduction, however the inclusion of color photographs in a paper must be agreed with Editor in advance.

Reporting analytical and spectral data

The following is the recommended style for analytical and spectral data presentation:

1. **Melting and boiling points:**

mp 163–165°C (lit. 166°C)

mp 180°C dec.

bp 98°C

Abbreviations: mp, melting point; bp, boiling point; lit., literature value; dec, decomposition.

2. **Specific Rotation:**

$[\alpha]_{23}^D -222$ (*c* 0.35, MeOH).

Abbreviations: α , specific rotation; D, the sodium D line or wavelength of light used for determination; the superscript number, temperature (°C) at which the determination was made; In parentheses: *c* stands for concentration; the number following *c* is the concentration in grams per 100 mL; followed by the solvent name or formula.

3. NMR Spectroscopy:

^1H NMR (500 MHz, DMSO- d_6) δ 0.85 (s, 3H, CH₃), 1.28–1.65 (m, 8H, 4'CH₂), 4.36–4.55 (m, 2H, H-1 and H-2), 7.41 (d, J 8.2 Hz, 1H, ArH), 7.76 (dd, J 6.0, 8.2 Hz, 1H, H-1'), 8.09 (br s, 1H, NH).

^{13}C NMR (125 MHz, CDCl₃) δ 12.0, 14.4, 23.7, 26.0, 30.2, 32.5, 40.6 (C-3), 47.4 (C-2'), 79.9, 82.1, 120.0 (C-7), 123.7 (C-5), 126.2 (C-4).

Abbreviations: δ , chemical shift in parts per million (ppm) downfield from the standard; J , coupling constant in hertz; multiplicities s, singlet; d, doublet; t, triplet; q, quartet; and br, broadened. Detailed peak assignments should not be made unless these are supported by definitive experiments such as isotopic labelling, DEPT, or two-dimensional NMR experiments.

4. IR Spectroscopy:

IR (KBr) ν 3236, 2957, 2924, 1666, 1528, 1348, 1097, 743 cm^{-1} .

Abbreviation: ν , wavenumber of maximum absorption peaks in reciprocal centimetres.

5. Mass Spectrometry:

MS m/z (relative intensity): 305 (M⁺H, 100), 128 (25).

HRMS–FAB (m/z): [M+H]⁺calcd for C₂₁H₃₈N₄O₆, 442.2791; found, 442.2782.

Abbreviations: m/z , mass-to-charge ratio; M, molecular weight of the molecule itself; M⁺, molecular ion; HRMS, high-resolution mass spectrometry; FAB, fast atom bombardment.

6. UV-Visible Spectroscopy:

UV (CH₃OH) λ_{max} (log ϵ) 220 (3.10), 425 nm (3.26).

Abbreviations: λ_{max} , wavelength of maximum absorption in nanometres; ϵ , extinction coefficient.

7. Quantitative analysis:

Anal.calcd for C₁₇H₂₄N₂O₃: C 67.08, H 7.95, N 9.20. Found: C 66.82, H 7.83, N 9.16. All values are given in percentages.

8. Enzymes and catalytic proteins relevant data:

Papers reporting enzymes and catalytic proteins relevant data should include the identity of the enzymes/proteins, preparation and criteria of purity, assay conditions, methodology, activity, and any other information relevant to judging the reproducibility of the results¹. For more details check Beilstein Institut/STREND A (standards for reporting enzymology data) commission Web site (<http://www.strenda.org/documents.html>).

¹ For all other data presentation not mentioned above please contact Editor for instructions.

Submission Checklist

The following list will be useful during the final checking of an article prior to sending it to the journal

for review:

- E-mail address for corresponding author,
- Full postal address,
- Telephone and fax numbers,
- All figure captions,
- All tables (including title, description, footnotes),
- Manuscript has been "spellchecked" and "grammar-checked",
- References are in the correct format for the journal,
- All references mentioned in the Reference list are cited in the text, and *vice versa*.

Submissions

Submissions should be directed to the Editor by e-mail: glasnik@pmf.unsa.ba, or glasnikhtbh@gmail.com. All manuscripts will be acknowledged on receipt (by e-mail) and given a reference number, which should be quoted in all subsequent correspondence.



Glasnik hemičara i
tehnologa
Bosne i Hercegovine

Bulletin of the Chemists and Technologists of Bosnia and Herzegovina

Print ISSN: 0367-4444
Online ISSN: 2232-7266

Zmaja od Bosne 33-35, BA-Sarajevo
Bosnia and Herzegovina
Phone: +387-33-279-918
Fax: +387-33-649-359
E-mail: glasnik@pmf.unsa.ba
glasnikhtbh@gmail.com

Sponsors

prevent.



Nema tajne niti neke čarobne formule, u pitanju je samo mukotrpan rad, produktivnost i težnja za većim ostvarenjima

www.prevent.ba



HYDRO-ENERGY FACILITIES

SYSTEM FOR WATER TREATMENT

INFRASTRUCTURE



HIGRACON d.o.o. Sarajevo
Dzemala Bijedica br.2
71000 Sarajevo
Bosnia and Herzegovina

Tel. +387 33 718 286
Fax. +387 33 718 285
GSM: +387 62 994 254
E-mail: higracon@bih.net.ba

www.higracon.ba

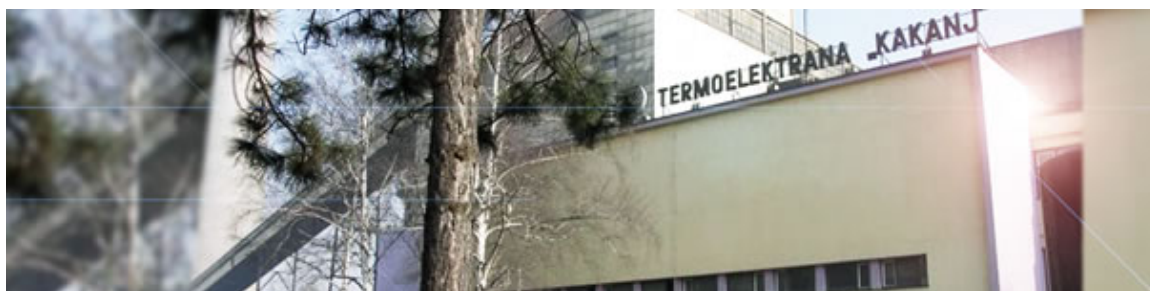


Glasnik hemičara i
tehnologa
Bosne i Hercegovine

Bulletin of the Chemists and Technologists of Bosnia and Herzegovina

Print ISSN: 0367-4444
Online ISSN: 2232-7266

Zmaja od Bosne 33-35, BA-Sarajevo
Bosnia and Herzegovina
Phone: +387-33-279-918
Fax: +387-33-649-359
E-mail: glasnik@pmf.unsa.ba
glasnikhtbh@gmail.com



www.elektroprivreda.ba/stranica/te-kakanj



www.fmon.gov.ba

Zahvaljujemo se **Federalnom ministarstvu obrazovanja i nauke** na finansijskoj pomoći za izdavanje ovog broja *Glasnika hemičara i tehnologa Bosne i Hercegovine*.

Redakcija GLASNIKA-a